A COMPUTATIONAL MODEL FOR THE INVESTIGATION OF NUCLEAR MANY-BODY EFFECTS: FROM REACTION DYNAMICS TO PHASE TRANSITIONS

by

James N. Glosli

B.Sc., Simon Fraser University, 1981

M.Sc., Simon Fraser University, 1983

A THESIS SUBMITTED IN PARTIAL FULFILLMENT OF

THE REQUIREMENTS FOR THE DEGREE OF

DOCTOR OF PHILOSOPHY

in the Department

of

Physics

SIMON FRASER UNIVERSITY

March, 1990

APPROVAL

Name: James Glosli

Degree: Doctor of Philosophy

Title of Thesis: A computational model for the investigation of nuclear many-body effects: from reaction dynamics to phase transitions

Examining Committee:

Chairman: Dr. E.D. Croizer

Dr. D.H. Boal
Senior Supervisor

Dr. M. Plischke

Dr. R.M. Woloshyn

Dr. L.E. Ballentine

Dr. S. Das Gupta
External Examiner
Department of Physics
McGill University

Date Approved: 23 March, 1990

PARTIAL COPYRIGHT LICENSE

I hereby grant to Simon Fraser University the right to lend my thesis, project or extended essay (the title of which is shown below) to users of the Simon Fraser University Library, and to make partial or single copies only for such users or in response to a request from the library of any other university, or other educational institution, on its own behalf or for one of its users. I further agree that permission for multiple copying of this work for scholarly purposes may be granted by me or the Dean of Graduate Studies. It is understood that copying or publication of this work for financial gain shall not be allowed without my written permission.

Title of Thesis/Project/Extended Essay

A Computational Model for the Investigation of Nuclear Many Body Effects: From Reaction Dynamics to Phase Transitions.

Author: _____
(signature)

James Norman Glosli
(name)

March 26/90
(date)

ABSTRACT

A Hamiltonian model is advanced which provides a computationally efficient means of investigating nuclear many-body effects. The Hamiltonian includes both Coulomb and isospin dependent terms, and incorporates antisymmetrization effects though a momentum-dependent potential. Unlike many other classical and semiclassical models, the nuclei of this simulation have a well-defined ground state with a nonvanishing $\langle p^2 \rangle$. The ground state nuclei produced by the model compare favorably in energy and RMS radius with the experimentally observed values.

The model provides a means to investigate the time scales associated with various reaction mechanisms found in heavy ion collisions. In particular, the thermalization in heavy ion collisions is investigated by examining the kinetic energy distributions and excited state populations predicted by the model. It is found that the apparent temperature scales obtained from these distributions are different, and their predicted magnitudes are in agreement with experiment.

The model is also used to explore the phase diagram of infinite nuclear matter. In the phase diagram study it is found that finite size effects for systems of masses typical of heavy ion collision are sufficiently large to prevent one from making any clear association of the fragmentation process with the nuclear phase diagram.

ACKNOWLEDGEMENTS

There are many people that deserve acknowledgment and to whom I am exceedingly grateful for their support and assistance that made this thesis possible. At the risk of neglecting a few people, I wish to mention some names. I would like to thank the Computing Services staff of Simon Fraser University for their assistance and support of large scale computing that made this program possible. In particular, I would thank Ian Reddy for his many hours of consultation that made the transition to a new computing system much easier. I am very grateful to my family because they have always supported me in my educational pursuits, with this latest degree being no exception. I would like to thank my sister Dora and her husband Glen for allowing me to commandeer their office and PC to write the thesis. With the thesis finished I am sure their kids will be much happier now that they don't have to check with Uncle Jim before playing computer games. I am also grateful to the Physics Department of Simon Fraser University for providing a comfortable environment to learn and to do research. I would like to thank Mike Plischke for his support and willingness to entertain questions. I am exceedingly grateful to Ed Levinson, with whom I have shared the graduate school experience for many years, for his courage in offering to be the first to proofread my initial and somewhat raw attempts at composition. Finally, I would like to mention my advisor David Boal. David deserves to be blamed and thanked (mostly the latter) for encouraging me to restart my PhD program. David's character and support made this experience both rewarding and enjoyable. I also thank him for his critical reading of the thesis and his many suggestions for improvement.

TABLE OF CONTENTS

List of Tables

List of Figures

I INTRODUCTION

Heavy ion collision experiments have been used to probe the nuclear interaction at both low (5-10A∘MeV[1]) and high (0.1-10A∘GeV) bombarding energy[2] experiments. Recently, much effort has gone into the study of intermediate energy reactions (10-100A∘MeV) with the construction of new accelerators at Michigan State University and GANIL. These intermediate energy reactions have yielded a rich assortment of nuclear phenomena and are thought to be a good tool to explore the many-body aspects of nuclear systems [GT86,GB87].

It is useful in the description of nuclear reactions to subdivide them into two classes based on impact parameter: central collisions (small impact parameter) and peripheral collisions (large impact parameter). The peripheral collisions are the least complex. For the most part these collisions result in only a small amount of energy and mass being exchanged between the collision pair. Whereas the physics of peripheral collisions tends to be insensitive to bombarding energy, the nature of the reaction processes in central collisions is qualitatively different for low and high bombarding energies.

For low energy central collisions, the reactions are dominated by the soft tails of the nuclear interaction, often called the nuclear mean field. In these reactions, for all but very heavy nuclei, the projectile and target

---

[1] The notation A∘MeV is an energy unit of A times one MeV, where A is the number of nucleons in the system under consideration.

[2] The bombarding energy is the kinetic energy of the centre of mass of the projectile as measured in the lab frame.

fuse together to form an excited compound nucleus. The excitation energy is sufficiently small that the system can equilibrate before it decays. These decays are statistical in nature and are dominated by particle and gamma ray emission.

At high energies the central collision reaction processes are dominated by the hard core of the nuclear interaction, with the nuclear mean field having little effect. The physics of these reactions can be described in terms of the participant-spectator model, which assumes only the nucleons that geometrically overlap during the collision (participants) interact, and that the other nucleons (spectators) are largely unaffected.

An intermediate-energy-range central collision produces a rich array of fragments. This process, known as multifragmentation, illustrates the many-body nature of these reactions and presents an interesting theoretical challenge. The energy is neither large enough to justify the participant-spectator picture, nor so low that the complete fusion and subsequent statistical decay picture is adequate. It is because these reactions cannot be modeled in simple ways that they are interesting to consider.

A conjecture that intermediate energy reactions may yield information about the nuclear equation of state, which is believed to be dominated by the nuclear mean field, also adds to the interest in these reactions. At very high energies the mean field affects the reaction only in a small way and therefore these reactions yield very little about the equation of state. On the other hand, low energy reactions, though dominated by the mean

field, can only explore the equation of state for low temperatures and near-normal nuclear matter densities, ρ_o. In the transition from low to high energy, where mean field effects are still important, and the system can make large excursions from the ground state, there is the possibility of exploring the equation of state at points in the T-ρ plane far away from T=0 and $\rho=\rho_o$. The nature of multifragmentation reactions may yield information about the equation of state.

To begin the discussion of multifragmentation, consider the temporal evolution of a colliding nuclear pair at low to intermediate energy. At large distance the dynamics of the nuclei are set by the initial bombarding energy and the Coulomb interaction. As they approach each other, the nuclei slow as they climb over the Coulomb barrier. Once over the Coulomb barrier they are drawn into each other by the attractive part of the nuclear potential. As the nuclei collide they begin to lose their individual identity through nucleon-nucleon collisions. The initial bombarding energy is converted in part to compressional and thermal energy. By the time of maximum overlap of the nuclei, it is reasonable to describe the system in terms of a compressed and highly excited compound nucleus, which then expands and breaks apart.

A number of scenarios have been proposed to explain the nature of the break-up. One suggestion, often called spinodal decomposition, is that the break-up is caused by the compound system expanding into the mechanical instability region of the liquid-vapour phase diagram of nuclear matter [BS83,LS84]. Another model is based on site-bond percolation where, as the system expands, bonds are broken causing the percolated cluster to break

into fragments [BPD86,DBN87]. Fragmentation is also modeled in terms of evaporation from hot quasi-equilibrium compound nuclei [Bon85]. A large number of variants of this idea has been proposed. For a review of these thermal models see Das Gupta and Mekjian [DM81]. Still another model depicts fragmentation in terms of a cold shattering of the nuclei, much like the splattering of a mercury droplet upon impact [AHI84]. We now briefly review these approaches.

The spinodal decomposition model assumes that the break-up process is controlled by the nuclear equation of state [BS83,LS84]. By examining the distribution of fragments one may learn about the equation of state and in particular the liquid-gas coexistence region of nuclear matter (nuclear matter denotes an infinite neutral system of nucleons in thermal equilibrium). The connection between reaction systems and nuclear matter, however, is complicated. One needs to consider Coulomb effects, finite size effects and relaxation times in order to make a such a connection.

A number of approximate models [BG86,GKM84,LS84] of infinite neutral nuclear matter have been solved to find the equation of state, from which the nuclear phase diagram can be calculated. Fig. 1.1 is representative of the equation of state that these models predict [BG86]. The conventional Maxwell construction can be used to extract the phase diagram of nuclear matter from the equation of state (See Fig. 1.2). A number of features of the phase diagram are worth noting. First of these to notice is the phase boundary (LGC) itself which represents the boundary of thermodynamic stability of the homogeneous phase. Inside the boundary the mixed phase of gas and liquid is thermodynamically favoured over the homogeneous phase.

Second, notice the isothermal spinodal (ITS) and isentropic spinodal (IES) curves which represent the solution to the equations $(\partial P/\partial \rho)_T=0$ and $(\partial P/\partial \rho)_S=0$ respectively (P, ρ, T and S denote pressure, density, temperature and entropy respectively). These curves delimit the region of mechanical stability of the homogeneous phase. A homogeneous system is mechanically unstable to the formation of clusters at fixed temperatures inside the ITS curve and at fixed entropy inside the IES curve.

In terms of the liquid-vapour phase diagram the fragmentation process is explained as follows. In the compressional phase of the reaction the system quickly thermalizes. It then under goes an isentropic expansion, but remains in thermal equilibrium. During this process both temperature and density drop allowing the system to be driven into the isentropic instability region. Once in this region, clusters begin to condense out of the vapour and are driven away from each other by both their initial radial velocity and Coulomb repulsion.

The percolation model is typically used in conjunction with a hydrodynamic calculation [BPD86,DBN87]. During the first part of the expansion, fluctuations are small and hydrodynamics is appropriate to describe the expansion of the homogeneous droplet. Beyond the onset of cluster formation, the assumptions of hydrodynamics are invalid and one resorts to the percolation model to describe the fragmentation.

To specify a site-bond percolation model we need to define p, the ratio of occupied sites to total sites, and q, the ratio of bonds left to the initial total number of bonds at T=0. An infinite system will under go a

transition from a state with only one cluster (percolation) to a state with many clusters (fragmentation), as a function of p and q. Fig. 1.3 show the percolation phase diagram [Cer88]. In applying this model to the expanding nuclear system, we imagine that p and q are time-dependent quantities. As the system expands, the number of particles, of course, remains fixed. However the volume (number of sites) that those particles can occupy increases. As well, the thermal energy in the system will change, which will alter the number of effective bonds, and hence q, in the system. Fragmentation will occur if the trajectory in p-q space crosses the percolation transition boundary.

The cold shattering model is based on nonequilibrium physics [AHI84]. The fragmentation process is similar to the shattering of glass, though one should not take the analogy too far. Fragmentation is modeled as a two step process. In the first step the participant nucleons form a fireball, and the spectator matter remains cold. In the second step the fireball decays. Some participants escape without further collision, mostly in the forward direction. Other participants enter the spectator matter and deposit energy and momentum. Locally, bonds are weakened and the spectator matter is destabilized globally and cracks. Then, the momentum deposited and the Coulomb force push the pieces apart.

All the above scenarios represent very different physical processes, but all share the common goal of trying to understand fragmentation in terms of a small set of collective variables. The motivation for the development of these collective variables models is two-fold: first, to have a simple picture of the physical processes to aid one's intuitive understanding of

fragmentation and second to have a model which is computationally tractable.

The correct answer to what is the essence of fragmentation may be found in one of the above models, none of the above or perhaps in a combination of several of the above. From an experimental point of view it may be very difficult to find a discriminator to choose from these or other models as the correct way to view multifragmentation. A computer simulation provides the opportunity to probe the nuclear system in detail not accessible by experiment and may be a good method to ascertain the essence of the fragmentation process.

Numerical simulations have been used for many years in the study of physical many-body systems. Most studies are concerned with properties of macroscopic systems, whose large particle numbers prevent the direct simulation of the actual system. Typically one simulates a small finite system and extrapolates to get the infinite system properties. On the other hand, nuclear systems comprise at most several hundred particles, thereby providing a novel opportunity to simulate the system of interest directly. Although the simulation of full quantum mechanical models of nuclear systems is still beyond present-day computer technology, the rapid advancement in computational hardware has made it possible to study a class of semi-classical nuclear models.

In this thesis we develop an A-body model for the description of the nuclear system. The model is approximate but we feel that much of the essential physics has been incorporated. Furthermore the model is

tractable by simulation techniques (both Molecular Dynamics (MD) and Monte Carlo (MC)). Using these techniques we are able to examine in microscopic detail the temporal evolution of our model via MD and explore its thermodynamic properties via MC. We are also able to investigate relaxation times, finite size effects, and both equilibrium and nonequilibrium processes that should be present in real nuclear systems.

The remainder of the thesis is organized as follows. Chapter II reviews the various numerical techniques that have been applied to heavy ion collisions. In Chapter III the assumptions that our model is based upon are introduced. These assumptions lead to a model where the antisymmetrization effects are mocked-up by a Pauli potential acting between classical objects that we call quasiparticles. As a test of the model we consider the its predictictions for a number of free fermion systems. In the first part of Chapter IV the real space potential between the quasiparticles due to the nuclear interaction is introduced. The remainder of the chapter presents the model's predictions for the ground state properties of finite nuclear systems and makes comparison with experiment. The dynamics of the model are examined in Chapter V. In the first part of the chapter a collision term is introduced to model the hard core of the nuclear interaction. In the last part of the chapter the time scales associated with early reaction processes are investigated. In Chapter VII the model's predictions for the kinetic and chemical temperatures are compared with experimental results. Chapter VII also considers the thermodynamic properties and finite size effects of the model. As well, the effects of entropy and temperature on the fragmentation of finite nuclei are explored. Finally, in Chapter VIII we present our

conclusions regarding the interplay of fragmentation in nuclear reactions and the nuclear equation of state.

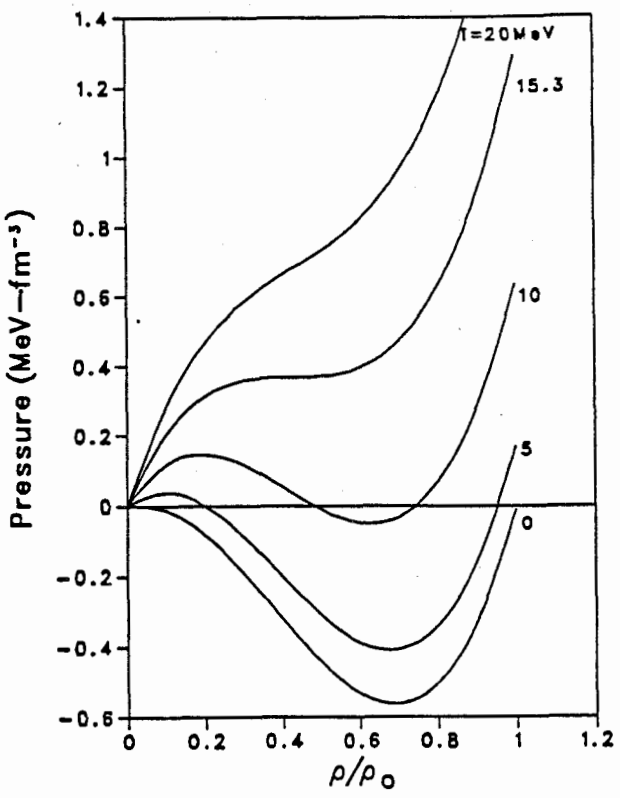

Fig. 1.1. Equation of state predicted for neutral nuclear matter using a zero range Skyrme-type interaction. [BG86]

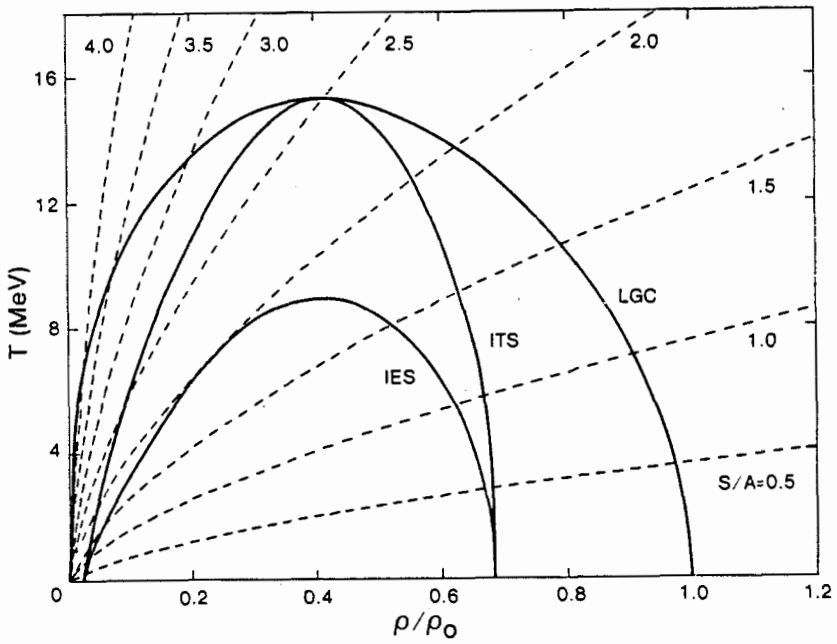

Fig. 1.2. Phase diagram constructed from the isotherms of Fig. 1.1. Isentropes of given S/A are shown by the dashed curves. The liquid-gas coexistence curve is labeled LGC; the isothermal and isentropic spinodals are labeled as ITS and IES respectively. [BG86]

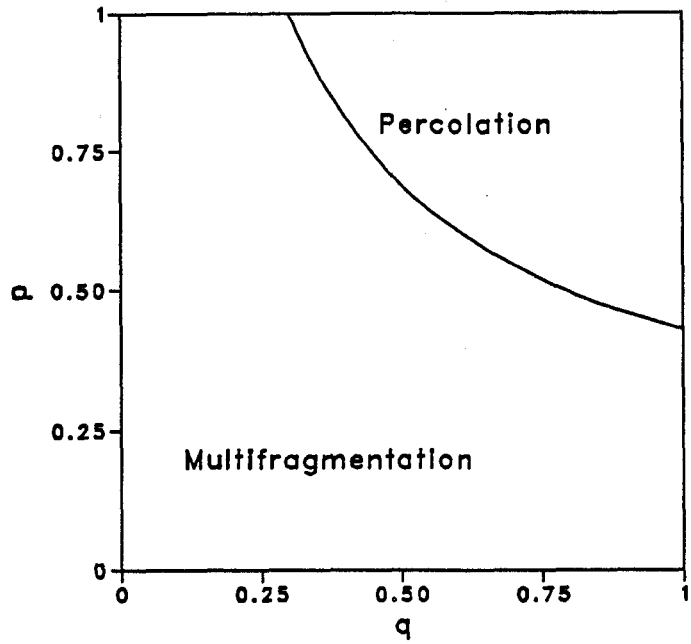

Fig. 1.3. A schematic percolation phase diagram for a site-bond percolation model [Cer88]. The variable, p, is the probability that a site is occupied and q is the probability that a bond is not broken.

II Numerical Models

The study of nuclear reactions within an exact theory, would require at least the solution of a time-dependent many-body relativistic quantal set of equations with particle production and absorption. Such a theory at present (as well as the foreseeable future) is not only intractable analytically but numerically as well. In light of these limitations, to make progress one must introduce approximations. Some possible simplifications are:

1) relativistic ⟶ nonrelativistic

2) quantum mechanics ⟶ classical mechanics

3) time dependent ⟶ equilibrium

4) many-body properties ⟶ one-body properties

5) particle production ⟶ no particle production

6) many-body interaction ⟶ isolated two-body collisions

7) microscopic description ⟶ macroscopic description

Combinations of these simplifications have been used to develop numerous models whose validity is necessarily restricted by the approximations. However, by limiting the detail of the information sought and the range of systems to which the models are applied, the effects of the approximations can be minimized.

The various numerical models can be separated into two broad classes based on the nature of the physical quantities to be calculated. The earlier and computationally least demanding techniques are only concerned with extracting one-body information from the calculations. The Internuclear cascade model, hydrodynamics, time-dependent Hartree Fock (TDHF), Vlasov

equation and Vlasov-Uehling-Uhlenbeck equations (VUU) are included in this class of calculations. Recently much interest has been focused on the many-body nature of nuclear reactions. To understand the fluctuations and correlations found in nuclear reactions a new set of techniques have been developed. A many-body quantum approach is still beyond reach; however, a number of classical and semiclassical methods have been developed and do provide insight into the many-body nature of nuclear reactions.

Internuclear Cascade Model

In the limit that the mean free path λ of the nucleons involved in a nuclear reaction is large compared to the range of the nuclear interaction, simplification 6) is justified. In this approximation many details of the nuclear interaction are neglected. In its simplest form this method, known as the internuclear cascade model, [Seb47,Gol48] consists of a sequence of two-body collisions within a set of nucleons moving in a force-free space. The nature of the two-body collisions is chosen to reproduce the correct experimental free NN cross sections. The model can be extended to include both quantum and relativistic effects in an approximate way. The fermionic nature of the nucleons can be included by checking if a collision is prohibited by the Pauli exclusion principle. As well, modifications allowing pion production and absorption can be made. The effects of the nuclear potential have been included in a one-body sense in a number of variants of the model. A nuclear mean field is defined, and the kinetic energy before and after a collision is modified, to reflect the change of the particle's potential energy between its current collision position and its last collision position. Despite the simplicity of the model, useful

information about some aspects of nuclear reactions can be found. In particular the emission spectra of high energy nucleons produced in large bombarding energy nuclear reactions compare favourably with experiment. [YF79,YF81]

The obvious failing of the model is that it has no binding of the nucleons. One notable problem with the lack of binding is the inability to construct ground state nuclei to be used in the reaction. An *ad hoc* procedure that is used in a number of calculations, is to assign momenta to individual nucleons based on a degenerate Fermi gas distribution and then spatially confine them with an external potential. If the final products of interest in the simulation are not sensitive to binding energy and the purpose of the potential is simply to ensure the correct initial geometry, then the arbitrariness of this procedure is of little concern.

Hydrodynamics

In hydrodynamics, [BL55,BL56,Nix79] the microscopic degrees of freedom are integrated out to leave a model expressed in terms of the macroscopic degrees of freedom of particle density $\rho(\mathbf{r})$, energy density $e(\mathbf{r})$, and momentum density $\mathbf{M}(\mathbf{r})$. The criteria to ensure that the hydrodynamic description is valid are:

1) many degrees of freedom in the system
2) short mean free path
3) short mean stopping length
4) short equilibration time compared to reaction time
5) short de Broglie wavelength

The extent to which these criteria are satisfied in a nuclear reaction is dependent not only on the type of reaction but on the stage of the reaction as well. For zero impact parameter heavy ion collisions with bombarding energy per nucleon in the several hundred MeV range, it is reasonable to apply a hydrodynamic approach during the compression and initial expansion stage of the reaction. However, as the reaction continues, the system breaks apart so that the collision rates drop, rendering the hydrodynamic approach invalid past this stage.

The relativistic form of the hydrodynamic equations of a single ideal fluid can be written;

$$\begin{aligned}
&\frac{\partial N}{\partial t} + \nabla \cdot (\mathbf{v}N) = 0 \\
&\frac{\partial M^{\alpha}}{\partial t} + \nabla \cdot (\mathbf{v}M^{\alpha}) = -(\nabla P)^{\alpha} \qquad \alpha = x,y,z \qquad (2.1) \\
&\frac{\partial E}{\partial t} + \nabla \cdot (\mathbf{v}E) = -\nabla \cdot (\mathbf{v}P)
\end{aligned}$$

where N, **M**, and E are the nucleon number density, momentum density and energy density respectively as measured in the computational frame of reference. The velocity of matter relative to the computational frame is denoted by **v**, and P is the pressure in the rest frame. The computational frame quantities N, **M**, and E can be related to the rest frame number density (n), pressure (P) and energy density (ε) by the relations,

$$N = \gamma n$$

$$\mathbf{M} = \gamma^2(\varepsilon + P)\mathbf{v}$$

$$E = \gamma^2(\varepsilon + P) - P$$

where $\gamma=(1-v^2)^{-1/2}$.

Both finite difference and particle-in-cell methods have been used to solve the hydrodynamic equations of motion. To apply these equations to nucleus-nucleus collisions one must deal with the fact that the system will go out of equilibrium as it expands and breaks-up. A number of hybrid models have been developed that use hydrodynamics in the early stages of the reaction and apply statistical models after break-up. For a general review of hydrodynamic calculations see the review by Clare and Strottman [CS86].

Mean field theory -- TDHF and Vlasov equations

A theory that expresses the time dependence of the one-body density matrix $\hat{\rho}$ can be developed under the approximation that nucleon-nucleon correlations are neglected . This approach leads to a set of equations referred to as the time-dependent Hartree-Fock equation. By the nature of the approximation this approach is a mean-field theory. In the classical limit, the TDHF equation is called the Vlasov equation and has the form of a collisionless Boltzmann equation.

The development of this mean-field theory begins by expressing the quantum Hamiltonian in the second quantized notation:

$$\hat{H} = \sum_{i,j} \langle i|T|j\rangle a_i^\dagger a_j + \frac{1}{2} \sum_{i,j,k,l} \langle ij|V|kl\rangle a_i^\dagger a_j^\dagger a_l a_k . \qquad (2.2)$$

The one-body density matrix, ρ, is defined by its matrix elements

$$\rho_{ij} = \langle\psi|a_i^\dagger a_j|\psi\rangle . \qquad (2.3)$$

The time dependence of ρ_{ij} is given by the standard equation

$$\dot{\rho}_{ij} = \frac{1}{i} \langle\psi| [a_i^\dagger a_j, \hat{H}] |\psi\rangle \quad . \tag{2.4}$$

Under the approximation that correlations can be neglected, the four-particle operator can be replaced by the product of single-particle densities,

$$\begin{aligned} \langle\psi|a_i^\dagger a_j^\dagger a_k a_l|\psi\rangle &\approx \langle\psi|a_i^\dagger a_l|\psi\rangle \langle\psi|a_j^\dagger a_k|\psi\rangle - \langle\psi|a_i^\dagger a_k|\psi\rangle \langle\psi|a_j^\dagger a_l|\psi\rangle \\ &= \rho_{il}\rho_{jk} - \rho_{ik}\rho_{jl} \end{aligned} \tag{2.5}$$

This allows the equation of motion of the density matrix to be expressed in terms of a single particle Hamiltonian, $H_{MF} = T + U$,

$$\dot{\rho}_{ij} = -i \sum_k \left\{ \rho_{ik} \langle j| H_{MF} |k\rangle - \langle k| H_{MF} |j\rangle \rho_{kj} \right\} \quad . \tag{2.6}$$

Then, the single-particle potential U is implicitly dependent on ρ and is given by the expression,

$$\langle j|U|i\rangle = \sum_{km} \left((\langle jk|V|im\rangle - \langle jk|V|mi\rangle) \rho_{km} \right) \quad . \tag{2.7}$$

Equations 2.6 and 2.7 constitute the TDHF approximation.

A useful representation of the above equation can be made by expressing the density matrix in terms of a Wigner function. The Wigner function can be expressed as a Fourier transformation of either the coordinate space, or momentum space representation of the density matrix,

$$\begin{aligned} f(\mathbf{r},\mathbf{p}) &= \int d\mathbf{s}\ exp(i\mathbf{p}\cdot\mathbf{s})\ \langle \mathbf{r}+\mathbf{s}/2|\rho|\mathbf{r}-\mathbf{s}/2\rangle \\ f(\mathbf{r},\mathbf{p}) &= \int (d\mathbf{q}/(2\pi)^3)\ exp(-i\mathbf{q}\cdot\mathbf{r})\ \langle \mathbf{p}+\mathbf{q}/2|\rho|\mathbf{p}-\mathbf{q}/2\rangle \quad . \end{aligned} \tag{2.8}$$

If the exchange term is ignored, the Wigner representation of the TDHF equation is given by:

$$\frac{\partial}{\partial t} f + \frac{1}{m} \mathbf{p}\cdot\nabla_r f - \sum_{n=0}^{\infty} \left(\frac{\hbar}{2i}\right)^{2n} \nabla_r^{(2n+1)} U \cdot \nabla_p^{(2n+1)} f = 0 \quad . \tag{2.9}$$

Taking the classical limit $\hbar \longrightarrow 0$, the TDHF equation reduces to

$$\frac{\partial}{\partial t} f + \frac{1}{m} \mathbf{p}\cdot\nabla_r f - \nabla_r U \cdot \nabla_p f = 0 \quad . \tag{2.10}$$

This collisionless Boltzmann equation with the self-consistent field U, is known as the Vlasov equation.

In principle one could calculate the mean field, U, from some assumed fundamental interaction. Various attempts (see Sec. 40-41 of [FW71]) at this approach have not yielded completely satisfactory results. For example, the predicted binding energies and density of nuclear matter are not in agreement with empirical saturation properties. In light of these difficulties it is customary to simply assume some form for the effective Hamiltonian that satisfies the known empirical results. Common choices for the effective density-dependent mean field are;

$$U(\rho) = -124\ (\rho/\rho_o) + 70.5\ (\rho/\rho_o)^2 \ \text{MeV} \tag{2.11a}$$

$$U(\rho) = -356\ (\rho/\rho_o) + 303\ (\rho/\rho_o)^{7/6} \ \text{MeV} \tag{2.11b}$$

where $\rho_o = 0.17\ fm^{-3}$.

Both of the above forms for U satisfy the constraint that the ground state of nuclear matter has an energy minimum at $\rho = 0.17\ fm^{-3}$ of E=-15 MeV per nucleon. Equations 2.11a and 2.11b are referred to as stiff and soft because of their respective coefficients of compressibility of K=380 MeV and K=200 MeV.

The TDHF and Vlasov equations' validity are restricted to the low excitation energy domain. At low energies the nucleons tend only to sample the slowly varying tail of the nuclear interaction and this makes the mean-field approximation reasonable.

Beyond Mean Field -- The Vlasov-Uehling-Uhlenbeck Equation

For higher energies, the mean-field approximation begins to break down. This has been shown graphically in a number of simulations of heavy ion collisions in the 100 MeV per nucleon bombarding energy range. For both the TDHF and Vlasov equation the incident nuclei pass almost transparently through each other with very little scattering of their constituent nucleons [SCM81,AS85]. This failing of the mean-field theory is not surprising. At higher energies, the nucleon-nucleon correlations neglected in the mean-field approximation will become important as it is energetically possible for the hard core of the nucleon-nucleon potential to be sampled. A natural refinement to the mean field theory would be to allow collisions between nearby pairs of particles.

To introduce the effects of the hard core potential, V_c, into the mean-field approximation, a perturbation theory can be used. The full Hamiltonian of the system can be split into the mean-field Hamiltonian, H_{MF}, plus a small correction term, V_c. Within second order perturbation theory, the off-diagonal elements of the density matrix evolve according to the mean field and the diagonal elements $n_i=\rho_{ii}$ satisfy the following equation of motion:

$$dn_i/dt=2\pi \sum_{jlm} <ij|V_c|lm>^2 \delta(\varepsilon_i+\varepsilon_j-\varepsilon_l-\varepsilon_m)(n_l n_m (1-n_i)(1-n_j)-n_i n_j (1-n_l)(1-n_m)) \quad . \tag{2.12}$$

A classical version of this expression can be written by using the Wigner representation and introducing the Born approximation for the particle-particle scattering cross section σ. This yields the total time derivative for the Wigner density function $f(\mathbf{r},\mathbf{p})$.

$$Df(\mathbf{r},\mathbf{p})/Dt= -\int \frac{dp_2 dp_3 dp_4}{(2\pi)^6} v_{pp_2} \sigma(pp_2 \rightarrow p_3 p_4)(ff_2(1-f_3)(1-f_4) - f_3 f_4 (1-f)(1-f_2)) \times \delta(\mathbf{p}+\mathbf{p}_2-\mathbf{p}_3-\mathbf{p}_4) \quad . \tag{2.14}$$

The inclusion of collisions within the mean field theory modifies Eq. 2.10 by replacing the RHS with Df/Dt. This modification to the Vlasov equation was first suggested by Nordheim in 1928 [Nor28] and Uehling and Uhlenbeck in 1933 [UU33].

Though computationally taxing, the solution of the VUU equation is within the grasp of present day computer hardware. One popular technique is based on the particle-in-cell method of numerical hydrodynamics [HAN76]. The method replaces the phase space density function $f(\mathbf{r},\mathbf{p})$, with a set of test particles each with its own momentum and position. The number of test particles is normally between 10-100 per nucleon. To evaluate the density-dependent forces, the system is divided into a mesh of cells. The density of each cell is evaluated by counting the number of test particles in each cell and dividing this number by the volume of the cell times the number of test particles per nucleon N_n. Then the force is found by taking the numerical gradient of the density dependent mean field. This procedure gives the evolution of the system between collisions. Each test particle

is only allowed to scatter off $1/N_n$ of the other test particles. If the trajectories of two test particles allows a pair to collide, a test is made to see if the Pauli exclusion principle will prohibit the scattering. This is done stochastically by allowing the scattering with probability $(1-f(r_1,p_1'))(1-f(r_2,p_2'))$, where r_1 and r_2 are the positions of the scattering pair at the time of the collision, and p_1' and p_2' are the new momenta of the particles if the scattering is allowed.

Many Body Physics -- The Classical Approach

The study of correlations and fluctuations in nuclear reactions requires more than just the one-body distribution that the previously discussed methods predict. The calculation of two-body and higher order correlations within a quantum mechanical framework is most difficult. Most of the studies of fluctuations within nuclear systems have involved the study of an A-body classical equation of motion within a molecular dynamics simulation.

Classical Dynamics

In most classical systems it is sufficient to specify a spatially-dependent potential to define the equations of motion. A number of different phenomenological potentials have been used in various simulations of nuclear systems. Infinite hard core potentials were used in nuclear simulations by both Amsden et al. [AGH77] and Bondorf et al. [Bon76,BFG76,BSG76]. Lennard-Jones 6-12 potentials were used by Pandharipande et al. [VJP85,LP86,SP87] in the study of the fragmentation of

argon droplets and nuclear droplet analogs. Various potentials consisting of sums of attractive and repulsive Yukawa terms have been used to model the nuclear interaction by Bodmer and Panos [BP77,BPM80] and by Wilets et al [WHK77,WYC78,CWY79]. In some of the works of Bodmer and Panos the potential included momentum dependence to take in account relativistic retardation effects.

Wilets et al. included momentum dependent interactions in their work as well, but for reasons very different than Bodmer and Panos. For most classical systems the kinetic energy of the ground state vanishes. This is certainly true of all classical systems with the momentum only entering as a p_i^2 term in the Hamiltonian. For a quantum system, particularly one containing fermions, the kinetic energy does not vanish in the ground state. For nuclear systems the Pauli exclusion principle causes the kinetic energy to make nontrivial contributions to the total energy. To simulate the effect of Pauli exclusion, Wilets et al. [WHK77] introduced a momentum-dependent interaction into the nuclear potential of the form,

$$V_p(\mathbf{r}_{ij},\mathbf{p}_{ij}) \sim exp\{-\alpha(|\mathbf{r}_{ij}||\mathbf{p}_{ij}| - 1)\} / |\mathbf{r}_{ij}|^2$$

This approach represented a significant advancement in the simulation of nuclear systems. It was the first time within a classical framework that both ground state and dynamic properties could be simulated within the same model.

With the success of the VUU theory in predicting one-body distributions, it is tempting to consider if fluctuations can be calculated in the theory. Within the original Vlasov approach it is not possible to extract

fluctuation information since all the correlations are neglected. However, with the VUU theory, the collision term is introduced to include the effect of the correlations and in turn information about the fluctuations may be possible to extract.

Motivated by this possibility, Gale and Das Gupta developed a hybrid model to study the fluctuations in nuclear reactions [GD85]. During the approach and interpenetration phase of the reaction, a cascade model which neglects binding is used to propagate the nucleons. At the end of this phase the collisions are turned off and the nuclear binding is turned on. At the start of the second stage, each nucleon is replaced by a collection of test particles spread out in phase space in a gaussian manner. This collection of test particles is then allowed to evolve via the Vlasov equation for the remainder of the simulation. This procedure has the dramatic effect of enhancing the fluctuations introduced in the first stage of this reaction and yields clusters of various masses. Thereby, in a qualitative way it mimick the multifragmentation processes seen in intermediate energy heavy ion collisions.

Another approach [BBW87,BBG87,BG88,AS87] is to limit the number of test particles in the solution of the VUU equation to one per nucleon and then examine the fluctuations. The potentials used in this calculation are the density dependent mean-field potentials. In order to calculate the force on the individual nucleons, a procedure for evaluating the density as a function of position needs to be developed. There is a certain amount of arbitrariness in defining the density of a collection of point particles. One procedure is to choose some fixed radius sphere centered on the point

where the density is to be evaluated and count the number of particles within this sphere. The density is simply this number divided by the volume of the sphere. Of course, this procedure does not allow fluctuations smaller than the radius of the sphere to be studied and has the troublesome feature that the density defined in this way is not a continuous function of position. Another alternative is to assign a smoothing function to each nucleon, (i.e. think of each nucleon as being smeared out in space) so that the density is just the sum of the individual smoothing functions. This procedure still has a cutoff to the length scale of fluctuations that can be calculated, due to the range of the smoothing function, but unlike the previous approach, it is a continuous function of position for a continuous smoothing function. A common choice for a smoothing function is a gaussian distribution. Such a procedure is used in [BBW87]

In the following chapters we develop a model that borrows many of the successful ideas of the previously discussed models. In particular, a momentum-dependent potential is introduced to ensure a well-defined ground state with nonvanishing kinetic energy. A density dependent potential, much like the mean field of TDHF, is used for the nuclear interaction because of its success in modeling the ground state properties. A collision term is introduced, to remove the transparency effects associated with the mean field.

Although many of these ideas are ad hoc, we hope to start with a quantum mechanical picture and follow along a reasonable, though not exact, path of simplifications to develop a microscopic A-body semi-classical model in

which the ground state and dynamical properties can be explored.

III The Quasiparticle Model

III.1 Introduction

The main motivation for developing this model is the desire to explore the physical processes responsible for multifragmentation. Although a model that could be applied to all of nuclear physics would be a grand goal, it is felt that such a goal would be most illusive. Instead a simpler objective is pursued. The model is only required to be applicable in the range of energies, densities and times associated with the multifragmentation processes.

The energy scale for multifragmentation is set by the nuclear binding energy. Typical binding energies are in the 8 MeV/nucleon range. For symmetric heavy ion collisions (i.e. ^{40}Ca + ^{40}Ca), where the bombarding energy is much lower than 6 MeV/nucleon, the projectile cannot overcome the Coulomb barrier, so there is no fragmentation. On the other hand, when the bombarding energy of the Ca projectile is greater than 200 MeV per nucleon, the composite system of projectile and target almost completely disintegrates into single nucleon products during a central collision. For the high energy collision the binding energy is of little importance, and the particle distribution is governed by the nucleon-nucleon cross section. The area of interest in multifragmentation is the intermediate bombarding energy range of 10-100 MeV/nucleon (lab frame) where the many-body effects associated with nuclear binding are still important.

The setting of an energy scale also sets the maximum density of interest. Consider the density (ρ) expansion of the ground state energy per nucleon (E), about the equilibrium density (ρ_o);

$$E(\rho) = E_o + K\,(\rho/\rho_o - 1)^2/18 + \text{higher order} \qquad (3.1)$$

where K is the compressibility coefficient and E_o is the ground state energy per nucleon at $\rho = \rho_o$. Experimental data on giant monopole resonances suggest the compressibility coefficient is of the order of 200 MeV [Bla80]. Using this equation we can set an upper bound on the density by using the maximum energy that can go into compression. In a symmetric heavy ion collision with a projectile bombarding energy of 100 MeV per nucleon, the maximum energy available for compression will be 25 MeV per nucleon (i.e. bombarding energy of target and projectile as measured in the center of mass). From Eq. 3.1 this would correspond to a density 2.5 times normal nuclear matter density.

The minimum density is set by the range of the nuclear interaction. At 1/4 normal nuclear matter density the volume per nucleon would be 25.0 fm^3 corresponding to a nearest neighbour distance of 2.9 fm. This distance is greater than the range of the nuclear interaction (1.5-2.0 fm) and hence densities less than 1/4 ρ_o will be of little interest in the study of multifragmentation.

A number of different time scales exist within a nuclear reaction. Our model focuses on the processes associated with the far-from-equilibrium state of the initial impact through the relaxation phase to the near-equilibrium state of the reaction. These hadronic processes are short

lived with most of the relaxation being completed several hundred fm/c (10^{-21}sec.) after the initial impact. The reaction will continue to evolve after this time but the study of long-time-frame evaporative processes is best handled by a statistical model in which the fragments decay by a stochastic method based on excitation energy.

For the energy, density and time ranges of interest, relativistic effects, pion production and photon decay can safely be neglected. The relativistic factor γ is less than 1.1 for 100 MeV nucleons, so relativistic effects will be small and a nonrelativistic picture suffices. The onset of pion production becomes important if the bombarding energy exceeds 300 MeV, which is well above the maximum energy thought to be relevant for multifragmentation. Photon decays occur 10^{-17} seconds or longer [Eng66] after the collision, which is long compared to the hadronic decay times. Though not thought to be important in understanding multifragmentation processes, these decays affect the experimentally measured distribution function.

Having discussed what is not included in the model the question remains of what is included. As discussed above, the model neglects the production of pions, photons and exotic particles, enabling the description of the system completely in terms of nucleon degrees of freedom. In principle the nucleons are quantum mechanical particles with two fermionic indices. One fermionic index describes the spin of the particle and the other describes the isospin. The effects of quantum mechanics are important in nuclear systems but a full quantum mechanical treatment of all but the most simple systems is beyond today's analytic and computational methods. Hence this

model incorporates only some aspects of quantum mechanics. In particular the effects of the Heisenberg Uncertainty Principle and the Pauli Principle, will be introduced in an approximate way.

Often, basic symmetries of a system can account for much of the physics that is observed. In developing a model to describe a physical system it is wise to insure that the model possesses as many of the symmetries, hence conservation laws, of the real system as possible. The model developed in this thesis incorporates the standard conservation laws of energy, linear momentum, and angular momentum.

A model is sought that also can describe both the dynamics and ground state properties in a consistent framework. Many of the previous approaches that handled the dynamics only treated the ground states in an ad hoc way. A model based on a Hamiltonian formulation would be able to treat both the dynamics and ground states.

A last requirement of the model is that it be tractable from a computational point of view. This constraint limits the scope of the model to one whose energy can be found in no more than $O(A^2)$ operations, where A is the number of nucleons in the system.

III.2 Assumptions

The development of the model begins with two assumptions. These assumptions are made so that some quantum mechanical effects are included in the model, yet the model is kept computationally tractable. The first

of these assumptions includes the Heisenberg Principle, while the second approximates the effect of the Pauli Principle.

The Heisenberg Principle is incorporated into the model by simply associating a wave function with each particle in the system. To keep the calculation simple it is assumed that each nucleon can be represented in terms of a fixed-width gaussian wave packet of the form

$$\phi_k(\mathbf{r},t)=\left[\frac{\alpha^2}{\pi}\right]^{3/4} exp\left[-\frac{\alpha^2}{2}(\mathbf{r}-\mathbf{R}_k(t))^2\right] exp\left[\frac{i}{\hbar}\mathbf{P}_k(t)\cdot\mathbf{r}\right]\chi_k^I\chi_k^S \qquad (3.2)$$

where $\mathbf{R}_k(t)$ and $\mathbf{P}_k(t)$ are respectively, the expectations of the position and momentum of the k^{th} particle at time t. Here, χ^I and χ^S are the isospin and spin wave functions.

The simplest antisymmetrization is just the Slater determinant of the A single particle ϕ_k's whose wave function has A! terms. Manipulating such a wave function with out approximation is an exceedingly arduous task for large A. Instead we assume the completely antisymmetrized wave function of the ϕ_k's can be replaced by a product state of the form,

$$\Psi(\mathbf{r}_1, \ldots, \mathbf{r}_A) = \prod_{k=1}^{A} \phi_k(\mathbf{r}_k, t) \qquad (3.3)$$

plus some effective potential $\hat{V}_{eff}$, to mock up the effect of the Pauli Principle.

Given these two assumptions it is sufficient to specify the set

$\{(R_k,P_k)|k=1,..,A\}$ to describe the A-particle system completely. Furthermore, as will be shown in Chapter V, these assumptions imply that (R_k,P_k) obey classical equations of motion, based on an energy function

$$H(R_1P_1,\ldots,R_AP_A) = \langle\Psi|\hat{H} + \hat{V}_{eff}|\Psi\rangle \qquad (3.4)$$

where $\hat{H}$ is the Hamiltonian of the quantum mechanical system and $\hat{V}_{eff}$ is the effective interaction discussed above. Since the dynamics of (R_k,P_k) are particle-like, it is natural to associate a particle with each of the phase space coordinates (R_k,P_k). To distinguish these particles from the underlying real quantum mechanical particles, they shall be referred to as quasiparticles (QP).

III.3 The Pauli Potential

An ansatz has been made that the antisymmetrized state could be replaced by a product state plus some effective potential, $\hat{V}_{eff}$. From Eq. 3.4 one sees that this effective potential contributes to the quasiparticle energy. This contribution, because of its role in mocking up the Pauli principle, will be called the Pauli potential V_P. It is worth stressing that V_P is the expectation of the quantum operator $\hat{V}_{eff}$, and represents an energy interaction term in the classical quasiparticle Hamiltonian.

To gain insight into the form of the Pauli potential, consider a two particle system with single particle wave functions ϕ_a and ϕ_b with associated quasiparticle (QP) coordinates (R_a,P_a) and (R_b,P_b) respectively. The antisymmetric two particle wave function is

$$\Psi_{ab}(r_1,r_2) = \frac{\Phi_a(r_1)\,\Phi_b(r_2) - \Phi_a(r_2)\,\Phi_b(r_1)}{\left[\int\int |\Phi_a(r_1)\Phi_b(r_2) - \Phi_a(r_2)\Phi_b(r_1)|^2\, dr_1 dr_2\right]^{1/2}} \qquad (3.5)$$

The expectation of the kinetic energy operator with respect to this wave function is given by

$$\langle \hat{K} \rangle_{ab} = \frac{1}{2m}\left[P_a^{\,2} + P_b^{\,2} + 3\alpha^2\hbar^2 + \alpha^2\hbar^2 \frac{X_{ab}}{e^{(X_{ab})} - 1}\right]$$

where (3.6)

$$X_{ab} = \frac{1}{2}\left[\, \alpha^2(R_a - R_b)^2 + (P_a - P_b)^2/(\alpha\,\hbar)^2 \,\right]$$

The first two terms in the kinetic energy look like the kinetic energy of a pair of classical particles, while the third term reflects the fact that the gaussian wave packets are spread out in momentum space. The last term is identified as the two-body potential between quasiparticles with phase space coordinates (R_a,P_a) and (R_b,P_b). This is the Pauli potential for a two particle system.

The Pauli potential has a number of desirable properties. First, it is a function of X_{ab}, which is a measure of the quasiparticle separation in phase space. Secondly, as the quasiparticle separation in phase space is made large (i.e. $X_{ab} \longrightarrow oo$) the potential vanishes. Finally, the potential is repulsive for all finite phase space separations.

Note that the potential does not diverge as $X_{ab} \longrightarrow 0$. At first thought this may seem unreasonable since the potential allows the two quasiparticles to share the same point in phase space. However this does not imply that the two quantum mechanical particles share the same region in their phase space. The real particles are randomly distributed in gaussian fashion about the quasiparticle positions in phase space. Even when the two quasiparticles share the same point in phase space, the probability that the two real particles share a region of phase space of volume $v = d^3x\, d^3p$ will be of $O(v^2)$. Therefore after integrating over all possible regions in phase space, the total probability of finding two real particles in the same volume will be of $O(v)$, which vanishes for small v.

If the above approach were to be applied to a three particle system, all of the above two-body terms would be found plus an additional three-body term. Similarly in a four particle system all of the terms of the three particle system would be present with the addition of a four-body term, and so on as larger and larger systems were considered. Proceeding in this fashion would quickly depart from the goal of keeping the cost of the computation to $O(A^2)$ operations. Instead we choose to include the effects of the higher-body terms approximately by rescaling the two-body Pauli potential. Motivated by the two particle calculation, the following ansatz is made for the Pauli potential;

$$V_p(X_{ab}) = V_s \frac{\alpha^2 \hbar^2}{2m} \frac{X_{ab}}{e^{(X_{ab})} - 1} \delta_{s_a s_b} \delta_{\chi_a \chi_b} \tag{3.7}$$

where s_i and χ_i denotes the spin and isospin repectively of particle i

(i=a,b) and V_s is the scale factor introduced to approximate the effects of the higher-body terms.

III.4 Ground State Properties of Non-Interacting Systems

The introduction of a momentum-dependent potential can have a dramatic effect on the ground state. In classical models with no momentum-dependent interaction, the ground state possesses the property $P_i=0$ for all particles. However the introduction of a momentum-dependent term in the Hamiltonian can break that symmetry. For example consider the QP Hamiltonian for a system of N noninteracting fermions in a periodic box of length ℓ.

$$H(R_1P_1, \ldots, R_NP_N) = \frac{1}{2m}\sum_{i=1}^{N} P_i^2 + V_s \frac{\alpha^2\hbar^2}{4m}\sum_{i\neq j} \frac{X_{ij}}{e^{(X_{ij})}-1}\delta_{s_i s_j}\delta_{\chi_i\chi_j} \quad (3.8)$$

The stability of the $P_i=0$ state can be examined by evaluating the energy curvature (with respect to P) matrix M at $P_i=0$. In Appendix A this matrix is calculated and for the case where the quasiparticles sit on a simple cubic lattice with lattice spacing, a, and the eigenvalues $\lambda(\mathbf{q})$ of M are found (note $\mathbf{q}$ is the eigenvector index). If $\lambda(\mathbf{q}) > 0$ for all $\mathbf{q}$ then $P_i=0$ is a minimum and is stable. However if there exists a $\mathbf{q}$ such that $\lambda(\mathbf{q}) < 0$ then $P_i=0$ is a saddle point and is unstable. This instability breaks the $P_i=0$ symmetry and the ground state occurs at nonzero momentum. In Fig. 3.1 for the case $V_s=1$ the value of λ for $q^x=q^y=q^z=q$ is plotted as a function of the product qa. Notice that by adjusting the lattice spacing, a, the stability of $P_i=0$ changes. For large aα all λ are greater than zero and

state P_i=0 is stable. This is just what one expects, since large $a\alpha$ implies a small Pauli term and the ground state should just be the P_i=0 state. However for small values of $a\alpha$ the value of λ changes sign as a function of q, hence P_i=0 cannot be the ground state.

Having shown that the QP ground state can have nonzero momentum it is of interest to see if the ground state energy of Eq. 3.8 can approximate a free Fermi gas. In making this comparison there are two parameters, α and V_s, that can be adjusted to fit the quasiparticle model to the exact results. By minimizing the QP Hamiltonian with respect to the quasiparticle phase space coordinates (R_k,P_k) the ground state energy of the quasiparticle system as a function of the parameters α and V_s is found. Then fitting this functional form to the exact T=0 free Fermi results over the density range of interest, the values of α = 0.5fm^{-1} and V_s = 1.9 are found. A comparison of the exact and QP model calculations are shown in Fig. 3.2 . As one can see from Fig. 3.2, the fit is reasonable in the density range 1/4 to 4 times normal nuclear matter density. The deviation at high density is a reflection of the approximation that is made to include the higher-body effects in the Pauli potential (i.e. the introduction of V_s). At low densities the failure of the gaussian wave packets to represent the true eigenstates of the system is responsible for the discrepancy. The true eigenstates of a free Fermi gas are nonlocalized, whereas the gaussian wave packets are localized in space. This difference becomes important at low densities. Despite the failings at high and low densities, the model approximates the correct results in the density range important to nuclear reactions at intermediate energy.

Whenever a model has a number of parameters one must be concerned that the similarities between the model and experiment may only be an artifact of the functional form's ability to fit an arbitrary function and may have little to do with incorporating the essential physics into the model. Although one could consider fitting α and V_s for each system under consideration, it would be unsatisfactory if this proved necessary. Our confidence that the essential physics is represented by the Pauli potential is strengthened by the fact that the model is able to reproduce known results for a variety of systems without further adjustment of these parameters. For this reason these parameters are fixed at the values found for the free Fermi gas of $\alpha = 0.5$ fm^{-1} and $V_s = 1.9$ in all remaining calculations.

As a further check on the validity of the Pauli potential approximation, consider the problem of a collection of N noninteracting fermions subject to a harmonic potential of the usual form $kx^2/2$, where k=4.038 MeV/fm. This value of k is the same value used in harmonic oscillator fits to experimental data of the ground state properties of ^{16}O [DW69], and therefore should be a representative value for finite nuclear systems. In Fig. 3.3 a comparison between the ground state energy per particle of the QP model and the exact quantum oscillator is made. The general agreement is good, though the the structure in the exact result curve, due to shell closing, is not reproduced by the Pauli potential model.

III.5 The T > 0 Properties of Non-Interacting Systems

The nonzero properties of the Fermi gas are explored by a Monte Carlo procedure. The inclusion of the Pauli potential makes the Monte Carlo procedure slightly more complicated than most traditional Monte Carlo algorithms. Unlike the QP model, many physical models have only quadratic momentum terms in the Hamiltonian with no coupling between momentum and spatial coordinate. In models whose Hamiltonian has this simple momentum dependence, the momentum integrals in the partition function can be done explicitly, leaving only the coordinate space integrals to be evaluated via Monte Carlo. In contrast, the Pauli potential couples momentum and coordinate space, so the Monte Carlo procedure must sample the full phase space.

To explore the finite temperature (T>0) properties, the standard Metropolis algorithm, in the constant volume, temperature and particle number ensemble is used, with both position and momentum of the quasiparticle being modified for each trial move. The step size of the Monte Carlo move is adjusted to keep the acceptance ratio in the range 0.4 to 0.6 and samples are collected every 5 Monte Carlo sweeps through the lattice. This sampling rate produces a sample that is somewhat correlated. To perform the error analysis on a correlated sample set we use the method of Jowett and Hannan [Mor75] to estimate the variances of the averages.

As a further validation of the Pauli potential approach, as well as a check of the Monte Carlo code, the free Fermi gas is simulated and compared with exact results. In Section III.4 we use a molecular dynamics approach to

find the ground state energy of a free Fermi gas. The results agree rather well with the exact expression. It is now of interest to see how well the finite temperature results agree with the exact solution. The energy per particle as a function of temperature of a free Fermi gas is estimated by a Monte Carlo simulation of a 64 particle QP model. For each T-ρ data point 500 samples are generated which is sufficient to reduce the statistical error in the energy estimate to less than 1%. By simulating a 128 particle system for a number of T-ρ points the finite size effects are estimated to be less that 2%. The Monte Carlo simulation results and the exact free Fermi gas results are shown in Fig. 3.4. The figure shows a general agreement between the QP model and exact results; however one can see that the slope of the E vs. T curve of the QP model is in error at zero temperature. The source of the discrepancy lies with the classical nature of the model. The continuum of energy states in a classical system results in a nonzero value for the T=0 specific heat. For comparison, the classical free gas result is shown on Fig. 3.4 as well.

In summary, it has been shown that for a number of noninteracting systems, a momentum-dependent Pauli potential seems to reproduce the real behaviour of a system of fermions reasonably well. Furthermore it is encouraging that the model is able to approximate these systems, without the need to alter α and V_s from their initial values. This leads one to believe that the Pauli potential incorporates much of the physics associated with the fermions. Although this is not the first calculation to use momentum-dependent potentials to mock up the Pauli principle, the form of the potential and motivation for that form are novel. Whereas previous approaches [WHK77,DDR87] assumed forms for the Pauli potential merely on

the grounds that they were repulsive in phase space, we try to extract a form, be it only approximate, from an examination of simple quantum systems. The beauty of this approach is that not only do we get a form for the Pauli potential, but also we are able to develop a picture that relates the underlying quantum mechanical system with the classical quasiparticle system that we simulate.

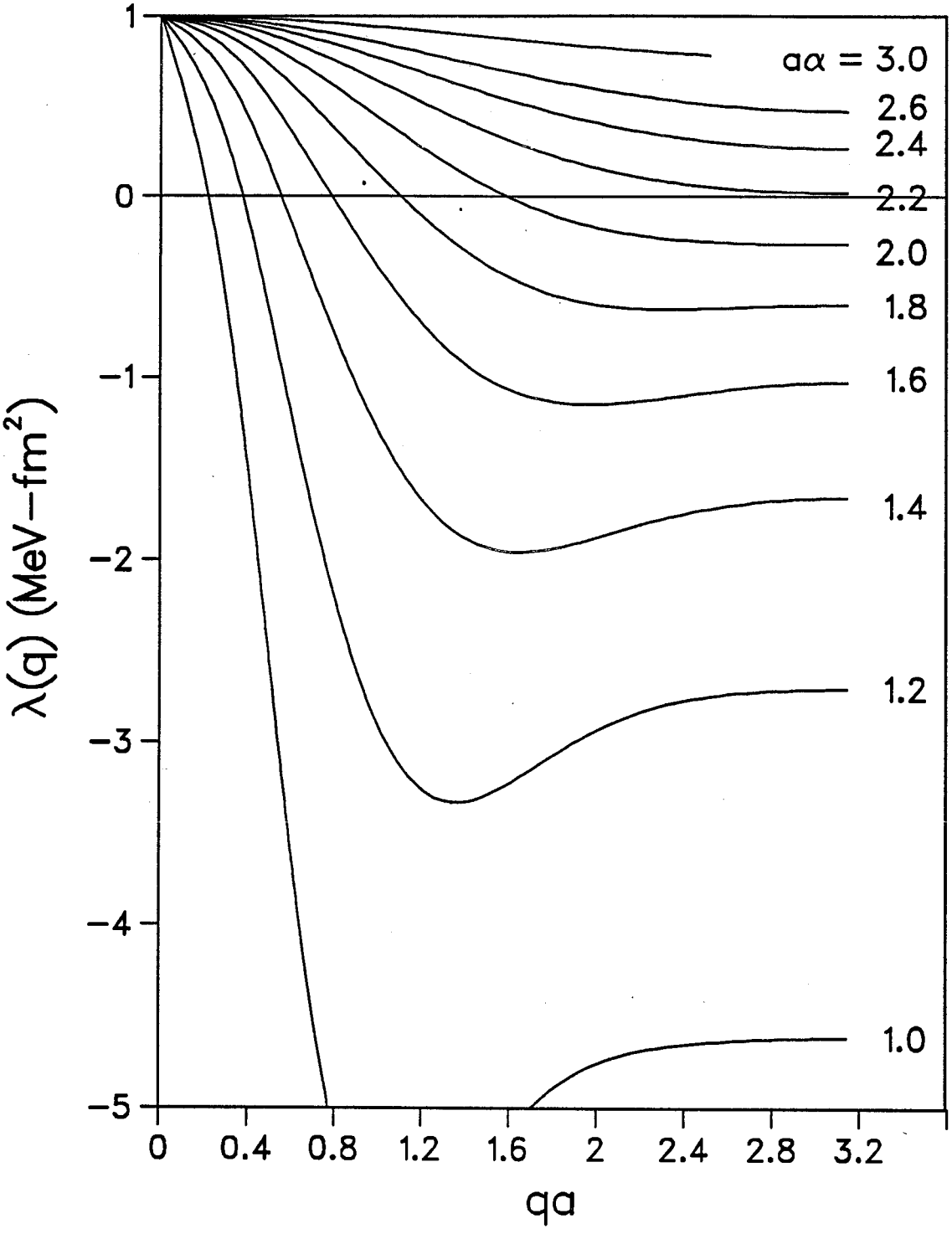

Fig. 3.1 Eigenvalues of the curvature matrix along the $q^x=q^y=q^z$ axis for various values of $a\alpha$.

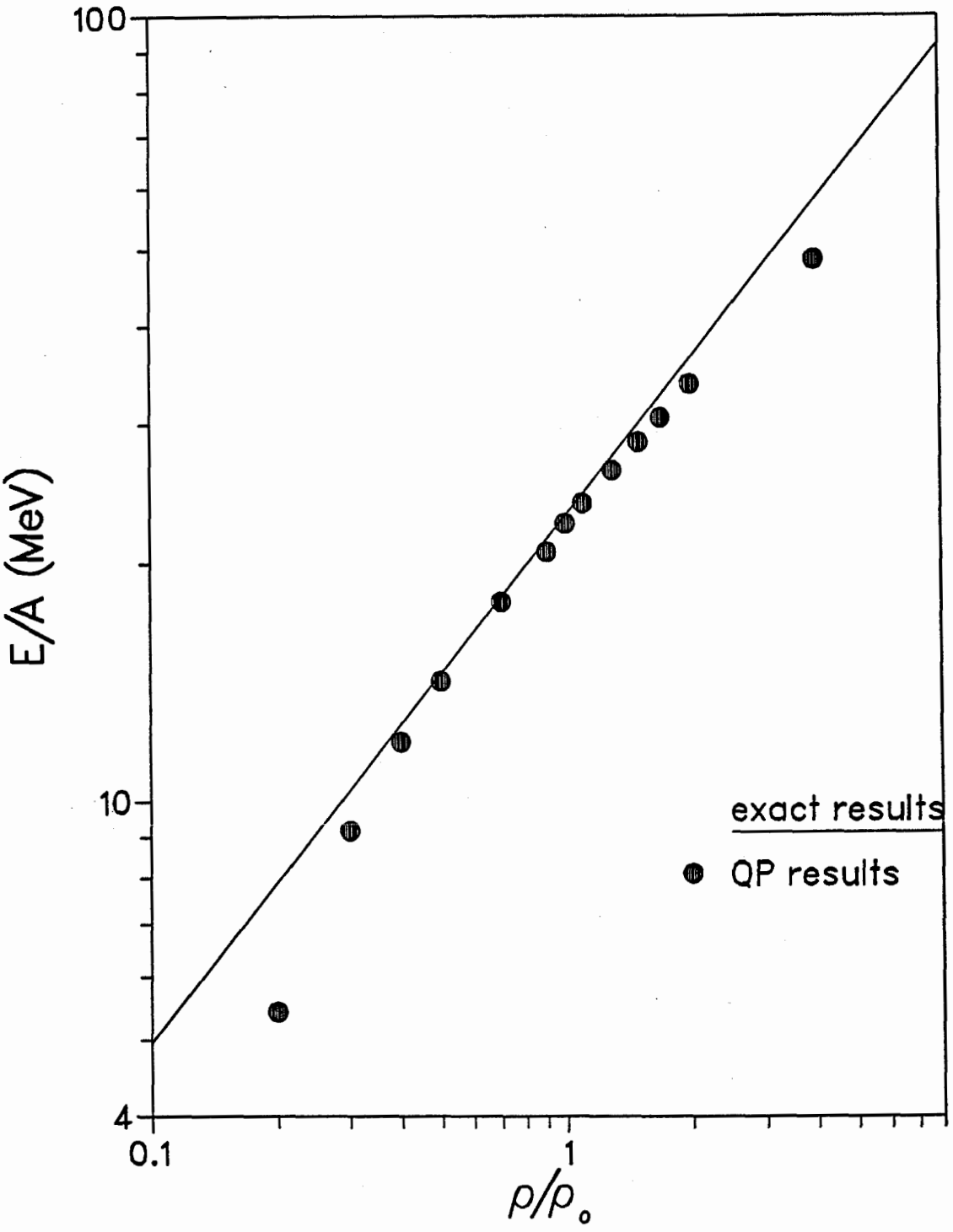

Fig. 3.2 Ground state energy per particle for a system of free fermions. The solid curve refers to the exact results and the ●● symbols refer to the QP results.

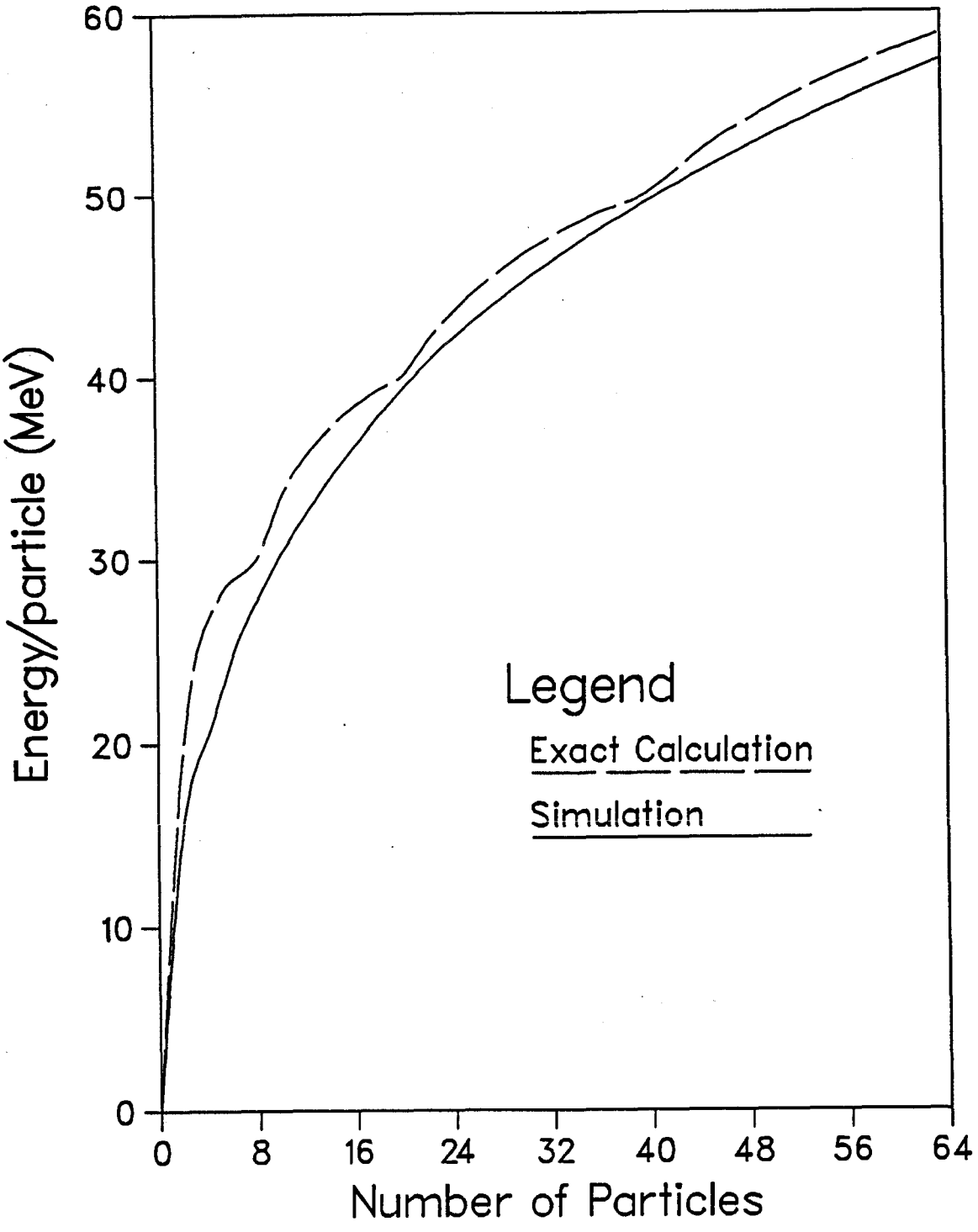

Fig. 3.3 Ground state energy per particle for a system of noninteracting neutrons in a harmonic potential with k=4.038MeV/fm^2. The dashed curve refers to the exact quantum mechanical calculation, while the solid curve is the result from the QP simulation.

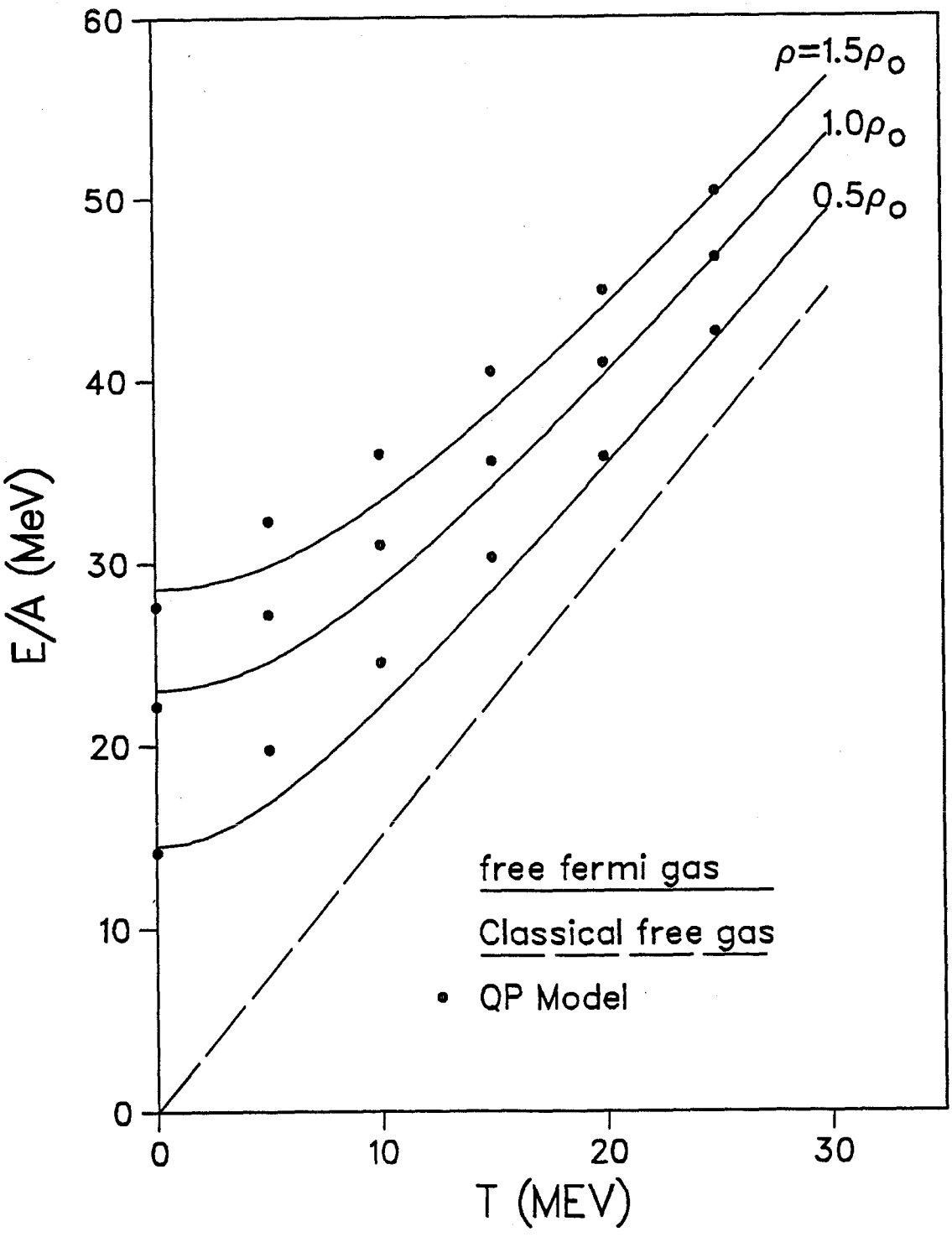

Fig. 3.4. A comparison between the exact free fermion results and the QP model's predictions of the energy per particle (E/A) as a function of temperature (T) for a number of densities. The energy per particle of the classical free gas is shown to illustrate the improvement that the inclusion of a momentum-dependent term can make in classical models.

IV Nuclear Ground States in the Quasiparticle Model

In this chapter a form is chosen for the nuclear interaction in the QP representation. This interaction combined with the Pauli potential and quasiparticle kinetic energy is the full nuclear QP Hamiltonian. The QP Hamiltonian as presented in Section IV.1 has a number of free parameters, and Section IV.2 discusses how these parameters are chosen. In the final section of this chapter the ground state properties of finite nuclear systems are presented and compared with experiment.

IV.1 Nuclear Interaction

The exact form for the nuclear interaction cannot be derived from first principles; therefore, simulations must resort to phenomenological potentials. A common approach is to assume that the nucleons interact through the zero-range Skyrme interaction [VB72]. This results in a density-dependent energy density of the form

$$V[\rho(\mathbf{r})] = \frac{a}{2}\frac{\rho^2}{\rho_o} + \frac{b}{3}\frac{\rho^3}{\rho_o^2} + \frac{c}{2}\frac{(\rho_p-\rho_n)^2}{\rho_o} + \frac{g_1}{2}(\nabla\rho)^2 \qquad (4.1)$$

where $\rho_p(\mathbf{r})$, $\rho_n(\mathbf{r})$ and $\rho(\mathbf{r})$ are the proton, neutron and total density respectively of the system as a function of position. Normal nuclear matter density is denoted by ρ_o and the constants a, b, c and g_1 are to be determined. The first term is an attractive term ($a<0$) which tries to drive the system to large densities. The second term is a repulsive term ($b>0$)

which favours low densities. The third term is isospin dependent, and favours (c>0) equal proton and neutron densities. The last term couples to spatial density fluctuations, and tends to dampen large density fluctuations.

The gradient term is usually not included in most simulation studies, but without it one would get the wrong surface tension for finite nuclei. Consider the variational problem where a density profile $\rho(\mathbf{r})$ is sought that minimizes the energy of the nuclear system subject to the constraint that the total number of particles in the system equals A. For simplicity assume ρ_p and ρ_n are equal. The total energy of the system includes both a potential and kinetic part. It is often assumed that the kinetic energy density of nuclear matter is free-Fermi-like (on a local basis). Under this approximation, known as a local Thomas-Fermi approximation, the kinetic energy density is

$$K(\rho(\mathbf{r})) = \frac{3}{5}\,\varepsilon_F(\rho/\rho_o)\,\rho^{2/3} \tag{4.2}$$

The total energy functional then has the form

$$E(\rho(\mathbf{r})) = \int d^3\mathbf{r}\left\{\left[\frac{3}{5}\,\varepsilon_F(\rho/\rho_o)^{2/3} + \frac{a}{2}\,(\rho/\rho_o) + \frac{b}{3}\,(\rho/\rho_o)^2\right]\rho + \frac{1}{2}\,g_1(\nabla\,\rho)^2\right\} \tag{4.3}$$

For infinite nuclear matter, the minimum $E(\rho(\mathbf{r}))$ occurs for $\rho(\mathbf{r})$ = constant. The parameters a and b are chosen such that the constant density solution of the infinite system has the same density as normal nuclear matter (i.e. $\rho(\mathbf{r}) = \rho_o$), with a binding energy per nucleon of 15.68 MeV.

In the finite case, if the gradient term is neglected, the minimum energy solution of Eq. 3.11, subject to the constraint $\int \rho(\mathbf{r}) d^3\mathbf{r} = A$, is simply

$$\rho(\mathbf{r}) = \begin{cases} \rho_o & r < \left[3A/(4\pi\rho_o) \right]^{1/3} \\ 0 & \text{otherwise} \end{cases} \qquad (4.4)$$

This step-function density profile is highly unrealistic for a finite nucleus. Dropping the gradient term causes the surface tension to vanish, and hence one obtains an unphysical density profile. To avoid this problem the gradient term has been retained in this model. It is useful to use integration by parts to replace the gradient term $(\nabla\rho)^2$ by $\rho\nabla^2\rho$ in the energy density functional.

Under the assumptions of this model, the total density is the sum of single particle densities $\rho_i(\mathbf{r})$ and can be written as

$$\rho(\mathbf{r}) = \left[\frac{\alpha^2}{\pi} \right]^{3/2} \sum_{i=1}^{A} exp[-\alpha^2(\mathbf{r}-\mathbf{R}_i)^2] \quad . \qquad (4.5)$$

Introducing the shorthand notation

$$\langle Q \rangle_i \equiv \int d^3\mathbf{r}\ \rho_i(\mathbf{r})\ Q(\mathbf{r}) \qquad (4.6)$$

enables us to write the nuclear potential in the form

$$U[\rho(\mathbf{r})] \equiv \int d^3\mathbf{r}\, V = \sum_{i=1}^{A} \left[\frac{a}{2} \langle \rho/\rho_o \rangle_i + \frac{b}{3} \langle \rho^2/\rho_o^2 \rangle_i + \frac{1}{2} g_1 \langle \nabla^2 \rho \rangle_i + \frac{c}{2} S_i \langle (\rho_p - \rho_n)/\rho_o \rangle_i \right] \qquad (4.7)$$

where $S_i = 1(-1)$ for protons (neutrons).

Since the density is just a function of gaussian forms it is easy to perform the integration associated with the $\langle \ldots \rangle_i$ expectation. However the term $\langle \rho^2/\rho_o^2 \rangle_i$ results in a three-body interaction between the quasiparticles. In order to keep the computational work no more than $O(A^2)$ the approximation

$$\sum_{i=1}^{A} \langle \rho^2/\rho_o^2 \rangle_i \approx \sum_{i=1}^{A} \left[\langle \rho/\rho_o \rangle_i^2 + \frac{1}{2} g_2 \langle \nabla^2 \rho \rangle_i \right] \qquad (4.8)$$

is used. The constants g_1 and g_2 multiply the same functional form and will be subsumed into $g = g_1 + g_2$.

There is also an interaction between the protons due to the Coulomb potential. The functional form of the Coulomb energy between two protons with a gaussian charge distribution is given by

$$V_c^g(|R_1-R_2|) = \frac{e^2}{4\pi\varepsilon_o} \int dr'dr'' \frac{\alpha^2}{\pi^6} \frac{exp\left\{-\alpha^2(r'-R_1)^2 - \alpha^2(r''-R_2)^2\right\}}{|r' - r''|}$$

$$= \frac{e^2}{4\pi\varepsilon_o} \Phi(\alpha|R_1-R_2|/\sqrt{2}) / |R_1-R_2| \qquad (4.9)$$

where Φ is the probability error function,

$$\Phi(x) = \frac{2}{\pi^{1/2}} \int_0^x dt\ exp(-t^2) \quad .$$

Evaluating the error function is computationally time consuming, so we choose to approximate it by a uniform spherical charge distribution. The potential for a uniform sphere of charge is

$$V_c^h(|R_1-R_2|) = \frac{e^2}{4\pi\varepsilon_o} \begin{cases} 1/|R_1-R_2|, & |R_1-R_2| > R_o \\ [3-(|R_1-R_2|/R_o)^2]/(2R_o), & \text{otherwise} \end{cases} \qquad (4.10)$$

where R_o is the hard sphere radius. Both the hard sphere and the gaussian potentials have the same asymptotic form as the interparticle separation becomes large (i.e. $V_c^h(R)/V_c^g(R) \longrightarrow 1$, as $R \longrightarrow oo$). These two potentials are made to agree at the origin (i.e. R=0) by choosing $R_o = 3\sqrt{2\pi}/4\alpha$. For this value of R_o the relative difference between the two potentials is less than 9% over the complete range of R. In any event, the calculations performed with the simulations have very little sensitivity to the gaussian or hard sphere forms taken for the charge distribution.

After substituting Eq. 4.8 into Eq. 4.7 and performing the integration, an explicit form for the nuclear interaction between quasiparticles is found. Including this with the Pauli and Coulomb terms, the energy of the quasiparticle system can be written as

$$H = \sum_i P_i^2 / 2m + \frac{1}{2}\sum_{i\neq j}\left[V_p(X_{ij}) + V_c(R_{ij}) \right] \qquad (4.11)$$

$$+ \frac{1}{2}\sum_{ij}\left[(a + cS_iS_j)/\rho_o + \alpha^2 g(3 - \alpha^2 R_{ij})\right]D(R_{ij}) + \frac{b}{3}\sum_i \left[\sum_j D(R_{ij})/\rho_o \right]^2$$

where

$$R_{ij} = |\mathbf{R}_i - \mathbf{R}_j| \ ,$$

$$D(R) = \left[\frac{\alpha^2}{2\pi}\right]^{3/2} exp(-\alpha^2 R^2/2)$$

and where $V_c(R_{ij})$ is given by Eq 4.10.

In summary, a classical quasiparticle Hamiltonian with a momentum-dependent interaction has been developed. The quasiparticles in themselves do not represent the real quantum particles of the systems, however the associated gaussian wave packets do. The gaussian wave packets insure that the Heisenberg Uncertainty Principle is not violated and that the Pauli potential has a form that allows the effects of the Pauli Principle to be

at least approximated. In the limit of noninteracting systems it has been shown that this approximation is reasonably good in the density range of interest. Furthermore this model possesses the necessary symmetries to ensure conservation of energy, linear momentum and angular momentum of both the quasiparticles and the underlying quantum mechanical particles. All of this has been accomplished within the context of a model whose energy can be determined in $O(A^2)$ operations.

IV.2 Parameter Determination

There are six free parameters (α, V_s, a, b, c and g) in the QP Hamiltonian, Eq. 4.11. The parameters α and V_s are fixed by comparison with the free Fermi gas at T=0 (See Chapter III). The parameters a, b and c are determined by comparing the results of a local Thomas-Fermi calculation to those of infinite nuclear matter. The value of g is the only parameter that is set within the context of the complete QP model. It is fixed by demanding that the binding energies of intermediate mass nuclei ($A \approx 50$ nucleons), as calculated by the QP model, with agree experiment. Although one could try to fit the binding energies over a larger range of mass number, A, it is found that fitting in a narrow range about A = 50 is sufficient to yield a good fit over the entire periodic table.

Using the local Thomas-Fermi approximation for the kinetic energy (see Eq. 3.10) the total energy per nucleon of the system can be written as, assuming homogeneity and small $\omega=(\rho_p-\rho_n)/\rho_o$,

$$E(\rho) = \frac{3}{5}\,\varepsilon_F\,(\rho/\rho_o)^{2/3} + \frac{1}{3}\,\varepsilon_F\,(\rho/\rho_o)^{2/3}\,\omega^2 + \frac{a}{2}\,(\rho/\rho_o) + \frac{b}{3}\,(\rho/\rho_o)^2 + \frac{c}{2}\,(\rho/\rho_o)\,\omega^2 \qquad (4.12)$$

where ε_F is the Fermi energy at normal nuclear matter density ρ_o. Normal nuclear matter refers to the preferred state of an infinite, neutral, nuclear system at T=0 (isospin symmetric). The value of ρ_o=0.17fm^{-3} is found by extrapolation of the mass formula to the neutral and infinite size system limit [Hof67]. Furthermore the extrapolation yields a binding energy, for small ω, of the form $B=B_o+a_s\omega^2$ where B_o=15.68 MeV and a_s=-28.06 MeV. Using these expressions for ρ_o and $B(\omega)$, and the fact that normal nuclear matter is stable (i.e. the energy is a minimum) the constants can be determined.

The binding energy as defined within the model will be the difference between the energy of Eq. 4.1 and the energy (E_{oo}) when the particles are infinitely separated. Typically it is assumed that ρ = 0, everywhere for infinite separation. Under this assumption *a*, *b* and *c* are determined to have the values of -124.11 MeV, 70.06 MeV and 30.54 MeV. However, with this model and with real systems the density at infinite separation is not identically equal to zero. The finite wave packet widths of Eq. 3.2 gives rise to a nonzero E_{oo} per particle given by

$$E_{oo} = \frac{a}{2}\,(\rho_1/\rho_o) + \frac{b}{3}\,(\rho_1/\rho_o)^2 + \frac{c}{2}\,(\rho_1/\rho_o) + \frac{1}{2}g\,\alpha^2\,\rho_1 \qquad (4.13)$$

where $\rho_1 = (\alpha^2/(2\pi))^{3/2} = 0.00794$ fm^{-3} at α = 0.5 fm^{-1}.

For this E_{oo} the solutions for a, b and c are slightly different from the values given above and dependent on g. The QP model now has only one free parameter, g, which is determined by matching the binding energies as calculated by the model with experimental values for a selection of nuclei. The method of calculating the ground states and the values of the ground state energies are presented in the next section. However to finish this discussion, the results of the parameter fitting are presented now.

A one parameter fit in g is made by requiring that the difference of the calculated binding energy and the experimental value be small for mass A≈50 systems. A good fit is found for g = 291 MeV-fm^5 and hence a=-129.69 MeV, b=74.24 MeV and c=30.54 MeV.

IV.2 Ground-State Properties for Finite Systems

The model presented above is phenomenological in nature. All of the parameters except one (g) are set by comparing the model to infinite systems. By examining a variety of finite systems not only is the value of g determined but a test is made of the validity of the model. In the remainder of this section the calculational method for determining the ground state is described, and a comparison of the calculated ground state energies and RMS radii is made with experiment.

The ground states are found in a dynamical way by inclusion of dampening in the equations of motion. The damped equations of motion for a system with mass number A, interacting via the Hamiltonian of Eq. 4.11, are

$$\dot{R}_i = \frac{\partial H}{\partial P_i} + \mu_1 \frac{\partial H}{\partial R_i} \qquad (i = 1,\ldots,A) \qquad (4.14)$$

$$\dot{P}_i = -\frac{\partial H}{\partial R_i} - \mu_2 \frac{\partial H}{\partial P_i}$$

where μ_1 and μ_2 are chosen to have the values of 400 (fm-c/MeV) and 0.426 (MeV/fm-c) respectively. Some care is needed in choosing μ_1 and μ_2 to ensure rapid enough convergence without over-dampening the system.

The initial configuration is constructed by placing the nucleons on a body-centred cubic lattice in a compact way until the desired mass A is obtained. The nucleons are then randomly labelled as protons or neutrons according to the nucleus of interest. The spins of the nucleons are assigned in such a way that the magnitude of the sum of the proton spin or neutron is never greater than 1/2. The momentum is assigned to each nucleon by choosing from a T=0 Fermi distribution with Fermi energy based on the local density.

The equations of motion are integrated via an adaptive fourth-order Runge-Kutta scheme until $\dot{\mathbf{r}}$ and $\dot{\mathbf{p}}$ are sufficiently small. For most systems it was found that $\dot{r} \sim 10^{-2}c$ and $\dot{p} \sim 0.5$ MeV/fm after 200 fm/c. The energy of the system appears stationary, with a rate of change less than 10^{-3} MeV-c/fm per nucleon. The calculated binding energy was only slightly sensitive to initial conditions. For different starting configurations the the energy of these systems after 200 fm/c only differed by a few hundredths of an MeV per nucleon.

To assess the ability of the model to reproduce ground state properties of real nuclei the binding energies and RMS radii of a range of elements are calculated and compared to the experimentally measured values. The RMS radius of the nuclear system is not just the RMS radius of the quasiparticle system. The width of the nucleon wave packet needs to be included. The RMS radius of a nucleus in this model is given by

$$R^2_{rms} = \frac{1}{A}\sum_i (R_i - R_{cm})^2 + 3/(2\alpha^2)$$

The first term of this expression is just the square of the RMS radius of the quasiparticle positions and the second term is the wave packet width contribution.

The comparison begins with a representative sample of elements from the periodic table. Table 4.1 compares the binding energy of the model with experiment [Eng66] and the predictions of Green's mass formula [Gre54], which has a comparable number of parameters as the QP Hamiltonian. As well the table compares the RMS radii of the QP model with the radii extracted from a Wood-Saxon fit to data [Hof67].

The agreement between the QP model and the data is in the 5% range for the binding energy and 10% for the radius. The agreement with data seems to be at the same level as that of Green's mass formula.

A comparison between model and data of the isospin dependence of the binding energy is made in Table 4.2, for two isobaric sequences of

intermediate mass systems. The masses of the systems chosen for study are A=32 and 51. Again the agreement with experiment is very reasonable.

Nucleus		Binding Energy per nucleon (MeV)			RMS radius (fm)	
A	Z	Model	Data	Green	Model	Data
10	5	6.77	6.48	6.67	2.47	2.58
20	10	7.34	8.03	7.89	2.80	2.96
40	20	8.19	8.55	8.47	3.27	3.42
52	24	8.75	8.78	8.74	3.41	3.65
58	28	8.60	8.73	8.65	3.57	3.76
88	38	8.80	8.73	8.69	4.03	4.21
108	47	8.70	8.54	8.57	4.27	4.47
197	79	8.07	7.92	7.90	5.17	5.35

TABLE 4.1 Model calculation of binding energies per nucleon and RMS radii of selected nuclei. The predictions for the binding energies are compared with both the data and mass formula of Green. The RMS radii are compared with that obtained in a Wood-Saxon fit to a range of nuclei.

Nucleus		Binding energy per nucleon (MeV)		
A	Z	Model	Data	Green
32	14	8.15	8.48	8.40
32	15	8.09	8.46	8.48
32	16	7.97	8.49	8.36
32	17	7.69	8.07	8.03
51	21	8.68	8.60	8.56
51	22	8.73	8.71	8.69
51	23	8.74	8.74	8.74
51	24	8.70	8.71	8.71
51	25	8.56	8.63	8.59

TABLE 4.2 Isospin dependence of binding energies per nucleon. The comparison is made among the model calculation, data and fit to the data.

The results for light systems are shown in Table 4.3. Light systems are the most difficult to approximate with a classical description and even the quasiparticle model shows some failings. The nature of the nucleon wave function becomes important, and the gaussian approximation begins to break down. The effects of shell closing, which the QP model has no way of approximating, also become significant. Nevertheless the comparison shown in Table 4.1 is not at all unreasonable. All the systems have finite radii and for A≥4 the binding energies are within 20% of the data. The model predicts the sharp decrease in the binding energy per nucleon for very light systems and also that ^{5}He is significantly less bound than ^{4}He (as is observed). However both ^{5}He and ^{8}Be are known to be unstable whereas the QP model predicts that they are stable against particle emission.

Nucleus		Binding energy per nucleon (MeV)			RMS radius (fm)	
A	Z	Model	Data	Green	Model	Data
2	1	2.71	1.11	1.34	2.45	2.2
3	1	4.37	2.83	0.61	2.45	1.70
4	2	6.24	7.07	4.09	2.45	1.63
5	2	5.84	5.48	4.06	2.48	unstable
6	3	6.06	5.33	5.37	2.45	2.54
7	3	6.52	5.61	5.49	2.45	2.40
8	4	7.09	7.06	6.14	2.45	unstable
9	4	6.88	6.46	6.29	2.47	2.40
10	5	6.77	6.48	6.67	2.47	2.45
12	6	6.97	7.68	7.05	2.54	2.50
14	7	6.91	7.48	7.33	2.55	2.45
16	8	7.10	7.98	7.56	2.68	2.65

TABLE 4.3 Binding energies and RMS radii for light nuclei. The comparisons are the same as Table 4.1.

The ground state energies and radii of the QP model agree with experiment within 5-10% ,except for very light systems ($A \leq 4$), where the nuclei are overbound and have too large a radius. It is the failure to obtain correct binding energies for small systems that results in the ^{5}He and ^{8}Be nuclei artificially stable. Despite these failings the QP model does have a number of unexpected successes. The peak in the binding energy as a function mass number not only exists, but occurs in nearly the correct location and has the right value. Furthermore the plateau in the RMS radii as a function of nucleon number, for light systems, is also reproduced by the model and extends over nearly the same observed range with approximately the correct value. This agreement with the data on finite systems is impressive when one recalls that all but one of the parameters are fixed by results from infinite nuclear matter, leaving only one parameter (g) to be fit to the finite systems.

V QUASIPARTICLE DYNAMICS

In the preceding chapters the QP model is developed and the ground state properties discussed. This chapter focuses on the dynamics of the model. First the equations of motion are derived. Next a discussion of the need for a collision term, and the form of such a term is given. Finally, as an example of the utility of the QP model, the time scales associated with intermediate energy heavy ion reactions are investigated.

V.1 Equations of Motion

In Chapter III the claim was made that the quasiparticles obey classical equations of motion. This claim will be justified now. The assumption has been made that the completely antisymmetrized state can be replaced by a product state, Ψ, plus some effective potential, $\hat{V}_{eff}$. The dynamics of the system is then governed by an effective Hamiltonian, $\hat{H}_{eff} = \hat{H} + \hat{V}_{eff}$. Following an approach similar to the proof of Ehrenfest's Theorem, we write the time dependence of a quasiparticle position and momentum in the following form:

$$\dot{R}_i = \frac{d}{dt}\langle\Psi|r_i|\Psi\rangle = \langle\Psi|[r,\hat{H}_{eff}]|\Psi\rangle / (i\hbar)$$

$$\dot{P}_i = \frac{d}{dt}\langle\Psi|p_i|\Psi\rangle = \langle\Psi|[p,\hat{H}_{eff}]|\Psi\rangle / (i\hbar) \qquad (5.1)$$

Now consider the gradients with respect to **R** and **P** of the energy

expectation, $\langle \hat{H}_{eff} \rangle$, which is just the QP Hamiltonian H(R,P).

$$\frac{\partial H}{\partial R_i} = \frac{\partial}{\partial R_i} \langle \Psi | \hat{H}_{eff} | \Psi \rangle = \langle \frac{\partial}{\partial R_i} \Psi \mid \hat{H}_{eff} \mid \Psi \rangle + \langle \Psi \mid \hat{H}_{eff} \mid \frac{\partial}{\partial R_i} \Psi \rangle$$

(5.2)

$$\frac{\partial H}{\partial P_i} = \frac{\partial}{\partial P_i} \langle \Psi | \hat{H}_{eff} | \Psi \rangle = \langle \frac{\partial}{\partial P_i} \Psi \mid \hat{H}_{eff} \mid \Psi \rangle + \langle \Psi \mid \hat{H}_{eff} \mid \frac{\partial}{\partial P_i} \Psi \rangle .$$

The partial derivatives of Ψ are easy to evaluate in the real space representation. Note that Ψ is a function of $(\mathbf{r}_i - \mathbf{R}_i)$ (see Eq. 3.2 and 3.3); therefore

$$\frac{\partial}{\partial \mathbf{R}_i} \Psi = - \frac{\partial}{\partial \mathbf{r}_i} \Psi \Rightarrow \mid \frac{\partial}{\partial \mathbf{R}_i} \Psi \rangle = \frac{-i}{\hbar} \hat{\mathbf{p}}_i \mid \Psi \rangle$$

(5.3)

$$\text{and} \quad \langle \frac{\partial}{\partial \mathbf{R}_i} \Psi \mid = \frac{i}{\hbar} \langle \Psi \mid \hat{\mathbf{p}}$$

Also note that the wave function depends on $\mathbf{P}_i$ only through the phase factor $exp(i\mathbf{P}_i \cdot \mathbf{r}_i/\hbar)$, therefore

$$\frac{\partial}{\partial \mathbf{P}_i} \Psi = \frac{i}{\hbar} \mathbf{r}_i \Psi \Rightarrow \mid \frac{\partial}{\partial \mathbf{P}_i} \Psi \rangle = \frac{i}{\hbar} \hat{\mathbf{r}}_i \mid \Psi \rangle$$

(5.4)

$$\text{and} \quad \langle \frac{\partial}{\partial \mathbf{P}_i} \Psi \mid = \frac{-i}{\hbar} \langle \Psi \mid \hat{\mathbf{r}}_i$$

Hence

$$\frac{\partial H}{\partial R_i} = \frac{i}{\hbar} \langle \Psi \mid [\mathbf{p}_i, \hat{H}_{eff}] \mid \Psi \rangle = -\dot{\mathbf{P}}_i$$

and

(5.5)

$$\frac{\partial H}{\partial P_i} = \frac{-i}{\hbar} \langle \Psi \mid [\mathbf{r}_i, \hat{H}_{eff}] \mid \Psi \rangle = \dot{\mathbf{R}}_i$$

which are just the classical equations of motion for the quasiparticle Hamiltonian H(**R**,**P**).

The above arguments depend on the existence of $\hat{V}_{eff}$ which has neither been calculated, nor shown to exist. Fortunately for calculational purposes all that is needed in this study is the expectation - not the complete operator.

V.2 Nucleon-Nucleon Collision Term

The density dependent potential used in this calculation resembles the mean field potential used in Boltzmann transport equations [BD88,BKD84,Boa87,SG86]. For the collisionless form of these equations, called the Vaslov equation, the predicted cross section for an intermediate energy nuclear reaction is much too small, allowing colliding heavy ions to pass though each other almost transparently. The reason the cross section is underestimated is because the correlations have been neglected by the mean field approximation. To approximate the effects of these correlations a collision term is introduced into the Vaslov equation. These modified Boltzmann equations, as they apply to fermions or bosons, are known as the Nordheim-Uehling-Uhlenbech (NUU) equation or Boltzmann-Uehling-Uhlenbech (BUU) equation [Nor28, UU33].

Given the similarities between the potential used in our calculation, and in the Boltzmann-like approaches, it is to be expected that the cross section in intermediate energy nuclear collisions will be underestimated. As with the Boltzmann-like approach, we therefore include a collision term

in the the model's dynamics. Although a collision term greatly affects the dynamics of the model it will have no effect on the zero temperature properties (i.e. the results of Chapter IV) since the quasiparticles are stationary in their ground state.

Although the inclusion of a collision term in the QP model is motivated by the Boltzmann equation studies, the form chosen for our study will be different than what is generally used in the NUU approach. The common elements in any collision algorithm are a specification of when the collision occurs and a prescription for determining new momenta for the scattering pair. In the algorithm commonly used in the NUU method, the collision occurs at the time of closest approach and the new momenta are chosen stochastically from a distribution that produces the observed NN cross section. This method has the features of conserving energy and linear momentum on an event-by-event basis, but conserves angular momentum only in an average over many events.

In this study it is desired to have a model that conserves not only energy and linear momentum on an event-by-event basis, but angular momentum as well. In developing a collision term for the model, these conservation laws are sufficient to determine uniquely the change of momentum once a collision geometry is specified. We return to this question below; at this point we wish to deal the kinematics.

The calculation of the change of momentum needs to be done numerically because of the momentum dependence of the Pauli potential. Consider the collision between two particles labelled 1 and 2. From the conservation of

linear and angular momentum the new momentum (P_i') is related to the old momentum (P_i) of particle i, by the relation

$$P_1' = P_1 + \Delta \hat{R}_{12}$$

$$P_2' = P_2 - \Delta \hat{R}_{12} \qquad (5.6)$$

where $\hat{R}_{12}$ is the unit vector along the $R_1 - R_2$ direction. The scalar, Δ, (which has the units of momentum) is determined by energy conservation:

$$E' - E = \frac{(P_1 - P_2)\cdot \hat{R}_{12}\Delta + \Delta^2}{m} + V(R_1,\ldots,R_N,P_1+\Delta\hat{R}_{12},P_2-\Delta\hat{R}_{12},P_3,\ldots,P_N)$$

$$- V(R_1,\ldots,R_N,P_1,P_2,P_3,\ldots,P_N) = 0 \quad . \qquad (5.7)$$

Notice that Eq. 5.6 has at least one solution, the trivial solution $\Delta=0$. To find the non-trivial root of the above equation a Steffensen iteration scheme [CB72] is used to solve the equation

$$\frac{(P_1 - P_2)\cdot \hat{R}_{12} + \Delta}{m} + \frac{1}{\Delta}\left[V(P_1+\Delta\hat{R}_{12},P_2-\Delta\hat{R}_{12},\ldots) - V(P_1,P_2,\ldots)\right] = 0 \qquad (5.6)$$

The initial Δ used in the iteration method is the value of Δ for scattering without any Pauli potential. Typically the method finds the root within 10 iterations. In our algorithm if the nontrivial solution is not found, the scattering is suppressed and the nonscattered solution $\Delta=0$ is accepted.

It remains to specify the point at which the collision occurs to complete the description of this model's collision process. In the NUU method the point of collision is deterministic (i.e. time of closest approach) and the

new momenta probabilistic. The assignment of new momenta for a collision with in the QP model is deterministic, with the conservation laws completely specifying the change of momenta. To make the scattering stochastic, the point of collision must be probabilistic. This is done by assigning a test particle to each quasiparticle. The test particle position about its quasiparticle is chosen at random from the gaussian distribution of the wave packet associated with the quasiparticle. If the distance between test particles becomes less than some given value, $2r_o$, the collision algorithm is invoked. If the trial scattered state is accepted (allowing for Pauli blocking of the collision), then a new momentum is assigned, and a new test particle position is given to each of the scattered quasiparticles.

The one free parameter, r_o, is determined by comparing the model's nucleon-nucleon (NN) cross section with experiment. The observed differential NN cross section is isotropic in the CM frame, with a total cross section of 28 mb [PDG70] at bombarding energies in the 100-200 MeV region. The total cross section in the model is made to agree with experiment by choosing r_o=0.944 fm. The model's differential NN cross section, which is calculated using numerical integration (see Fig. 5.1) is roughly isotropic, with some enhancement in the backward and forward directions. Though this enhancement is not physical, it should be of little significance in a heavy ion collision because of multiple scattering. Further this enhancement occurs only in a small range of solid angle. The effects of varying the NN cross section are being investigated separately [BW90] and have not been found to be substantial at low to intermediate bombarding energies.

To consider the NN scattering in the presence of other fermions the free scattering NN collision term must be generalized to include the effects of phase space occupation.. The fermionic nature of the particles makes the scattering sensitive to the occupation of phase space. The scattering may be suppressed: if the phase space that a particle is scattering into is saturated the scattering is prohibited. In the QP model a test is made for this Pauli blocking once a trial momentum is chosen for the scattering pair.

To calculate the probability of Pauli blocking it is convenient to go over to a phase space description of the system via Wigner transformations [BJ84,HOS84]. The Wigner transform of a single particle wave function $f(\mathbf{r},\mathbf{p})$ always has norm of unity (i.e. $\int f(r,p)drdp = 1$), so one is tempted to interpret it as a probability distribution in phase space. Although the Wigner transform is normalized for all wave functions, the transform $f(\mathbf{r},\mathbf{p})$ is not guaranteed to be non-negative, making the probability interpretation dubious. However, for the gaussian wave packets used in the QP model, $f(\mathbf{r},\mathbf{p})$ is always positive so a probability interpretation is reasonable.

The phase space distribution of a single particle, as given by the Wigner transform of Eq. 3.2, is

$$f_i(\mathbf{r},\mathbf{p}) = \frac{1}{(\pi\hbar)^3}\, exp\left(-[\alpha^2(\mathbf{r}-\mathbf{R}_i)^2 + (\mathbf{p}-\mathbf{P}_i)^2/(\alpha\hbar)^2]\right) \qquad (5.9)$$

The density of particles with a specific isospin, I, and spin, S, combination is given by (under the assumption of a simple product state)

$$f_T^{IS}(\mathbf{r},\mathbf{p}) = \sum_{i=1}^{A} f_i(\mathbf{r},\mathbf{p})\delta_{II_i}\,\delta_{SS_i} \tag{5.10}$$

Now consider the scattering of particle 1. Let f_1' be its new phase space distribution after scattering. Imagine phase space divided into cells of volume $(2\pi\hbar)^3$. The collision is Pauli blocked if particle 1 is scattered into a cell that is occupied by a particle with the same quantum numbers I,S . The probability that a cell is occupied by some particle other than particle 1 is

$$P_{occupied}(\mathbf{r},\mathbf{p}) = (2\pi\hbar)^3(f_T^{IS} - f_1) \tag{5.11}$$

where it is assumed that $f_T - f_1$ is a slowly varying function in phase space in the vicinity of $(\mathbf{r},\mathbf{p})$. The probability that the scattering of particle 1 is blocked is then given by

$$\begin{aligned} P^1_{blocked} &= \int d^3\mathbf{r}\, d^3\mathbf{p}\, f_1'(\mathbf{r},\mathbf{p}) P_{occupied}(\mathbf{r},\mathbf{p}) \\ &= (2\pi\hbar)^3 \sum_{i\neq 1} \delta_{II_i}\,\delta_{SS_i} \int d^3\mathbf{r}\, d^3\mathbf{p}\, f_1'(\mathbf{r},\mathbf{p})\, f_i(\mathbf{r},\mathbf{p}) \\ &= \sum_{i\neq 1} \delta_{II_i}\,\delta_{SS_i}\, exp\left(-\tfrac{1}{2}\,[\alpha^2(\mathbf{R}_1-\mathbf{R}_i)^2 + (\mathbf{P}_1'-\mathbf{P}_i)^2]/(\alpha\hbar)^2\right) \end{aligned} \tag{5.12}$$

Likewise, the blocking probability $P^2_{blocked}$ for the scattering of the other member of the scattering pair (particle 2) can be calculated. The probability that a collision is accepted is the probability that both particle 1 and particle 2 are not Pauli blocked,

$$P_{accept} = (1 - P^1_{blocked})\,(1 - P^2_{blocked}) \tag{5.13}$$

The above calculation assumes that the occupation of a phase space cell never exceeds unity. Although this is correct for a truly fermionic system, it can be violated in the quasiparticle model because of the approximations made. This violation of the occupation of the phase space cells can lead to a calculated $P_{blocked}$ that is larger than one. If this is the case, our algorithm assumes that $P_{blocked} = 1$, and hence the collision is rejected.

The collision term discussed above, along with the Eq. 5.5 completely specify the dynamics of our model. Eq. 5.5 represents the effect of the Pauli potential and nuclear interaction in determining the trajectory of the quasiparticles between collisions. If a collision occurs, the temporal integration based on Eq. 5.5 is suspended, the above collision prescription is applied instantaneously, after which the temporal integration is resumed. We refer to this model of the dynamics of the quasiparticle as QPD in the remainder of the thesis.

V.3 Reaction Time Scales

The time scales associated with a heavy ion collision are interesting for a number of reasons. First, from a computational point of view, it is desirable to know if the calculation will yield anything interesting within the limits of available computer time. Secondly, the establishment of various time scales of the reaction assists in identifying the physical processes responsible for fragmentation.

We now consider how the computational time requirements scale with system

size. The numerical scheme used to integrate the equations of motion requires the evaluation of the force on each particle at each time step. The simplest algorithm's running time then would scale linearly with the number of time steps and quadratically with the number of particles. The short range of the nuclear force introduces a natural cutoff length that can be used to define clusters of interacting particles. Then the nuclear force needs only to be calculated between particles within a given cluster. On the other hand, no such cutoff exists for the long range Coulomb force. Using the cutoff in the calculation of the nuclear force, the computational work required to evaluate both the nuclear and Coulomb force at time step can be can be written as

$$W(t) = \frac{w_n}{2} \sum_c \left[A_c(t)\right]^2 \quad +. \quad \frac{w_c}{2} Z^2 \tag{5.15}$$

where A_c is the number of particles in the cluster c, Z is the number of protons in the system and the sum is over all clusters. The constants w_n and w_c are the work required to calculate the nuclear and Coulomb forces respectively between two particles. The total computational work required to integrate the equation of motions for some time t_T is then

$$W_T = \frac{1}{\Delta t} \int_0^{t_T} dt\, W(t) = w_c Z^2\, t_T\, /\Delta t + \frac{w_n}{\Delta t} \int_0^{t_T} dt \sum_c \left[\, A_c(t) \,\right]^2 \tag{5.16}$$

where Δt is the length of one time step.

For a ^{40}Ca + ^{40}Ca reaction about 1 cpu minute on a IBM 3081 processor is required to propagate the equations of motion for a reaction time of 250 fm/c. Almost all of this time is spent evaluating the nuclear force terms

with less then 15% of the time being used to calculate the Coulomb force. Of course the total running time for any particular study is much longer than this. The statistical nature of the model requires integration of the equations of motion many times to ensure there are enough events to have reasonable statistics.

We wish to explore the time scales associated with a heavy ion collision for several values of the impact parameter, b, and the bombarding energy. Only a few reactions are considered in this study but it is hoped that they illustrate the general features. To investigate intermediate energy phenomenon, a Ca+Ca reaction is considered. This reaction is studied at b = 0, 3 and 6 fm., and 25A∘MeV bombarding energy. For each impact parameter, 500 events are generated, each for a total reaction time of 250 fm/c. A set of Ar+C reactions are used to explore the low energy fusion regime. The Ar+C reaction is simulated at 12A∘MeV bombarding energy and impact parameter values of b=2, 4 and 6 fm. For each of these systems, 250 events are generated, each with a total reaction time of 400 fm/c.

The time dependence of the cluster mass distribution is examined first. The following procedure is adopted for determining a cluster's characteristics at any given time. First the momenta and positions of all the particles of a reaction are written to storage every 10 fm/c during the simulation. The positions are then analyzed at each stored time step to determine which nucleons belong to a given cluster. A cluster is the set of all nucleons which can be linked together with separations of no more than 3.5 fm. For the Ca+Ca reaction at 25A∘MeV the time dependence of three mass bins is considered: 1-10, 11-40 and 71-80 nucleons. Fig. 5.2 shows

this dependence for b=0 and 6 fm. The figure representing the peripheral collisions, indicates that in such collisions the nuclei join to form a short lived, large system. This large system breaks up into a pair of nuclei each with nearly the same mass the original Ca nuclei, and with little exchange of energy between them. The central collision has a much different character. This reaction decays with time as well but is much more fragmented than a peripheral collision, with 5 times as many light fragments, and no heavy fragments. This high multiplicity is interpreted as evidence for much a larger excitation of central collision reaction products as compared with the large impact parameter reactions.

Further evidence of the relative mixing of target and projectile nuclei, and hence excitation, can be seen by examining the time dependence of the RMS radius of a set of nucleons that eventually emerge as a fragment. To calculate this quantity one determines which nucleons belong to a common cluster at some time, t_c, chosen such that the rapid decay associated with the initial impact is over. A value of t_c=150 fm/c suffices for the Ca+Ca reaction at 25A∘MeV. Next, for a given cluster, the positions of the constituent nucleons are examined for times previous to t_c, and the RMS radius of the nucleon positions is calculated. This RMS radius is averaged over all configurations that emerge as a cluster of a given mass A. In Fig. 5.3 the time dependence of the average RMS radii is shown for a number of cluster sizes: A=36, 44 and 76 in a Ca+Ca reaction at 25A∘MeV. The radius of the A=76 cluster is large at first, since the constituent nucleons are spread out over both target and projectile. For both the b=0 and 6 fm reactions, as the two nuclei approach each other the radius decreases, as expected. Both reactions also exhibit a growth in this

radius after the two nuclei collide. However, the central collision has a distinct decrease in growth rate at about 40 fm/c after the time of minimum radius, which is not seen in the peripheral reaction. The radius associated with this change of growth rate corresponds to a normal (near ground state) nuclear system of mass 80.

For the large impact parameter collisions the data support the conclusions that the initial nuclei stay intact and that the growth of the RMS radius is just due to the increase with time of the separation of the target and projectile centers-of-mass. For central collisions the picture is very different. After initial impact, the system is compressed, but then expands quickly to the size of a normal mass A=80 nuclear system, followed by a much slower expansion due to light particle evaporation.

These intermediate energy dynamics are now contrasted with the dynamics of low energy reactions. In Fig. 5.4 the time dependence of the mass distribution in Ar+C reactions at 12A∘MeV is shown. The peripheral reaction (shown in the lower frame) has the same qualitative behavior as the peripheral Ca+Ca reaction of Fig. 5.2, with the target and projectile linking together to form a loose system which breaks apart quickly. The central collision, however shows a qualitative difference between the intermediate and low energy reactions. In the low energy reaction the initial nuclei fuse to form an excited system that then de-excites by losing a few light particles. This behaviour seems to occur commonly for impact parameter b<4 fm.

In all the reactions discussed thus far there has been light particle

emission from the excited system after the collision. It is of interest to examine the time dependence of this emission. There are a number of possible definitions for particle emission, but the one chosen here is based on local density. If the local density in the vicinity of a nucleon falls below a cutoff of 0.07 fm^{-3}, the nucleon is said to be emitted. The time dependence of the nucleon emission rate for a Ca+Ca reaction at 25A∘MeV is shown for both b=0 and 6 fm in Fig. 5.5. The semilog plot shows the initial increase of emission as the nuclei overlap, followed by the exponential decay of the rate after maximum overlap. As expected, total nucleon emission is greater in the central collision, where more of the bombarding energy is transferred into internal excitation energy of the nuclei.

From Fig. 5.5 one can also extract an emission lifetime from the slope of the decay portion of the curve. Both reactions exhibit a long time emission lifetime of $9x10^{-23}$ seconds. However the central collision also has a short lifetime component of $3x10^{-23}$ seconds not found in the peripheral collision. This additional component is due to the rapid emission of particles during the initial violent impact of the target and projectile of the central collision, not found in the peripheral reaction. The long lifetime component corresponds to quasiequilibrium emission of nucleons for low excitation energy systems found with peripheral collisions and with central collisions after the energy loss associated with the initial rapid particle emission.

On the long time scale there are many other possible channels for decay of an excited nuclear system. Some of these processes can be described within

the context of this model, but certainly not all. On the long time scale one also needs to consider, for example, photon production, quantum tunneling of particles through the Coulomb barrier and fission processes. Although one could try to include some of these processes in the model, computer resources do not exist to run even the simpler QPD model to those times. Since most of the far-from-equilibrium processes have disappeared by 250 fm/c it makes sense to take the output of the QPD code and use it as input for a statistical decay code, in order to see these very long time decays.

In summary the time scales have been determined for several processes associated with the initial impact and separation phase of low and intermediate energy reactions. From Figs 5.2 and 5.4 it is seen that a quasiequilibrium state is reached between 150-250 fm/c. The QPD model lends itself to computer simulation up to this reaction time; however, much longer processes are out of the reach of this method. Nevertheless, after 250 fm/c these systems have relaxed sufficiently that more a efficient statistical method, such as one of the models reviewed by Das Gupta and Mekjian [DM81], could be used.

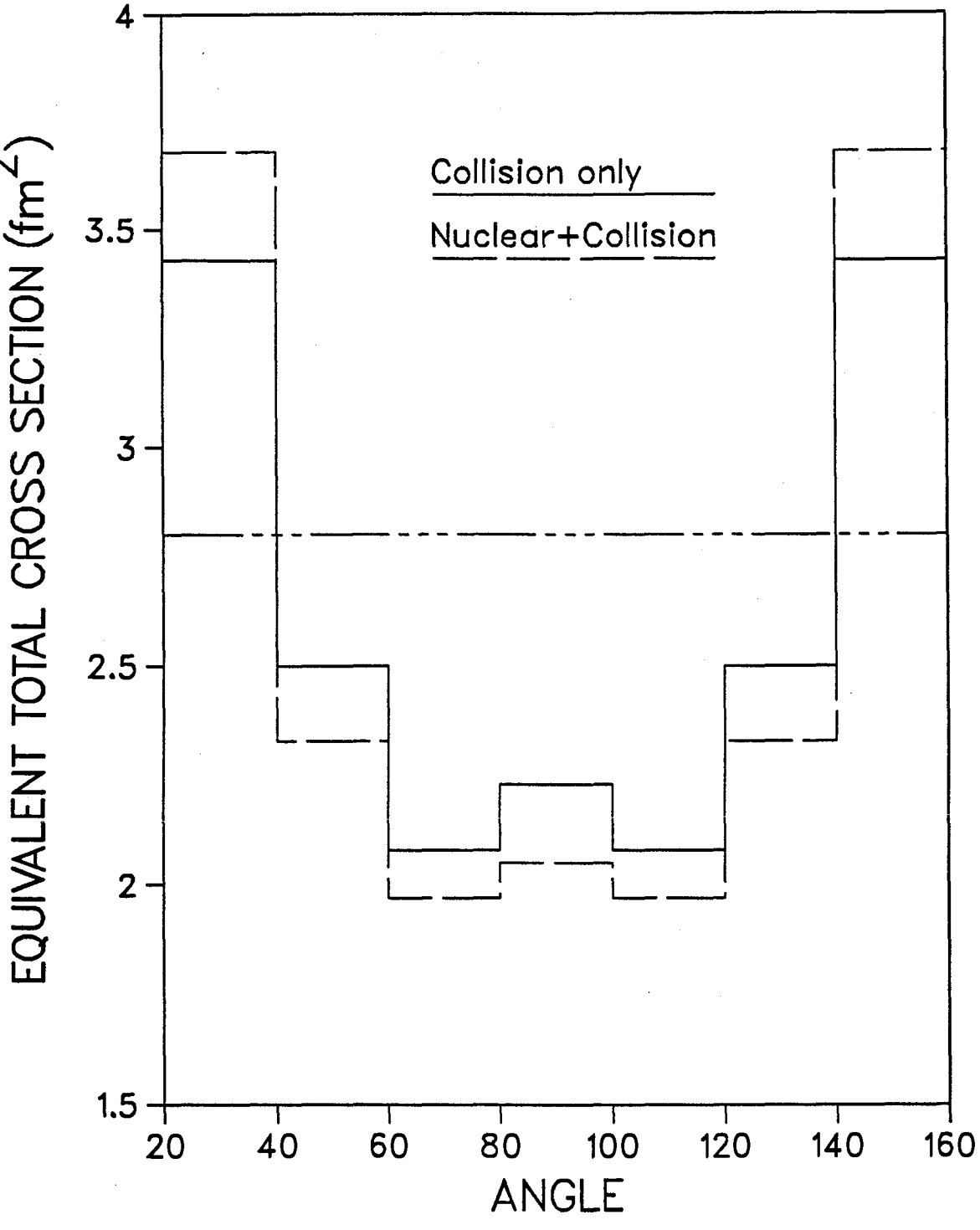

Fig. 5.1 Associated total NN cross section for the QP model with collision term (QPD). The cross section is calculated using a QPD simulation. The full curve is from the scattering term only, while the dash curve includes the scattering term plus the nuclear potential.

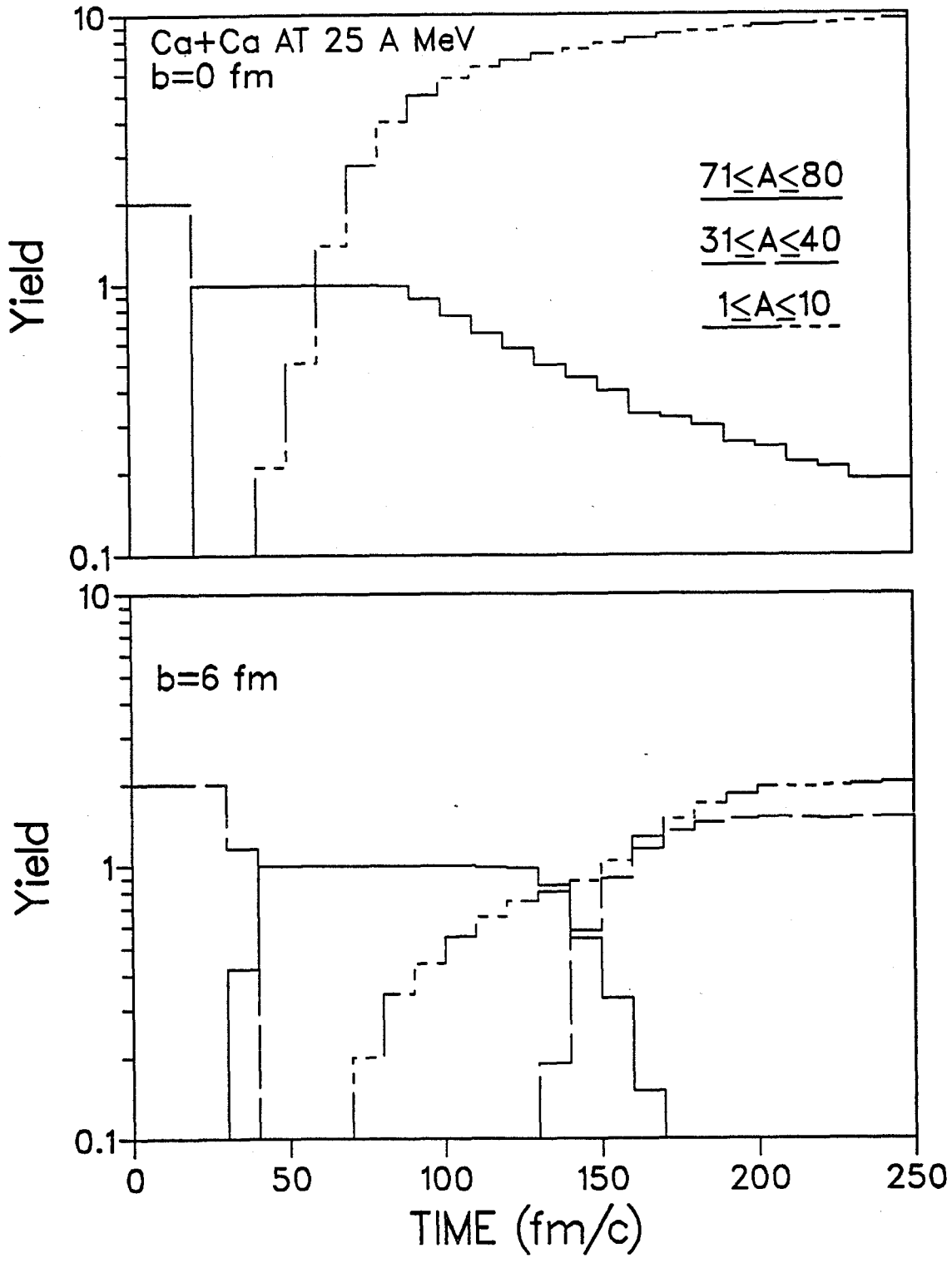

Fig. 5.2 Time dependence of the fragment mass distribution in a Ca+Ca reaction at 25A∘MeV for b=0 fm (top) and b=6 fm (bottom). Three mass bins are used in the figure, 1-10, 31-40 and 71-80 mass units.

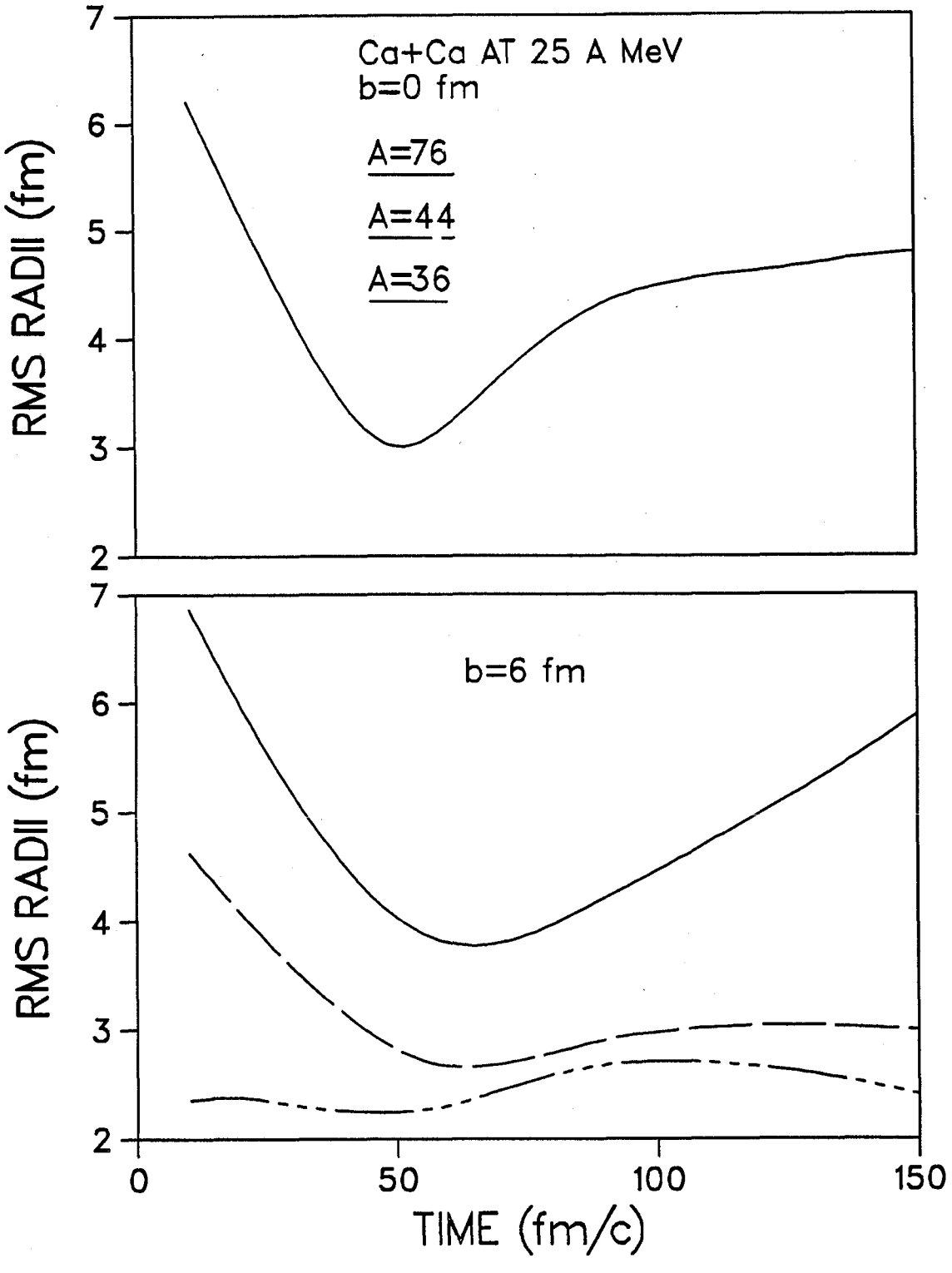

Fig. 5.3 Time dependence of the RMS radii of the nucleon positions of various fragments of fixed mass in a Ca+Ca reaction at 25A∘MeV for b=0 fm (top) and b=6 fm (bottom). The masses chosen for display are: 36, 44 and 76. See text for description of how the radii are determined.

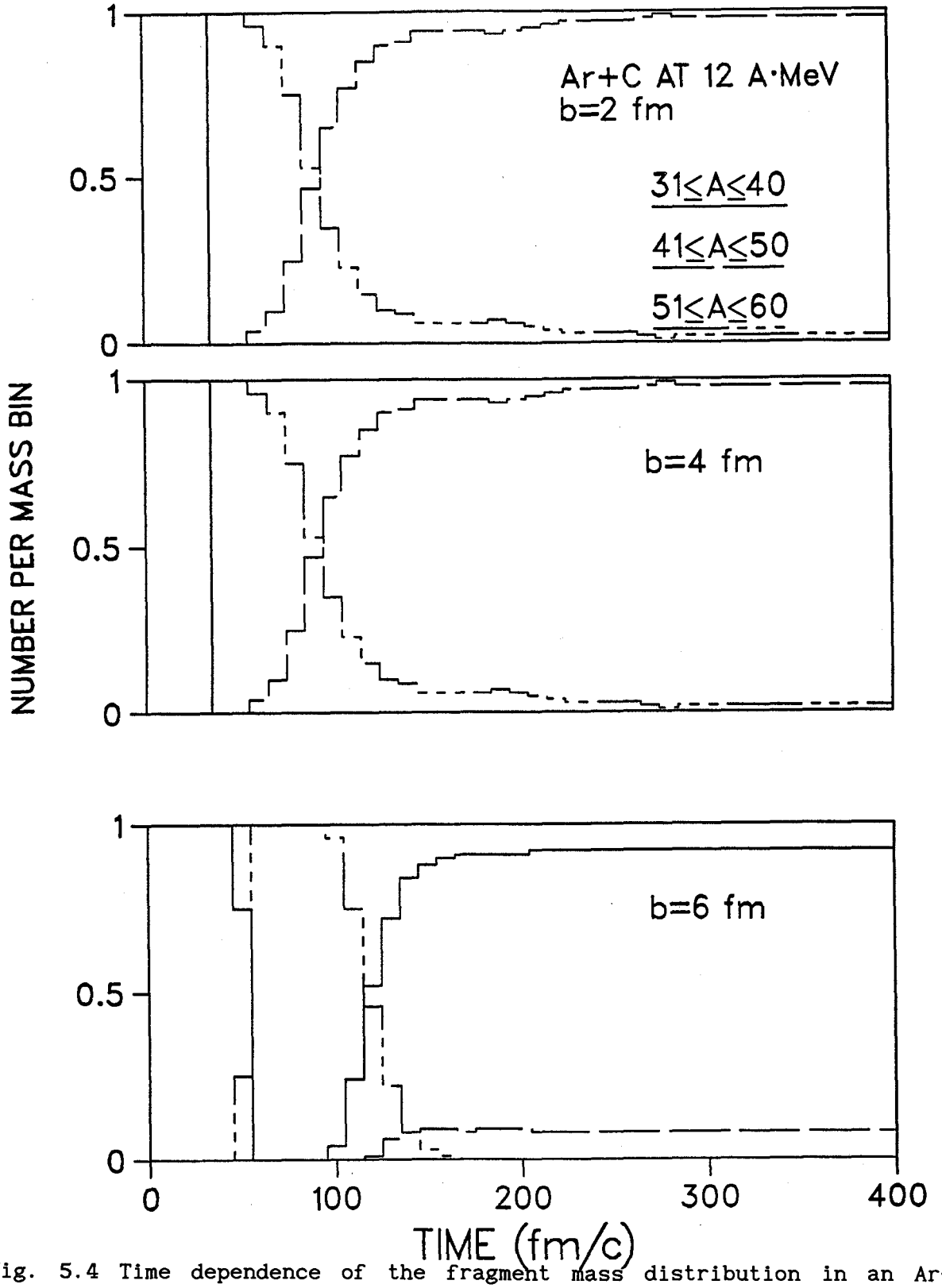

Fig. 5.4 Time dependence of the fragment mass distribution in an Ar+C reaction at 12A∘MeV for b=0 (top), 4 (middle) and 6 fm (bottom). Three mass bins are used in the figure, 31-40, 41-50 and 71-80 mass units.

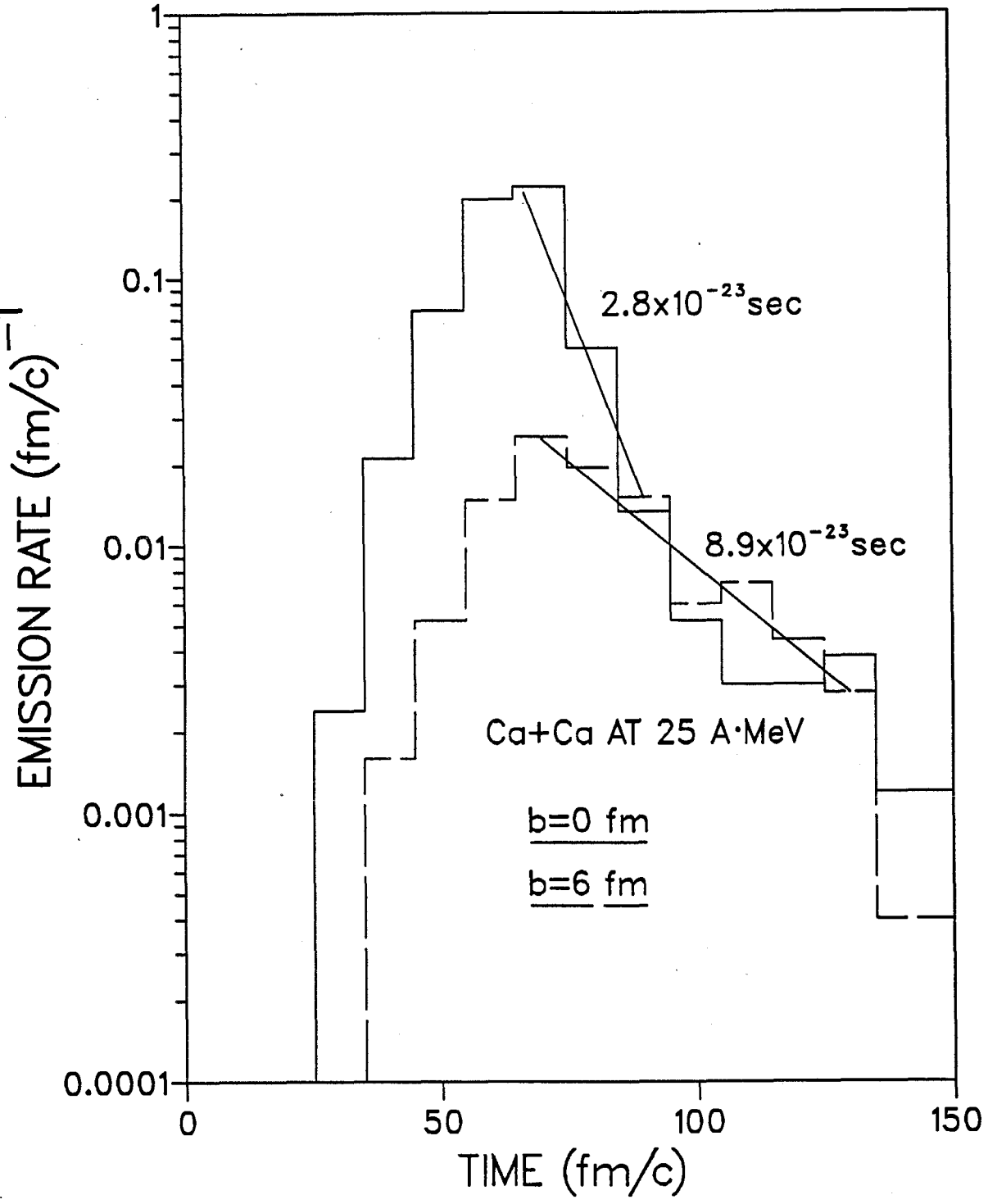

Fig. 5.5 Time dependence of nucleon emission rates for the two reactions of Fig. 5.2. A nucleon is considered "emitted" when the average local density around it falls below 0.07 fm for the first time.

VI TEMPERATURE MEASUREMENT

VI.1 Introduction

In Chapter I we introduce the concept that short lived composite systems formed in a nuclear reaction can be described in terms of a quasiequilibrium system. Although such a simplification would be most welcome, its justification is unclear. Nevertheless the notion is popular and begs the questions: If the system has thermalized, what is its temperature and how would it be measured? A number of experiments have been performed to address the question of temperature in nuclear reactions. The focus of this chapter is not to address the question of thermalization directly, but to make a connection with the analysis of experimental data based on the thermal equilibrium assumption. The temperatures we extract from our simulation, as well as the temperatures extracted from the experiments, may not be temperatures at all; however, for the purposes of this chapter and to make comparison with experiment, we will call them temperatures.

One of the common ways to extract a temperature from the data is to fit a Maxwell-Boltzmann distribution as observed in a moving frame to the single particle kinetic energy spectra [DM81]. The fit yields the velocity of the frame and a temperature. We call this the kinetic temperature (T_K).

A number of years ago an alternate method for determining the temperature was proposed based on the excitation energy distribution of the fragments produced in the reaction [Mor84]. If the distribution were thermal, one

could extract a temperature by fitting a Boltzmann distribution to the data. We call this the chemical temperature T_E^*.

Both of the above methods extract a temperature by fitting a distribution function to the data. The virtue of the kinetic energy method is that it leads to an analytic form of the associated thermal distribution function, whereas the thermal distribution of the excitation energy is not known analytically. Despite this virtue of the kinetic temperature, the chemical temperature is probably a better measure of the thermal energy in the system. We address this issue later in the chapter.

In the Hamiltonian of the system there is no coupling between the centre of mass motion of a fragment and its internal degrees of freedom. The decoupling of the centre of mass motion and excitation energy causes the kinetic and chemical temperatures to be statistically independent. Despite being independent, if the system were indeed in thermal equilibrium the two temperatures would have the same value. This is not observed in the experiments that have been performed. The kinetic temperature is found to be much larger than the chemical temperature [GB87], normally by a factor of four [Blo86,Po85a,Po85b] but factors of ten have been observed [Mor84,Mor85].

The temperature determination in nuclear reactions is confused by a number of factors. The system is expanding and hence, in principle can not be in thermal equilibrium. The hope in doing the thermal analysis of experimental data, is that the system is expanding sufficiently slowly so that it remains in a quasiequilibrium state and can be characterized by

some time-dependent temperature. As the system expands it reaches a point, called the freeze-out point, where the interfragment separation exceeds the range of the nuclear force. Past the freeze-out point, the individual fragments may have a distribution of excitation energies which is similar to a thermal equilibrium distribution, but the system as a whole cannot stay in thermal equilibrium because of the decoupling of the fragments. The temperature of a fragment species is then a measure of the temperature of the entire system at the time the fragment breaks away from the system (denoted by T_f).

Extraction of T_f, would be experimentally possible if the fragment distribution function remained fixed after freeze out. To some extent this is true; however long time decays tend to alter these distribution functions [Po85a,Po85b,Fie87,HS87]. It is also possible to perform a model dependent analysis [Blo87,Che87] of the data to try to remove the effect of the long time decays, but its removal has only a small effect on the predicted temperature and is not sufficient to explain the differences between the kinetic and chemical temperatures.

The QPD model is well suited to explore the temperature questions in nuclear reactions. First, it is sufficiently fast numerically that enough events may be propagated past the freeze-out point to have reasonable statistics. Secondly the model has well-defined ground states so excitation energies can be examined.

To investigate the general features of the temperatures in a nuclear reaction, Ca+Ca reactions are studied. The reaction is simulated at 35A∘MeV

and 100A◦MeV bombarding energies. Only central collisions are investigated since these produce the most fragments, and hence the best statistics. Also for statistical reasons, only ^{4}He and ^{6}Li fragments are considered, because of the relatively high number of these fragments produced.

VI.2 EXCITATION ENERGY DISTRIBUTIONS

To determine the temperature of a given mass fragment, information is needed about its excitation energy distribution. As mentioned in the introduction, the excitation energy distribution function is not known explicitly, so a Monte Carlo procedure is used to extract this information. The ^{4}He nucleus that we consider is the one in which the sum of the proton spin and the sum of the neutron spin both vanish. The ^{6}Li we consider has spin such that the magnitudes of the sum of the proton spin and the sum of the neutron spin are both equal to 1/2 (which is denoted by ^{6}Li(1/2,1/2)).

As discussed in Chapter III, the inclusion of the Pauli potential requires that the full phase space Monte Carlo procedure be used. Parenthetically, ^{4}He has no Pauli term, because of the pairing of the spins, so it would be possible to simplify the procedure by doing the momentum space integrals analytically. However the ^{4}He nucleus is sufficiently small that the full phase space Monte Carlo is not computationally taxing and evaluating the statistical properties of this nucleus via the full phase space Monte Carlo also provides a way to check the procedure against some analytic results.

In designing the Monte Carlo algorithm one must keep in mind the comparison that is to be made. In this study we wish to extract a temperature by

comparing the excitation energy distribution of a given type of cluster produced in a reaction with the excitation energy distribution of the same type of cluster generated via Monte Carlo. The excitation energy is just the excess of the internal energy (i.e. the energy as measured in the frame where $P_{tot} = 0$) over the ground state energy. To look at this distribution the Monte Carlo algorithm must consist of moves that keep $R_{cm}=0$ and $P_{tot}=0$. As well, the algorithm must keep the cluster intact since it is the temperature of a cluster of a given mass that is sought.

A trial Monte Carlo move is made by first selecting a particle. Then a new phase space coordinate for the particle is drawn from a uniform distribution in phase space centred at the old phase space coordinate with a width of 0.6fm and 60 MeV/c for each of the position and momentum coordinates respectively. The centres of mass and momentum are kept fixed by shifting the entire system in phase space such that $R_{cm}=0$ and $P_{tot}=0$. The new move is rejected if it causes the cluster to break up. (see section V.3 for the definition of a cluster). The final rejection or acceptance is just the standard Metropolis algorithm. The new configuration is unconditionally accepted if the change of energy of the system δE is less then zero and accepted with probability $exp(-\delta E/T)$ if $\delta E > 0$. Of course all probabilistic variables are in fact only pseudorandom. After each 50 sweeps of the total system, the configuration is stored, which is ample separation to insure that the samples are uncorrelated.

At least 10,000 samples are generated at each temperature. The 500,000 sweeps made at each temperature is more than what is needed in this study, but the systems are small and hence us give the opportunity to make

statistical uncertainties very small. For the Monte Carlo work described in the next chapter, the large system sizes make it computationally prohibitive to make as many sweeps.

Using this Monte Carlo method the average kinetic and excitation energy per nucleon for the ^{4}He cluster can be calculated. The results of this calculation are presented in Fig. 6.1. Since there is no Pauli term in the Hamiltonian for ^{4}He, it is easy to evaluate the expectation of the kinetic energy analytically. The Hamiltonian is quadratic in the momentum, so each momentum degree of freedom contributes $\frac{1}{2}T$ to the kinetic energy (note we have set the Boltzmann constant, k_B, to equal unity, so T has units of energy). The number of momentum degrees of freedom equals 3A-3 (with the 3 degrees of freedom removed to account for fixing $P_{tot} = 0$). For ^{4}He, A=4, so the kinetic energy per nucleon $\langle KE/A \rangle = \frac{9}{8} T$. This dependence is indicated in Fig. 6.1 by the solid straight line, which is consistent with the Monte Carlo data. As a function of temperature the excitation energy rises faster than the kinetic energy because of the presence of the potential term. At low temperature the quasiparticles make only small displacements from their ground state values and it is possible to evaluate the low temperature dependence of the excitation energy by expanding the Hamiltonian in a second order Taylor expansion. Doing this, we find the average excitation energy per nucleon, $\langle E^*/A \rangle \approx \frac{9}{4} T$, for small T. Similar results can be obtained for ^{6}Li and are presented in Fig. 6.2

The extraction of a temperature from a heavy ion collision using the excitation energy distribution of the fragments is complicated by the finite lifetimes of some fragments. The decays of these fragments can

alter the energy distribution from the distribution at emission, and hence the measured temperature. Some of the possible decay processes and their threshold energies for ^{4}He and ^{6}Li are shown in Table 6.1.

Reaction	E^*/A (MeV)
$^{4}He \longrightarrow n + {}^{3}He$	3.11
$^{4}He \longrightarrow {}^{2}H + {}^{2}H$	3.53
$^{4}He \longrightarrow 2n + 2p$	6.24
$^{6}Li \longrightarrow {}^{2}H + {}^{4}He$	0.99
$^{6}Li \longrightarrow {}^{3}H + {}^{3}He$	1.79
$^{6}Li \longrightarrow 3n + 3p$	6.06

TABLE 6.1: Threshold values of the excitation energy per nucleon for selected reactions of computational ^{4}He and ^{6}Li(1/2,1/2).

One can see that both nuclei are completely unbound for excitation energy over 7 MeV per nucleon, and there are possible decay channels for lower energies. If the decay processes were well understood, the large time energy distribution could be used to find the post-emission distribution and hence the temperature. Another approach is to focus on an excitation energy distribution in the range of energy where the fragments are long lived (compared to the time of observation). Though this is not the complete distribution, there is sufficient information to extract a temperature from it.

To determine the energy range needed to extract a temperature, the lifetimes of various energy ^{4}He fragments are examined. To do this, the ^{4}He configurations generated in the Monte Carlo simulation are grouped

according to excitation energy into 1A∘MeV bins and then propagated (using the molecular dynamics code) for 250 fm/c. A cluster search is performed every 10 fm/c to determine if the cluster is still connected. The time dependence of the fraction of connected clusters for various energy bins is shown in Fig. 6.3.

One clearly sees from Fig. 6.3 that the lifetime of ^{4}He depends upon excitation energy. For energies less than the energy of the lowest decay mode (3.11 MeV per nucleon), the nuclei are stable, as expected. For energies larger than the first decay mode, but less than the energy of vaporization (6.24 MeV per nucleon), the decay process appears to have two components: one that decays on an intermediate time scale and another with a very long lifetime. For ^{4}He nuclei, the 4-5 MeV per nucleon excitation energy bin shows the intermediate component has a lifetime of 220 fm/c. It is not possible to tell if the lifetime of the long lived component is finite from the data shown in Fig. 6.3 . However there is enough energy to allow the ^{4}He to decay, so all components in this energy range must have a finite lifetime. For energies above the vaporization threshold the nuclei are short lived, as depicted by the 6-7 MeV per nucleon bin, with a lifetime of 28 fm/c.

The above discussion on lifetimes indicates that excitation energies of less than 6 MeV per nucleon will be in the range of interest for extracting a temperature from the reaction data. States in this energy range are sufficiently long lived, compared to the reaction times of 100-200 fm/c, that the distribution of states is not altered appreciably by decays. It is useful in extracting a temperature from a reaction system to calculate the

expectation of the excitation energy subject to the constraint that $E^*/A <$ 6 MeV (denoted by $\langle E^*/A \rangle_c$). This expectation is calculated via Monte Carlo simulation for both ^{4}He and ^{6}Li(1/2,1/2) as a function of temperature with the results shown in Fig. 6.4.

In extracting a temperature for the reaction data it is assumed that the excitation energy distribution of the fragments is a Boltzmann distribution. To check this assumption, the excitation energy distribution function is calculated so that a comparison to the reaction data can be made. The distribution functions for both ^{4}He and ^{6}Li at temperatures of 2, 3 and 4 MeV are calculated and shown in Figs. 6.5 and 6.6. Because only a finite number of samples can be generated in a Monte Carlo simulation, the distribution function has been binned into 1 MeV per nucleon intervals to improve statistics. Furthermore the range displayed only focuses on the energies of interest (0-6 MeV per nucleon); however the distribution does fall off exponentially for higher energies as expected. The figures indicate reasonable agreement between the distribution seen in the reaction simulation and the distribution obtained for a system in thermal equilibrium.

VI.3 Temperature Determination

In this section the temperature is extracted from simulated reactions using the excitation energy distributions of ^{4}He and ^{6}Li, as presented in the previous section. The reactions which are studied are Ca+Ca collisions at impact parameter b=0 and bombarding energies of 35A$\cdot$MeV and 100A$\cdot$MeV. We choose these two reactions to be typical of the experimental systems

investigated so far. A total of 7000 events are generated at 35A∘MeV and 4500 events at 100A∘MeV. The higher multiplicity of the 100A∘MeV reaction over the 35A∘MeV reaction allows one to maintain the same statistics with fewer events.

The excitation energy distributions of these fragments are shown in Fig. 6.5 and 6.6, respectively, for a reaction time about 100 fm/c after maximum overlap of target and projectile Ca nuclei. In Table 6.2 the number of ^{4}He and ^{6}Li clusters at time t=150 fm/c is shown. The trend to notice is that the sample size increases with increasing bombarding energy but decreases with increasing emission angle and fragment mass.

As a probe of the degree of thermalization of the system, the angular dependence of the excitation and kinetic energies (and their associated temperatures) is considered. If the system is completely thermalized these quantities should be independent of angle. The angular dependence is studied by separating the fragments into two angular bins, one covering 0-60 degrees and the other 60-120 degrees.

Cluster Type	Bombarding Energy (A∘MeV)	Sample size between angles 0 - 60°	60 - 120°	Number of Events
^{4}He	35	375	27	7000
	100	1191	205	4500
^{6}Li	35	80	2	7000
	100	421	49	4500

TABLE 6.2: Summary of sample sizes of ^{4}He and ^{6}Li reaction products for various bombarding energies and emission angles at time t=150 fm/c subject to the cut $E^{*}/A < 6$ MeV.

A maximum likelihood estimate [Fre71] (MLE) $\hat{T}$ is made for both kinetic and chemical temperatures of the system, by assuming a Boltzmann distribution. (See Appendix B). For a collection of n nuclei of the type of interest (i.e. ^{4}He or ^{6}Li) the MLE of the kinetic temperature $\hat{T}_K$ is given by solving the equation,

$$\bar{K} \equiv \frac{1}{n}\sum_{i=1}^{n} K_i = \langle K(\hat{T}_K)\rangle = \frac{3}{2}\hat{T}_K \qquad (6.1)$$

where K_i is the center of mass kinetic energy of the i^{th} nucleus and <...> denotes an expectation with respect to the Boltzmann distribution. The evaluation of the expectation of a random variable with respect to the Boltzmann distribution is in general difficult; however, the expectation of center of mass kinetic energy is easy to calculate analytically and its value is shown in Eq. 6.1 as well.

The MLE of the chemical temperature $\hat{T}_E^*$ is given by

$$\bar{E}^* \equiv \frac{1}{n}\sum_{i=1}^{n} E_i^* = \langle E^*(\hat{T}_K)\rangle \qquad (6.2)$$

where E_i^* is the excitation energy of the i^{th} nucleus, drawn from an n-fold sample of nuclei satisfying the constraint that $E_i^* < 6$ MeV per nucleon. Unlike the kinetic energy, an analytic expression for the expectation of the excitation energy is not easy to obtain. In order to evaluate the RHS of Eq.6.2 a Monte Carlo procedure is used, as described in the previous section. The temperature dependence of $\langle E^*/A\rangle_c$ is shown in Fig. 6.4.

In this study we examine not only the dependence of these temperatures on

bombarding energy, emission angle and fragment species (all of which are measurable in a reaction experiment) but the time dependence of the temperatures as well. The examination of the time dependence provides insight, not accessible by experiment, into the reaction mechanisms responsible for the setting of these temperatures. The time dependence is explored by calculating the MLE $\hat{T}$ every 10 fm/c. During the first part of the reaction the statistics associated with $\hat{T}$ are poor because of the small number of fragments present, however as the reaction proceeds the number of fragments grows and statistics improve. Fig. 6.7 shows the relative number of ^{4}He nuclei as a function of time for several Ca+Ca reactions.

The temperatures from ^{4}He emitted at wide angles during a 100A$\cdot$MeV Ca+Ca reaction are considered first. In Fig. 6.8 the time dependence of both kinetic and chemical temperatures are shown. The features to notice are: the chemical temperature is nearly constant with time, the kinetic temperature has a strong initial time dependence (but this dependence vanishes for large time), and the chemical and kinetic temperatures differ greatly for all times. The asymptotic values of the temperatures set in at approximately 100 fm/c, roughly corresponding to the freeze-out time of the composite system (see Fig 6.9 for a pictorial representation of the system before and after freeze-out). Furthermore, these asymptotic values are approximately the temperatures observed experimentally. We conclude from the simulation data that the difference between the kinetic and chemical temperatures is established relatively early in the reaction (50-100 fm/c after the initial impact). Although long term decays are not needed to explain the temperature difference, they may lead to further changes in the energy distribution of the fragments, and hence changes in the

temperatures.

Now consider the effect of emission angle on the temperature. The upper part of Fig. 6.10 shows the temperatures for the same reaction as considered above, except now ^{4}He fragments at forward angles are examined instead. The qualitative features of Fig. 6.10 are the same as Fig. 6.8: the chemical temperature is nearly constant with time, the kinetic temperature has a strong initial time dependence, but the dependence vanishes for large time, and the chemical and kinetic temperatures greatly differ. From a quantitative examination we see the kinetic temperature at forward angles is much greater than the wide angle temperature but the chemical temperature has changed very little from its wide angle value.

To address the question of the dependence of the temperature on species, consider the energy distribution of the ^{6}Li fragments in the same reaction as discussed in the two previous paragraphs. A complete comparison is not possible because the total number of ^{6}Li fragments produced is much smaller than the number of ^{4}He; in particular there are too few ^{6}Li at wide angles to have sufficient statistics to extract a temperature. However, the situation for forward angles is not as bad, and a temperature can be extracted from the ^{6}Li nuclei. Fig. 6.10 shows both kinetic and chemical temperatures as determined at forward angles. The same qualitative features exist as seen in the previous temperature plots. Note also the close agreement of the upper (^{4}He) and lower (^{6}Li) parts of Fig 6.10, which reflects the insensitivity of the temperatures to species type.

Finally, the dependence of the temperature on bombarding energy is

considered. Experimentally, it is observed that the chemical temperature shows very little bombarding energy dependence [Che87]. To make a comparison, Ca+Ca reactions at bombarding energies of 35A∘MeV and 100A∘MeV are simulated. The kinetic temperatures, as expected, show a strong bombarding energy dependence whereas the chemical temperatures, in agreement with experiments, show very little dependence on bombarding energy as shown in Fig. 6.11.

Examination of the energy distribution of the fragments is, at best, an indirect probe of the temperature. Although a more direct method doesn't exist for experiment, one can conceive of more direct ways of determining temperatures in simulation studies. With a direct method one could consider the temperature of some local region in space and see if it is reflected in the emission products. For instance, consider the temperature around the position of the centre of mass (i.e. within a volume defined by $|R-R_{cm}| < 4$ fm). As a probe of the local temperature, the expectation of the transverse kinetic energy of free nucleons (i.e. those which are not bound in clusters) is used. The free nucleon approximation enables us to neglect the momentum dependence of the Pauli potential, making it easy to perform the expectation integrals. The temperature is then simply given by $\langle P_{\perp}^2/2m \rangle$ where $P_{\perp}$ is the momentum of a nucleon in the direction transverse to the beam. This expression is strictly true only after the system has relaxed to equilibrium. By considering the transverse motion the bias associated with the energy in the beam direction is at least partly removed and thereby provides a better measure of the thermal energy of the system. (The time dependence of temperatures in a model expanding system has been investigated analytically in [Aic83]).

The results of the transverse kinetic energy analysis are shown in Fig. 6.12. Notice that this kinetic temperature is much lower than the previously calculated kinetic temperature. Furthermore, its value of 3 MeV near the break-up time is not very different from the chemical temperature. As the system continue to expand there is a cooling of the central region below the 3 MeV value. This is consistent with the picture that the chemical temperature is set near the time of break-up.

VI.4 Discussion and Summary

The results presented in this chapter describe a physical picture very different than the quasiequilibrium description. A simple quasiequilibrium picture requires the kinetic and chemical temperatures to be the same. Furthermore, an equilibrium state should have no knowledge of its initial conditions therefore the temperatures should be independent of emission angles, which though true for the chemical temperature is certainly not the case for the kinetic temperatures. Some refinements of the quasiequilibrium picture have been advanced in an attempt to explain these discrepancies. One suggestion [Boa84,Blo88] is that as the composite system of target and projectile undergoes a free expansion, the temperature in a local co-moving frame drops. The difference between the kinetic and chemical temperatures can be explained by imagining that these temperatures represent the state of the system at different times. This explanation can only account for the difference in the measured kinetic and chemical temperatures, it is not intended to explain the angular dependence of the kinetic temperature. The chemical temperature, on the other hand, may in

fact reflect a true temperature of the system. First, it shows little emission angle dependence. Second, if we examine the excitation energy distribution of the fragments and compare it to the Monte Carlo data (see Fig. 6.5 and 6.6), there is a rough agreement. Although an observable of a system exhibiting a Boltzmann distribution does not imply a thermal equilibrium, (i.e. it is only a necessary condition not a sufficient condition), it is suggestive that the observable reflects the thermal component of the system.

The picture that we are advancing is based on the vague notion that there are thermal and nonthermal components of the system. For example, consider the two incident nuclei long before they collide. Each of these nuclei is in its ground state and represents a T=0 configuration. Although there is no thermal energy in the system, the total energy is certainly above its minimum value. This energy excess is associated with the kinetic energy of the relative motion of the nuclei toward each other. We associate this directional motion and related energy with the non-thermal component of the system. Upon impact the non-thermal energy begins to be converted into thermal energy. If this conversion process is fast enough (compared to the expansion of the system), or if the collision products were confined to a box, all of the energy associated with the directional motion would be converted to thermal energy. How to define, let alone measure, the thermal and non-thermal components of the energy during the relaxation period to equilibrium is not clear. The idea that we use is that the non-thermal energy of the system is associated with the directed motion (i.e. motion of the centre of mass, relative motion of two approaching nuclei, radial motion of expansion, etc) and the thermal energy is associate with the more

random motion of the particles after the directional motion has been removed.

It is argued above that the chemical temperature is a measure of the thermal energy of the system at the break-up point. Both experiment and this simulation show this temperature to be on the order of 3 MeV, independent of bombarding energy. This would imply, from Fig. 6.1, an energy of approximately 6.5 MeV per nucleon. This is on the order of the total excitation energy per nucleon (as measured in the centre of mass) of 8.75 Mev for the 35A∘MeV reactions and certainly below 25 MeV for the 100A∘MeV reactions. Therefore, for at least the 100A∘MeV reaction, at the time of breakup a large portion of the energy must be non-thermal.

In summary, we have used a computational model which possesses a well defined nuclear ground state to investigate the problem of temperature measurement in heavy ion collisions. The model is used in a Monte Carlo calculation to evaluate the fractional distribution of excitation energy of ^{4}He and ^{6}Li as a function of temperature. These distributions, in turn, are used to extract a temperature from a simulation of a heavy ion reaction. The reaction studied is Ca+Ca at fixed impact parameter and bombarding energies of 35A∘MeV and 100A∘MeV. The temperatures extracted from the simulation show the same characteristics as are observed experimentally: the chemical temperature have a value of 2.5-3.5 MeV - much lower than the kinetic temperatures and vary only slowly with bombarding energy. By examining the time dependence of the temperature, it is clear that the differences are established early in the reaction. Decays on the of order 10^{-21} seconds are not needed to produce this effect. We conclude

that a significant portion of the bombarding energy has not been thermalized. We proposed that the large kinetic temperatures do not reflect a temperature of the system but simply indicate the large amount of energy associated with directed motion.

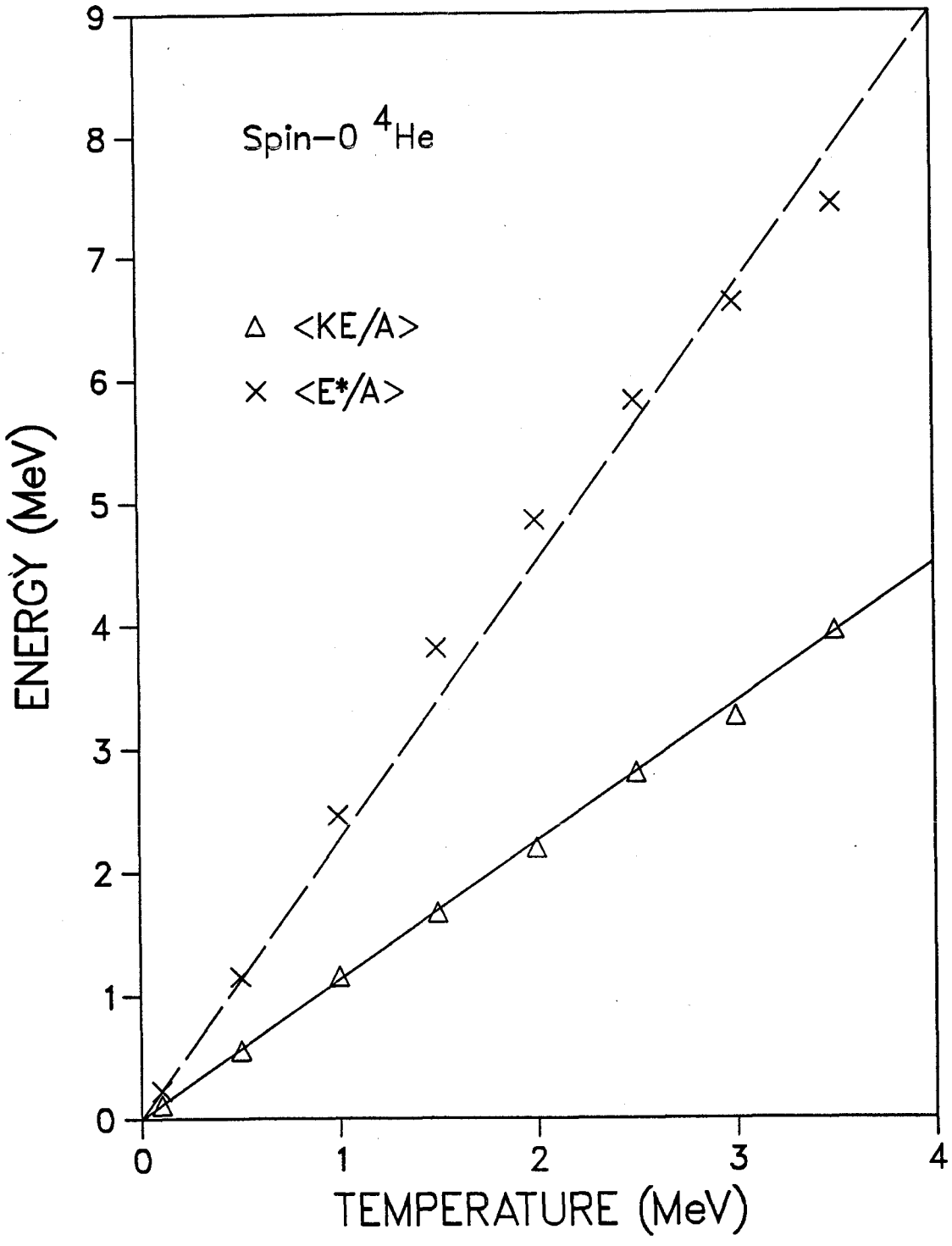

Fig. 6.1 Calculated kinetic energy per nucleon and excitation energy per nucleon as a function of temperature for computational zero spin ^{4}He nuclei.

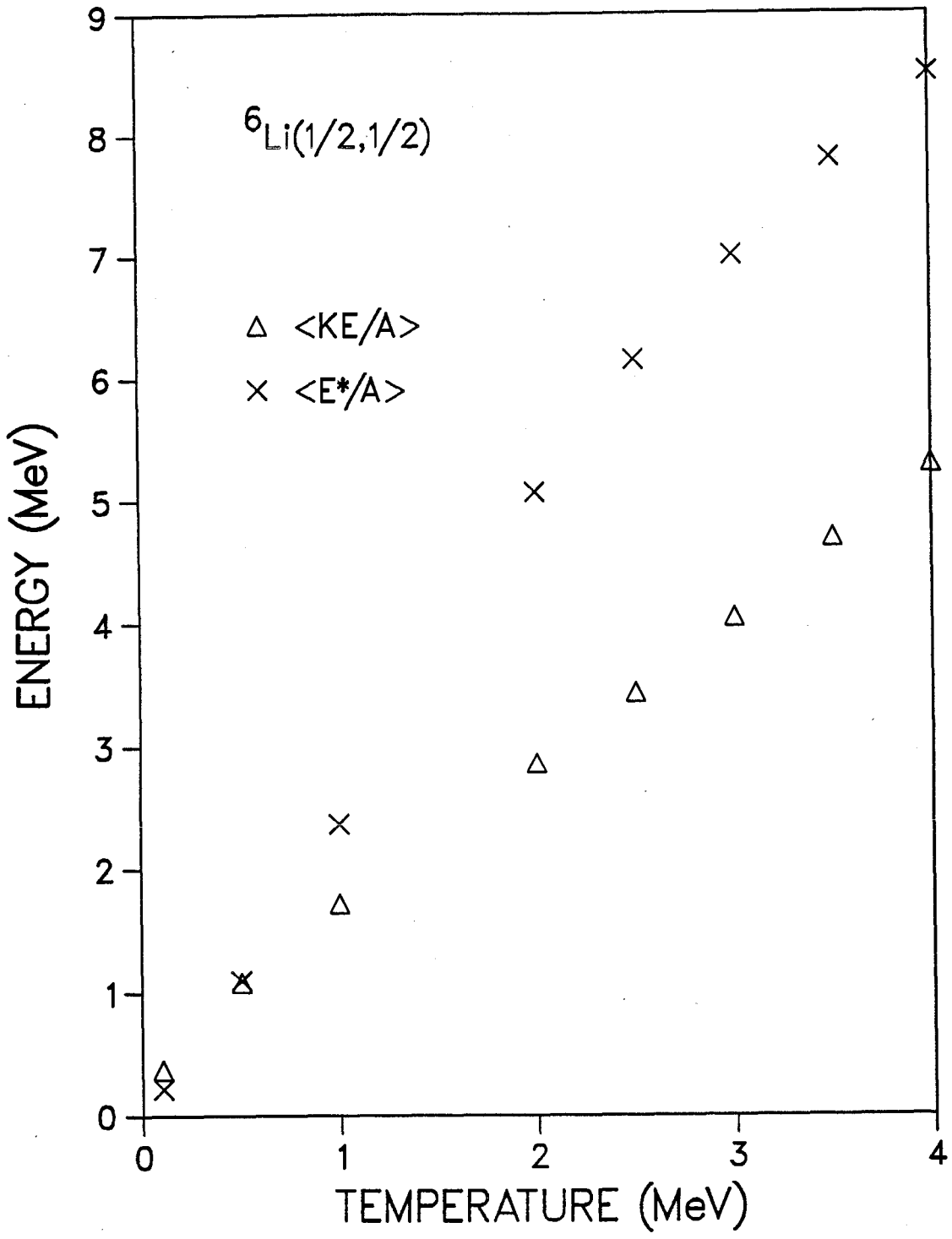

Fig. 6.2. Calculated kinetic energy per nucleon and excitation energy per nucleon as a function of temperature for computational ^{6}Li(1/2,1/2).

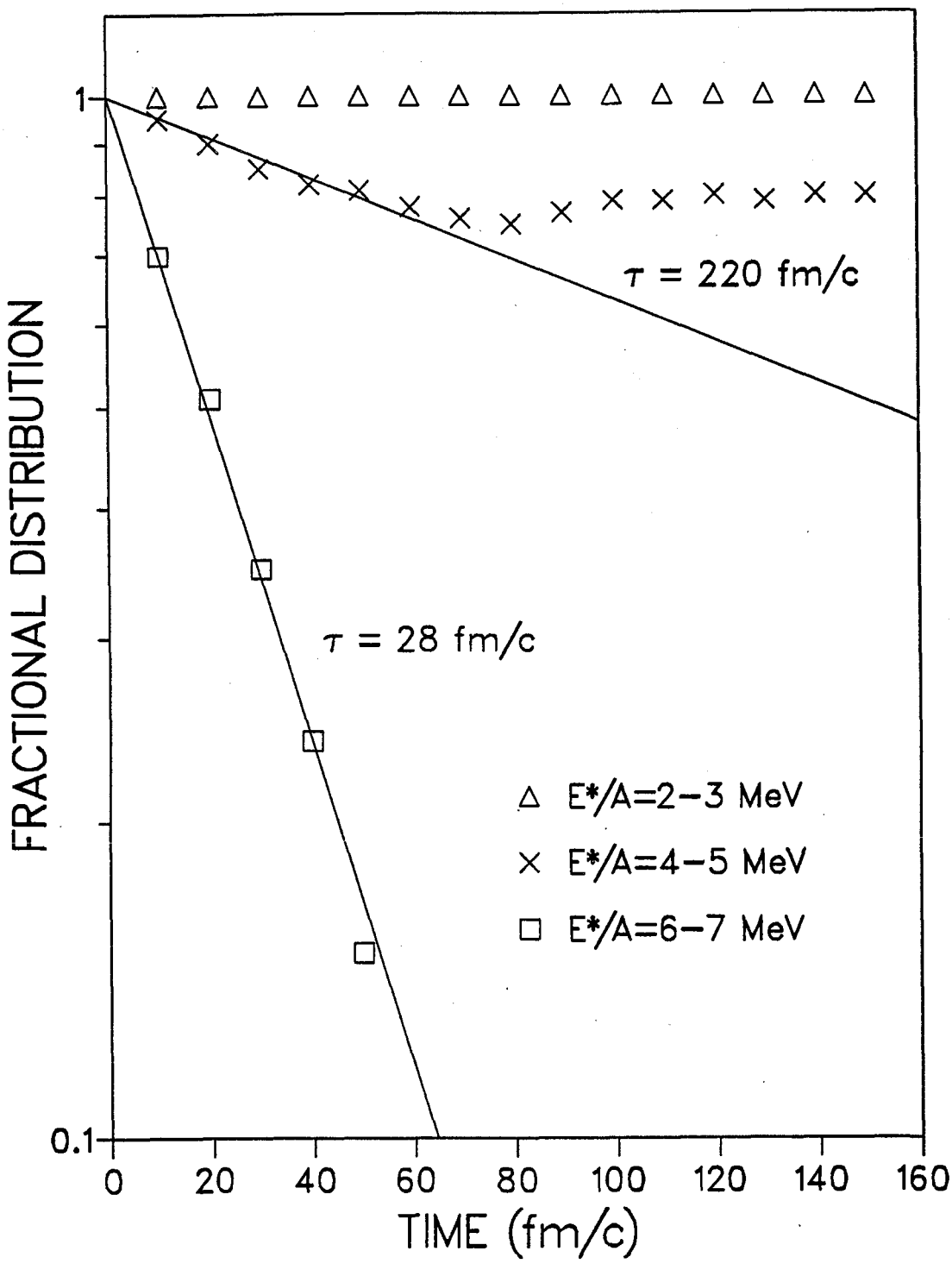

Fig. 6.3. Time dependence of the population of ^{4}He nuclei with various initial excitation energies: 2-3 A∘MeV (symbol Δ), 4-5 A∘MeV (symbol x) and 6-7 A∘MeV (symbol □). The initializations are chosen randomly from the phase space associated with a temperature of 2 MeV subject to the cluster connection constraint.

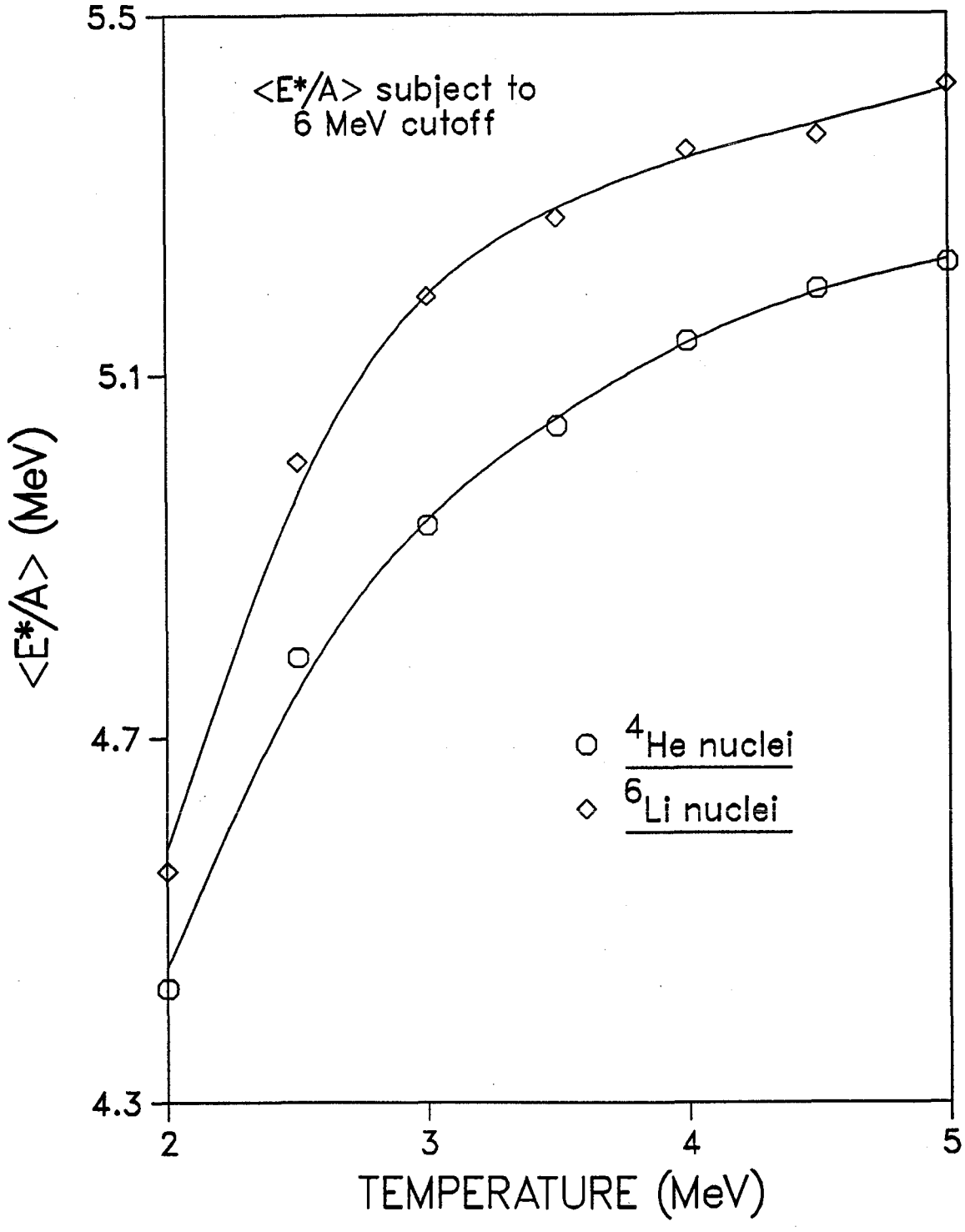

Fig. 6.4. Calculated average excitation energy per nucleon subject to 6.0 MeV cutoff for ^{4}He and ^{6}Li in their ground state spin configurations.

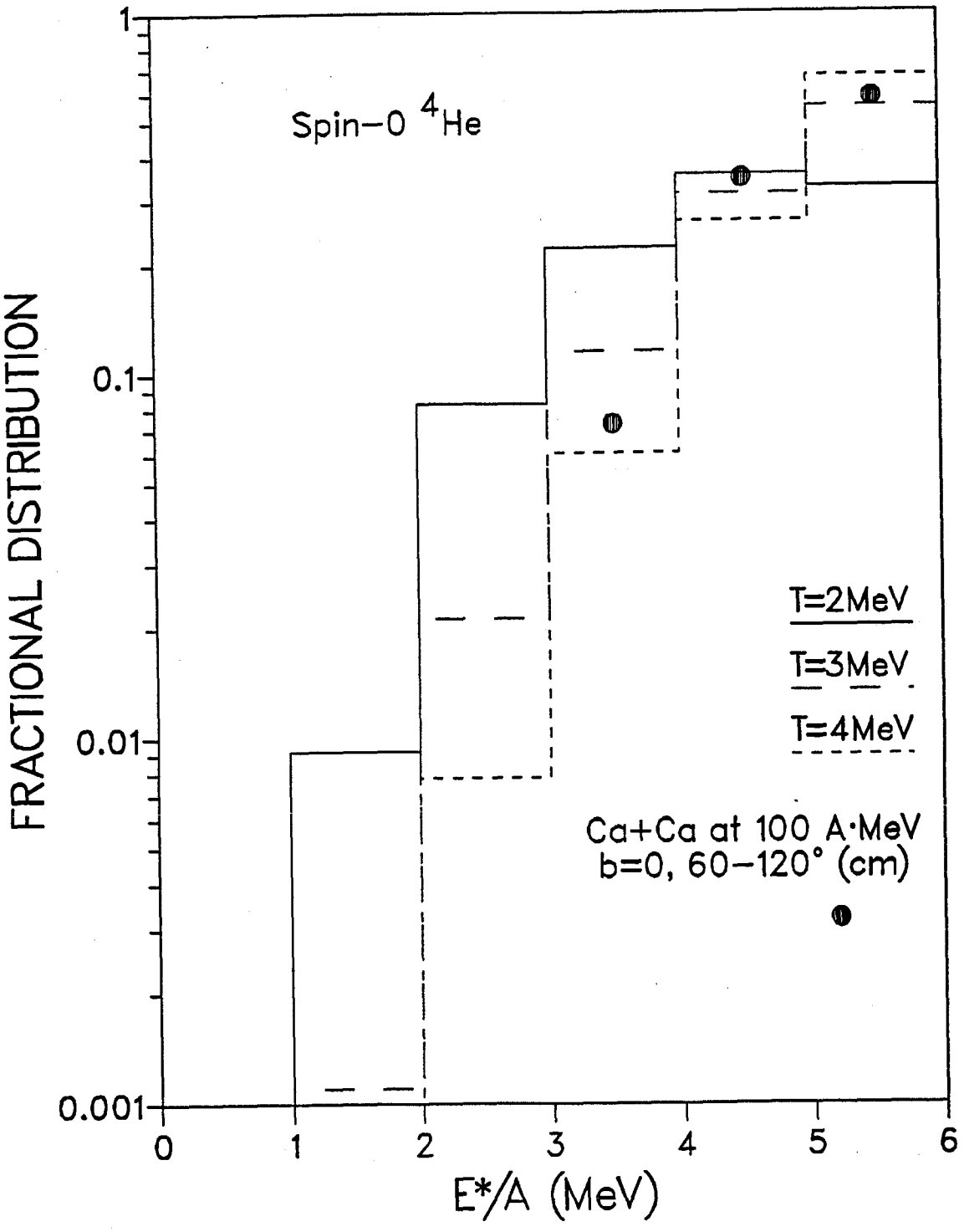

Fig. 6.5. Fractional distribution of excitation energies per nucleon predicted for the computational zero spin ^{4}He nuclei (subject to cluster constraint) for temperatures of 2, 3 and 4 MeV (histograms). The points are from the simulated Ca+Ca reaction at 100 A∘MeV and b=0 fm. All distributions have been normalized to unity over the 0-6.0 A∘MeV range in excitation energy. The ^{4}He nuclei are observed in the 60-120 degree range in the cm frame.

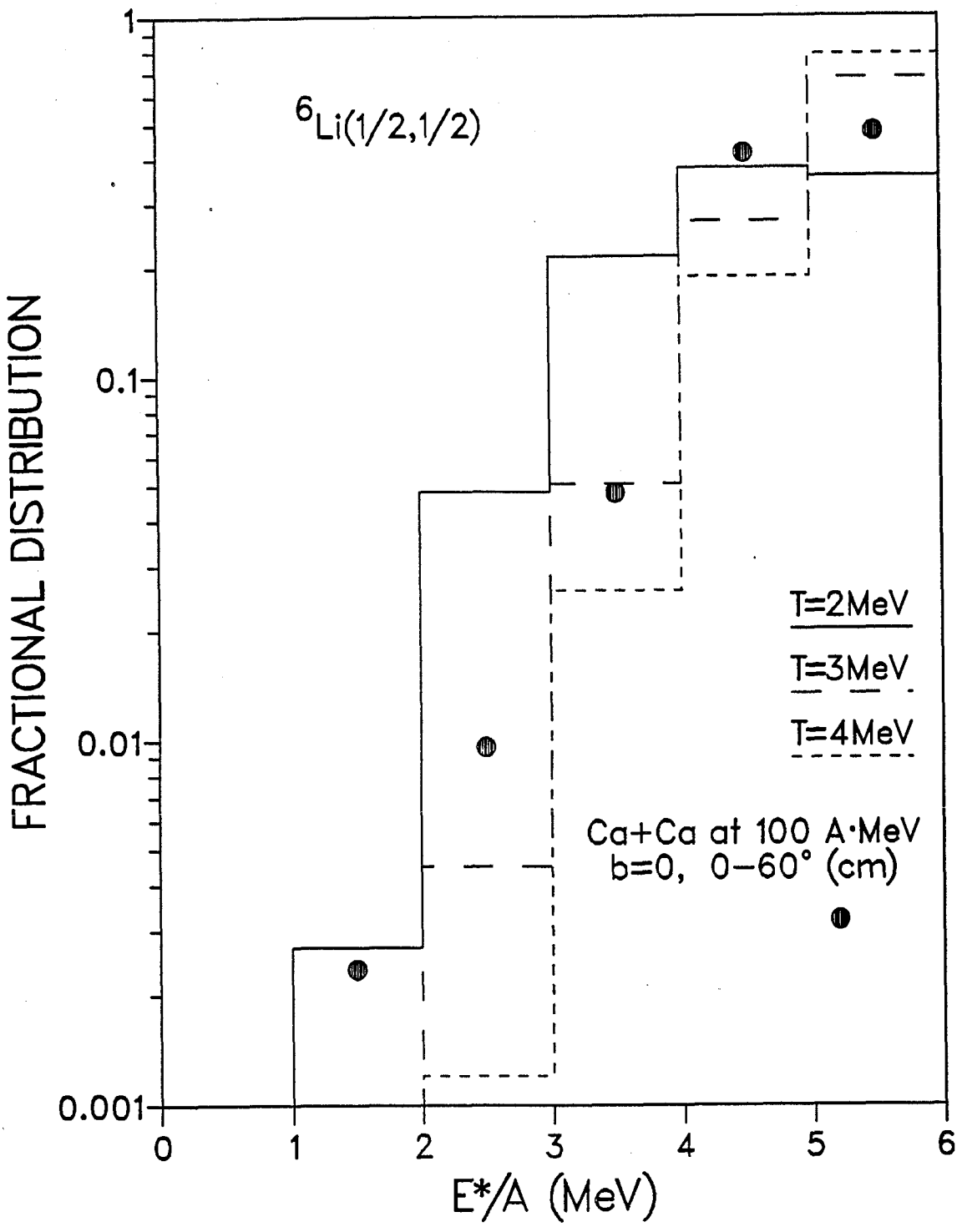

Fig. 6.6. Fractional distribution of excitation energies per nucleon predicted for the computational ^{6}Li(1/2,1/2) nuclei (subject to cluster constraint) for temperatures of 2, 3 and 4 MeV (histograms). The points are from the simulated Ca+Ca reaction at 100 A∘MeV and b=0 fm. All distributions have been normalized to unity over the 0-6.0 A∘MeV range in excitation energy.

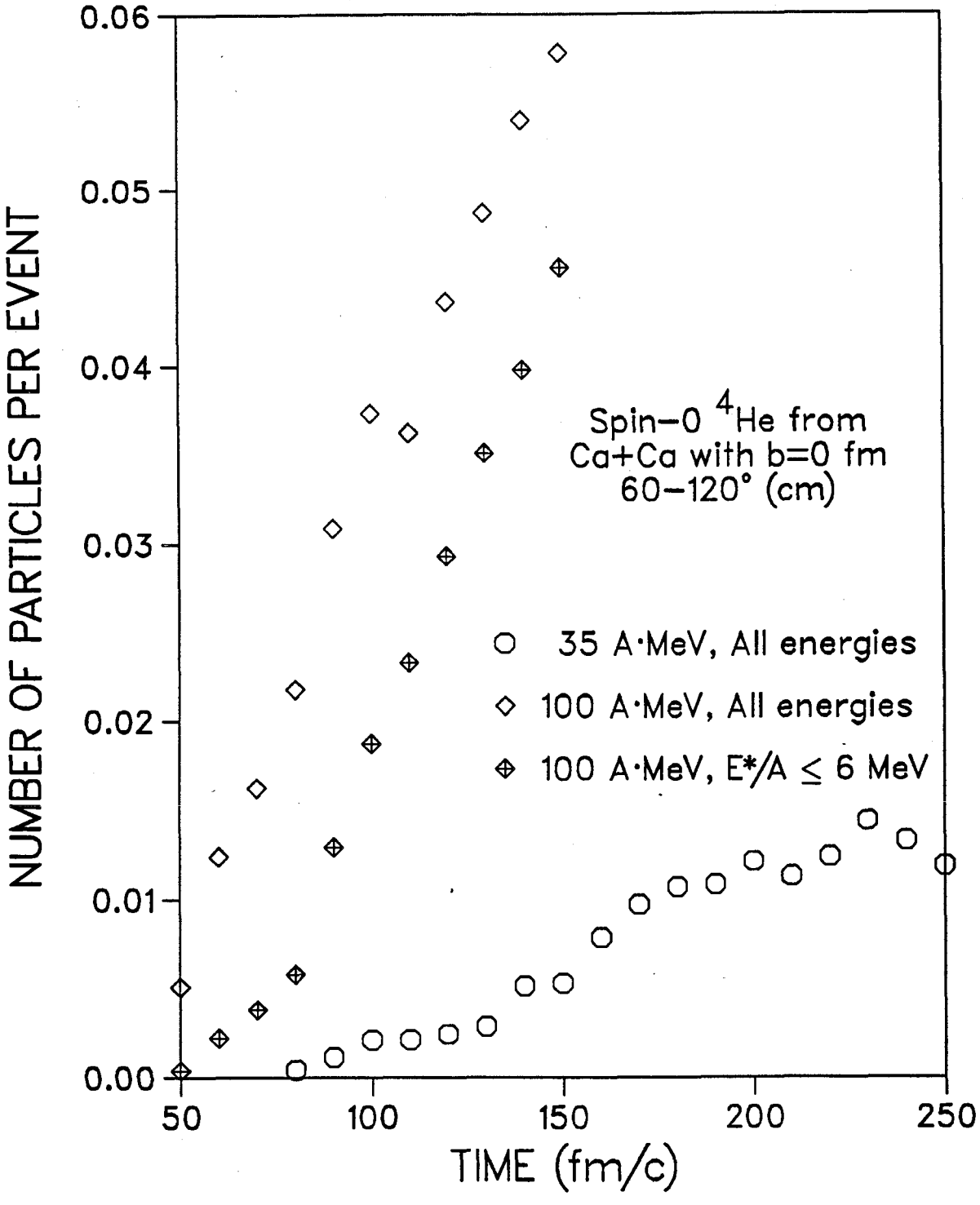

Fig. 6.7. Time dependence of the number of ^{4}He nuclei per event observed in the angular range of 60-120 degrees for the Ca+Ca reaction at 35 A∘MeV and 100 A∘MeV bombarding energy. The 100 A∘MeV populations are shown both with and without the 6 A∘MeV cut in excitation energy.

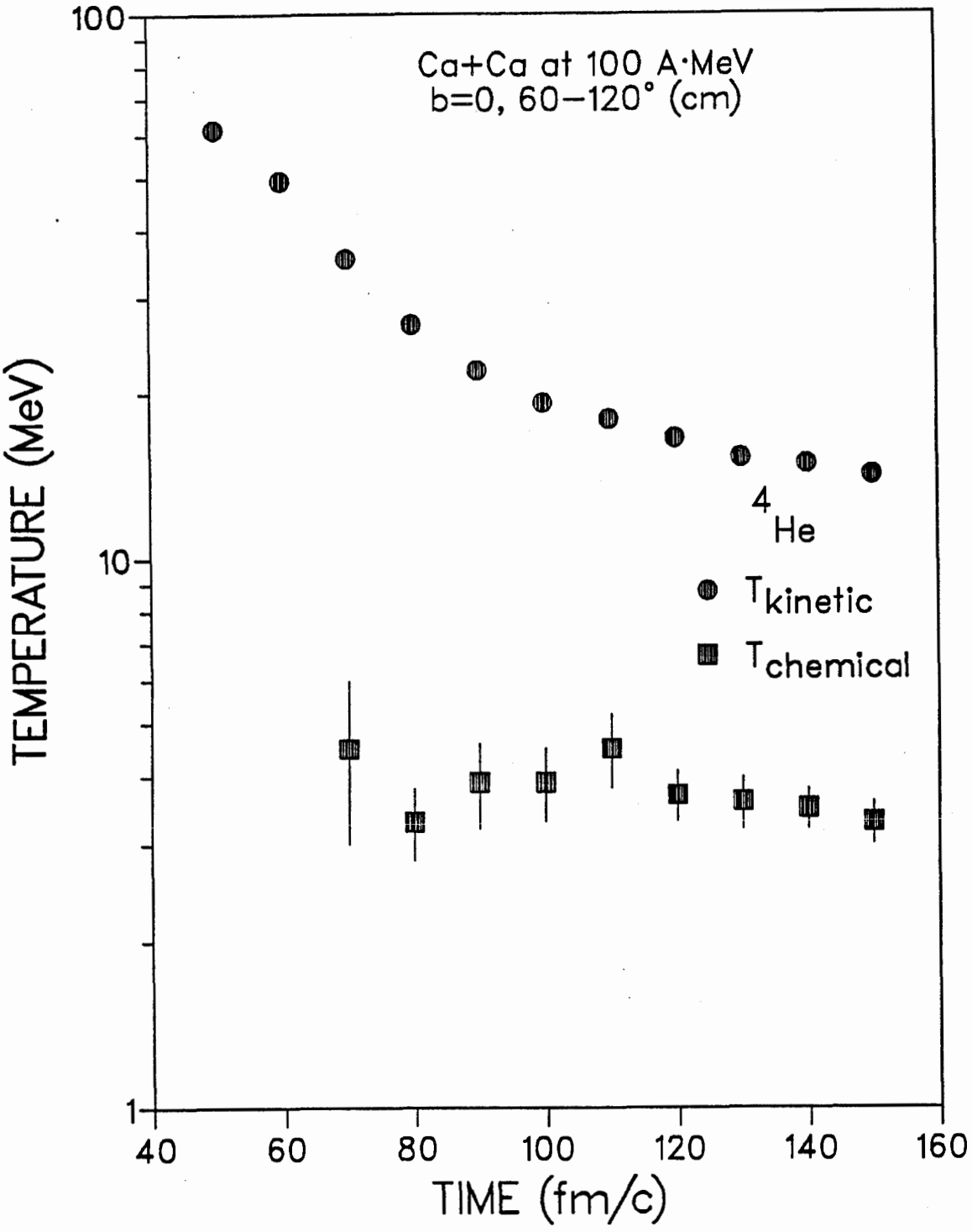

Fig. 6.8. Time dependence of the ^{4}He kinetic and chemical temperatures calculated for the Ca+Ca reactions at 100 A∘MeV and b=0 fm. The ^{4}He nuclei are collected in the 60-120 degree range in the cm frame.

Fig. 6.9. Representation of the quasiparticle positions in the Ca+Ca reaction at 100 A∘MeV and b=0 fm. The upper part of the figure is for an elapsed time of 60 fm/c while the lower part is for 120 fm/c. Each quasi-particle is represented by a solid sphere of radius 1/2 fm surrounded by 100 dots distributed according to a gaussian distribution.

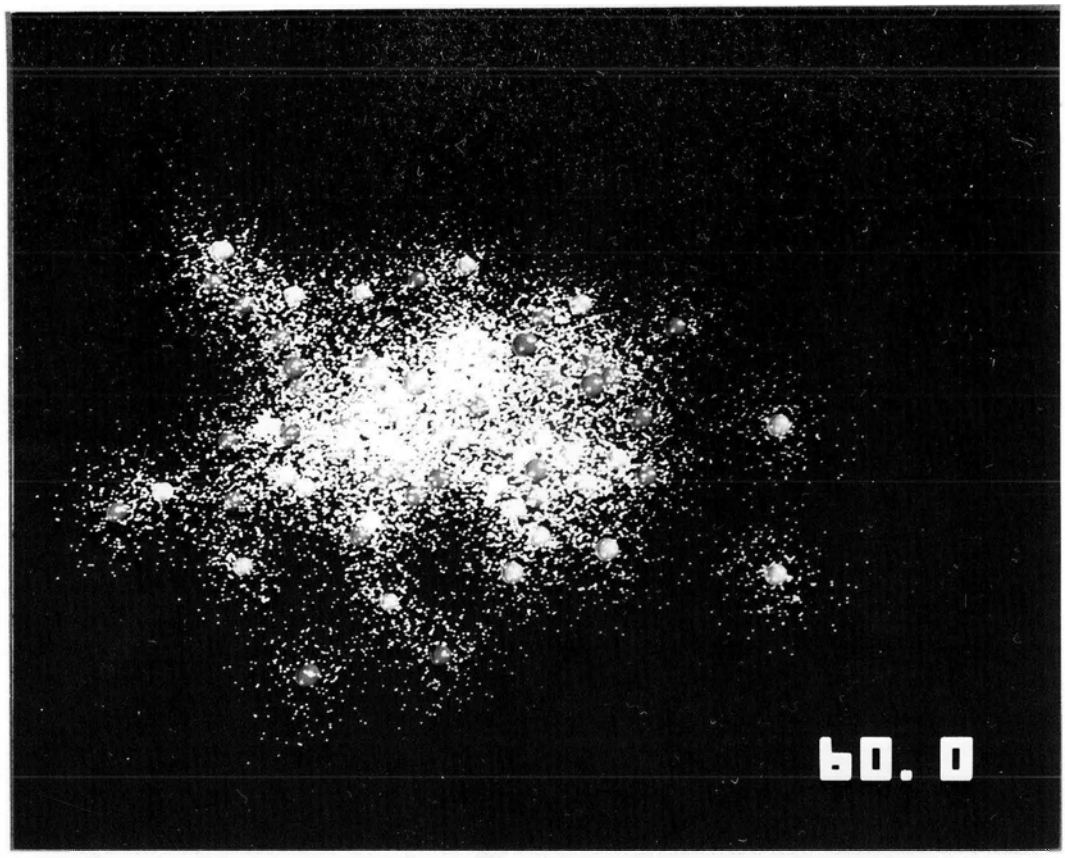
60. 0

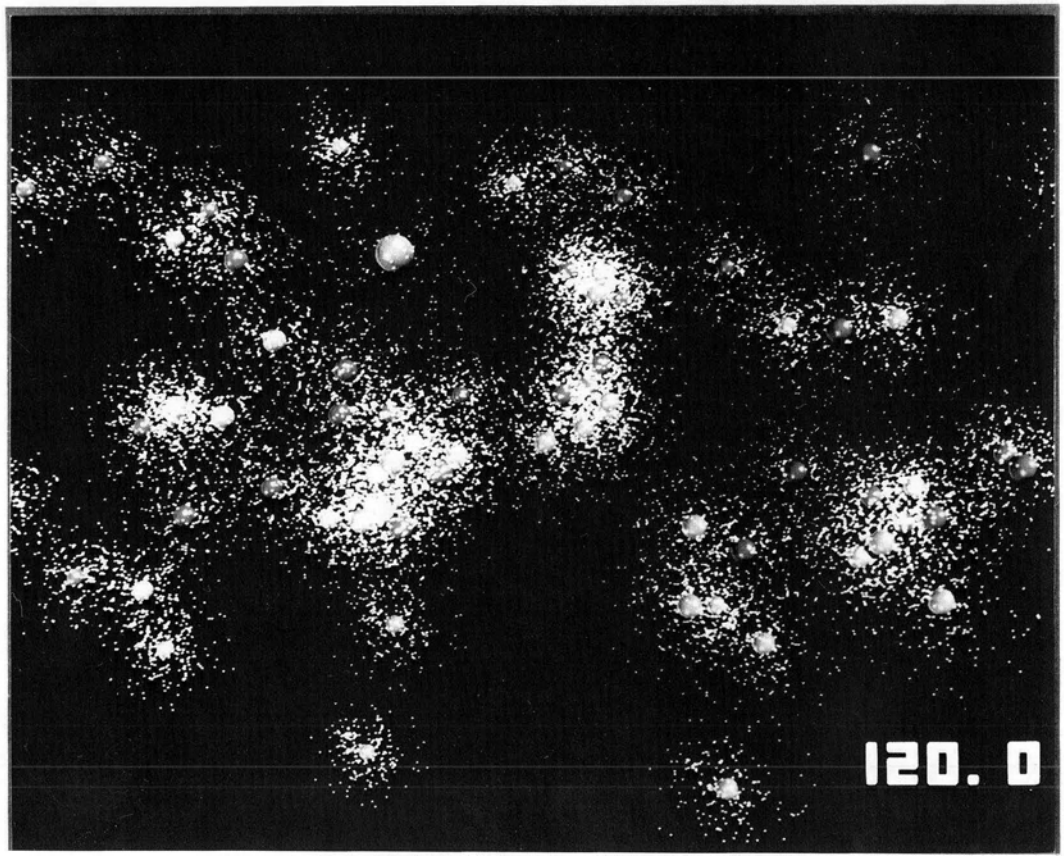
120. 0

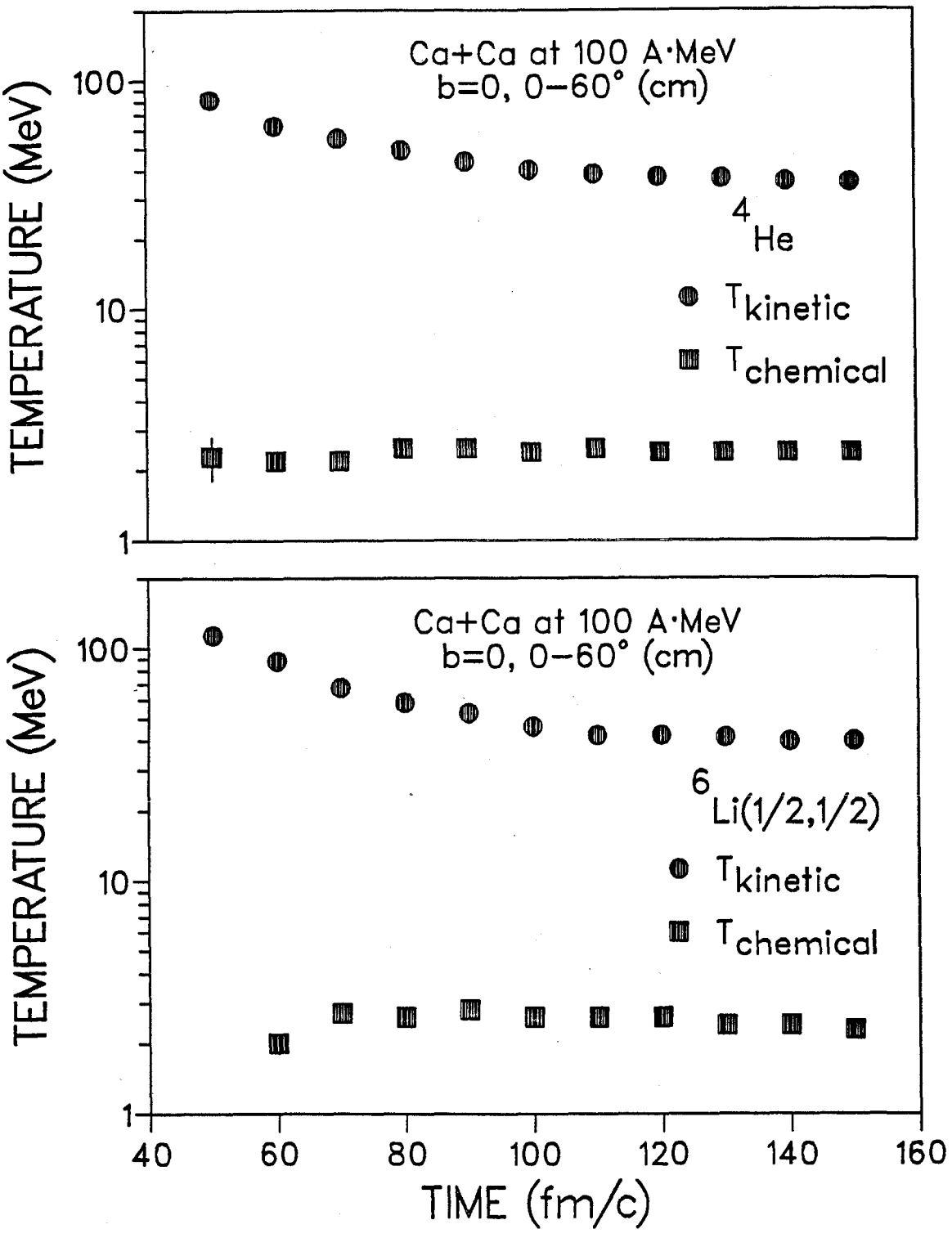

Fig. 6.10. Time dependence of the kinetic and chemical temperatures for nuclei emitted at 0-60 degrees in the Ca+Ca reaction at 100 A∘MeV. The upper part of the figure (a) is for ^{4}He nuclei while the lower part (b) is for ^{6}Li(1/2,1/2).

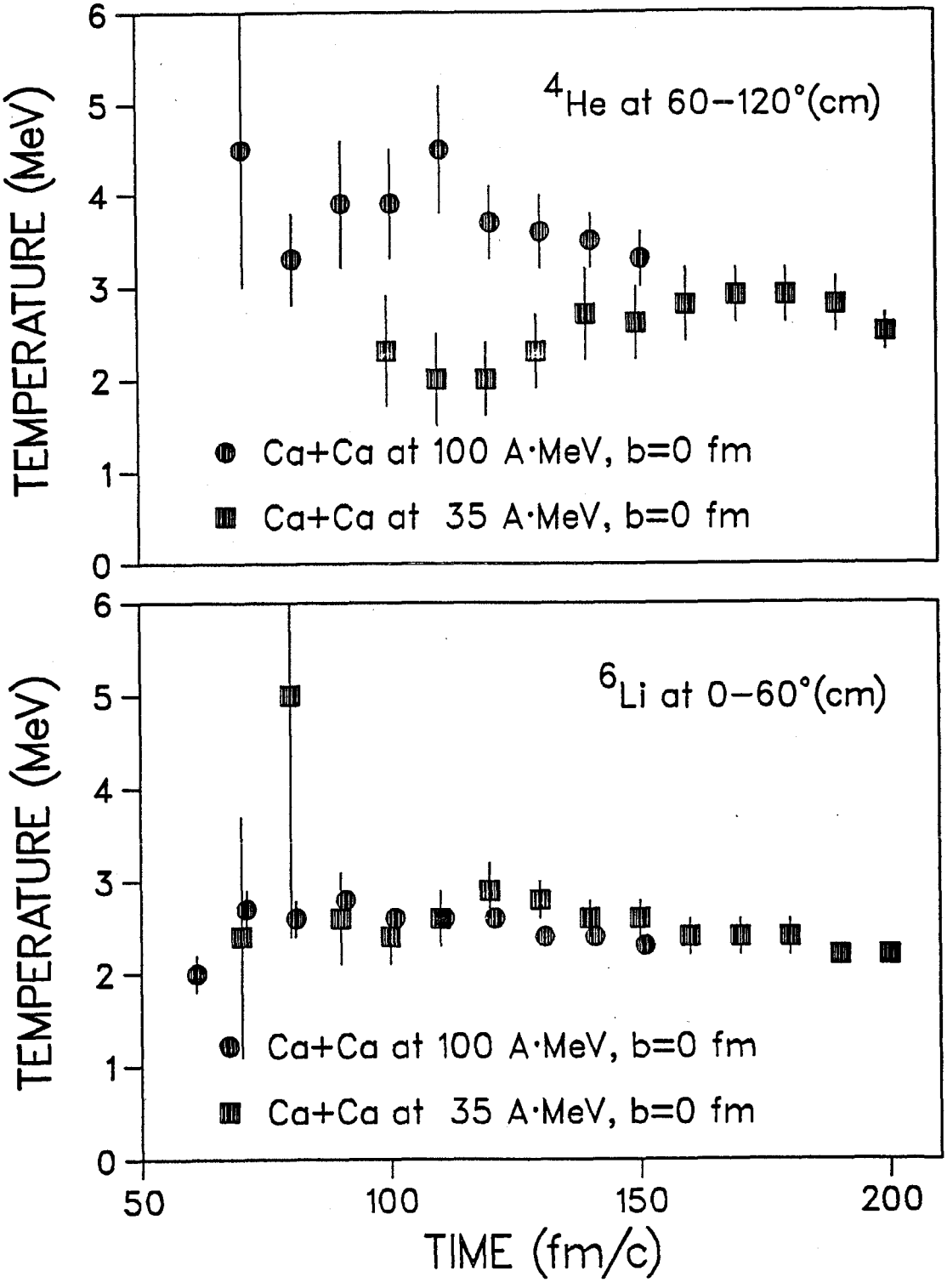

Fig. 6.11. Comparison of the chemical temperatures obtained in the Ca+Ca reaction at 35 A∘MeV and 100 A∘MeV bombarding energy. The top part of the figure is for ^{4}He nuclei in the angular range of 60-120 degrees, while the lower part is for ^{6}Li in the angular range of 0-60 degrees.

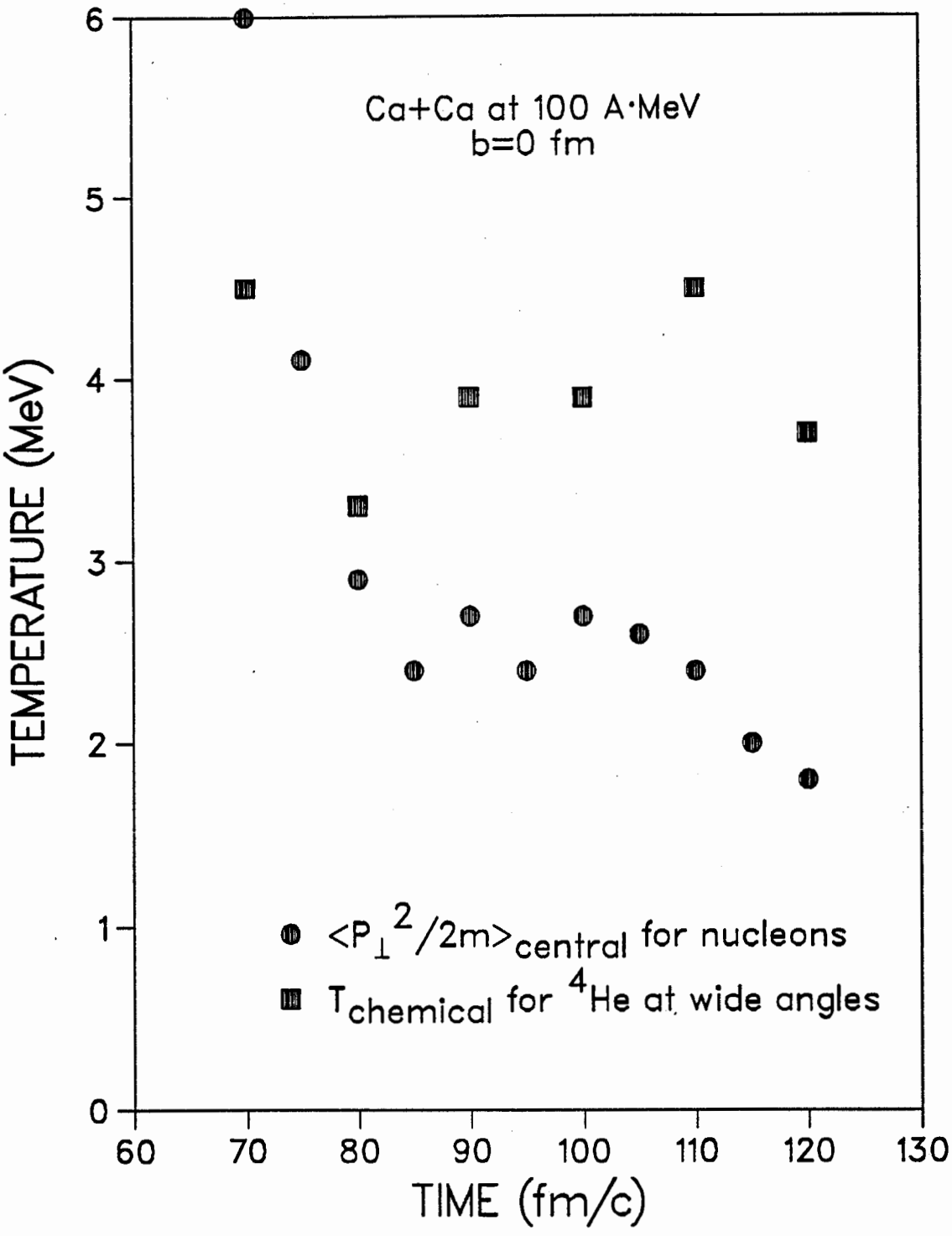

Fig 6.12. Time dependence of the free nucleon kinetic temperature in the local reference frame centered on the cm position of the reaction system. The reaction chosen is Ca+Ca at 100 A∘MeV and b=0 fm. Shown for comparison is the ^{4}He chemical temperature of Fig. 6.8.

VII THERMODYNAMICS

VII.1 INTRODUCTION

In this chapter the interplay of the thermodynamic properties and the dynamics of nuclear systems is examined. In particular we wish to explore to what extent the fragmentation processes present in heavy ion collisions are affected by bulk thermodynamic properties of nuclear matter. To study this connection and to see to what extent the assumptions of thermodynamics are valid in reaction systems we use the QPD model.

The chapter is organized as follow: In the next section the T=0 properties of the QPD model are considered. In Section VII.3 the temperature and density dependence of the energy and the specific heat for a number of finite system is estimated. From these results, finite size scaling is used to construct the liquid-vapour phase diagram of the infinite system. The fourth section is used to present the dynamics of excited nuclear droplets in terms of thermodynamic variables and in the final section a discussion of the connection between the thermodynamics and the dynamics of the droplet is made.

VII.2 T=0 Properties of Nuclear Matter

We begin the discussion of the thermodynamics of infinite neutral nuclear matter by presenting a few ground state properties. Simple energy arguments show that T=0 nuclear matter is a homogeneous state for $\rho>\rho_o$ and a coexistence state for $\rho<\rho_o$. Many analytic calculations [BG86,LS84]

determine the coexistence region by examining the instabilities of nuclear matter which is constrained to be homogeneous. In this section both the true ground state (coexistence state for $\rho<\rho_o$) and the constrained ground state (homogeneous for all ρ) of nuclear matter are found. In particular the energy per nucleon, E/A, for finite systems is estimated by Monte Carlo. Using finite size scaling, these results are extrapolated to the infinite system for both the coexistence and homogeneous states. The finite size scaling of the energy in the coexistence region enables one to also find the T=0 surface tension, σ(T=0). The compressibility is found as well by extracting the curvature of the T=0 energy isotherm of the homogeneous state (see Eq. 3.1).

It is worthwhile to introduce some notation. In other parts of this thesis we use ρ_o=0.17fm^{-3} to denote the density for which the ground state energy is a minimum and hence have identified it as the density of normal nuclear matter. In choosing the parameters in the QPD Hamiltonian we have tried to ensure that our model also has a minimum at $\rho=\rho_o$. However this calculation was not done using the full QPD Hamiltonian; the expectation of the kinetic energy operator was evaluated within the Fermi-Thomas approximation. As will be shown below this approximation does have an effect but it is small. To avoid confusion, we introduce ρ_{min} to denote the density of the minimum energy of the full QPD model and let ρ_o=0.17fm^{-3} denote the accepted value of nuclear matter density.

In this section, the ground states of the finite size, isospin symmetric QPD model are found with the dissipative equations of motion presented in Chapter IV; however the Coulomb term is dropped and periodic boundary

conditions imposed. It is found that the same damping factors used in Chapter IV (μ_1=400 fm-c/MeV, μ_2=0.426 MeV/fm-c) and integration times (t=200 fm/c) also suffice to find the ground states for the periodic isospin symmetric version of the QPD model.

To find the ground state energy of the homogeneous system we use a Lagrange multiplier method to impose the constraint that the variance of the density distribution is equal to a constant χ .

$$\int (\rho-\bar{\rho})^2 d^3\mathbf{r} = \int \rho^2 d^3\mathbf{r} - A\bar{\rho} = \chi \qquad (7.1)$$

where $\bar{\rho}$=A/V and ρ is given by equation 4.5. Since $\bar{\rho}$ is a constant (i.e. V and A are fixed) this constraint can be more simply expressed as $I[\rho]\equiv\int \rho^2 d^3\mathbf{r} = \zeta$, where $\xi = \chi + A\bar{\rho}$. The ground state of the constrained system can be found by minimizing the Lagrange function, ϕ.

$$\phi(\lambda) = E(\mathbf{R}_1\mathbf{P}_1,\ldots,\mathbf{R}_A\mathbf{P}_A) + \lambda\, I[\rho] \qquad (7.2)$$

In most Lagrange multiplier calculations λ is chosen such that the constraint, $I[\rho] = \zeta$, is satisfied. In this calculation we wish to choose λ such that $I[\rho]$ is a minimum (i.e. the system is homogeneous). For some positive value of $\lambda=\lambda_c$ the system becomes homogeneous and hence $I[\rho]$ is a minimum. For all values of $\lambda>\lambda_c$ the ground state remains unchanged. It therefore suffices to perform the calculation for any value $\lambda>\lambda_c$. Notice that the Lagrange multiplier term in Eq. 7.2 has the same functional form as the attractive term in the QPD Hamiltonian of Eq. 4.11. (i.e. the "*a*" term). If $\lambda=-a/(2\rho_o)$ then ϕ only has repulsive terms so that the ground state is homogeneous, and we can then find the energy of the constrained system.

Of course the calculation of both the constrained and unconstrained ground state energy must be performed on a finite system. To extract the infinite system values of E/A one must either go to a sufficiently large system so that finite size effects are small, or use finite size scaling to extract the infinite system values. For a homogeneous state the finite size scaling of the energy per particle $e(\rho,\ell)$ to first order is given by

$$e(\rho,\ell) = e(\rho,oo) + C_c \exp(-\ell/\xi) \tag{7.3}$$

where $\ell=(\rho A)^{1/3}$ is the periodic length, ξ is the correlation length of the infinite system and C_c is an unknown constant. For the coexistence state an interface exists, and the scaling of the energy will be given by

$$e(\rho,\ell) = e(\rho_{min},oo) + C_s/A^{1/3} \tag{7.4}$$

The coefficient C_s can be related to the surface tension, $\sigma=(4\pi\rho_{min}/3)^{2/3}C_s$. By fitting the finite size data to these forms the infinite system ground state energy per particle is found.

The energy per particle of the homogeneous state is found for system sizes of A=32,64,128 and 256 and for densities from $0.1\rho_o$ to $1.5\rho_o$ in $0.1\rho_o$ steps. For $\rho>\rho_o$ the true ground state is homogeneous and we do not need to constrain the system. Using Eq. 7.3 the infinite system ground state energy per particle is found and displayed in Fig. 7.1. Next we fit a quadratic form to this infinite system ground state energy in the vicinity of $\rho=\rho_o$ (i.e. $0.8 \leq \rho/\rho_o \leq 1.2$) A minimum energy per particle of e_{min}=-16.20 MeV at $\rho=\rho_{min}=1.03\rho_o$ is found. Regarding the earlier comment

on the difference of ρ_{min} and ρ_o we see that the approximation made in Chapter IV in estimating the QPD Hamiltonian parameters is quite appropriate The curvature of the T=0 energy isotherm can be related to the compressibility, $K=9\rho^2\partial^2 e(\rho)/\partial\rho^2$ [Nix79]. Using this relation we find K=400 MeV, as expected from our choice for the spatial part of the nuclear potential, but much larger than the experimentally determined value of 200 MeV [BGG76] (for a review see [Bla80]) base on monopole vibrations.

In Fig. 7.1 we also present the ground state energy of the coexistence state. For the infinite system this energy is simply e_{min} and independent of density. For finite systems the surface tension affects the ground state energy per particle of the system. From Eq. 7.4 we see that the finite size analysis can be used to extract the surface tension of the system. To find C_s we fit the data to the following form

$$(e(\rho,\ell) - e_{min})A^{1/3} = C_s + C_1/A^{1/3} + C_2/A^{2/3} \qquad (7.5)$$

A value of 17.2 MeV was found for C_s. This compares favourably with the surface term in binding energy formulas of Myers and Swiatecki [MS66], where C_s=18.56 MeV. The value of C_s=17.2 MeV implies a surface tension of 1.11 MeV/fm^2.

From the zero temperature energy isotherm the zero temperature pressure can be found with the relation (valid at zero temperature)

$$P(T=0) = \rho^2 \frac{\partial(E/N)}{\partial\,\rho}\Big|_{T=0} \qquad (7.6)$$

The pressure at zero temperature, as calculated within the QPD model, is displayed in Fig. 7.2 . For comparison the T=0 pressure isotherms, as calculated in a liquid drop model [NNL88,DBN87], are shown in Fig. 7.2 for both symmetric nuclear matter and ^{108}Ag as well. It is interesting that there is so little difference between them.

VII.3 **Phase Diagram**

The T-ρ phase diagram of the liquid-vapour transition is calculated by estimating the specific heat at constant volume C_v by Monte Carlo. Typically 8000 samples are used in the estimation of C_v, although near the critical point 12000 samples are generated. A pseudo-transition temperature is associated with the temperature $T_m(\rho,\ell)$ that maximizes the $C_v(T,\rho,\ell)$ of the finite system. The temperature $T_m(\rho,\ell)$ shows large finite size effects, so finite size scaling is used to estimate the infinite system transition temperature $T_t(\rho)=T_m(\rho,oo)$.

The high temperature phase of the system is homogeneous so the asymptotic ($\ell \longrightarrow oo$) form of the free energy per particle as a function of ℓ is given by:

$$f_h(T,\rho,\ell) = f_h^{\infty}(T,\rho) + A(T,\rho)\ \exp(-\ell/\xi) \qquad (7.7)$$

where $A(T,\rho)$ is an unknown function of T and ρ and f_h^{∞} is the free energy per particle of the infinite homogeneous system. At low temperature the system is in a coexistence state with an interface existing between the coexisting phases. This interface make a contribution to the free energy proportional to its area, so the asymptotic form of the free energy per

particle as a function of ℓ, is given by;

$$f_c(T,\rho,\ell) = f_c^{\infty}(T,\rho) + B(T,\rho) / \ell \qquad (7.8)$$

where $B(T,\rho)$ is an unknown function of T and ρ. The crossover from coexistence to a homogeneous phase is given by the relation that $f_c(T,\rho,\ell)=f_h(T,\rho,\ell)$. By substituting the finite size scaling form into this relation and neglecting the exponential term we find that

$$f_c^{\infty}(T_m,\rho) + B(T_m,\rho)/\ell = f_h^{\infty}(T_m,\rho) \quad . \qquad (7.9)$$

Expanding f_c , f_h, and B about T_t to first order in $1/\ell$ we find

$$f_c^{\infty}(T_t,\rho) + \varphi_c(T_m-T_t) + B(T_t,\rho)/\ell + b\ (T_m-T_t)/\ell = f_h^{\infty}(T_t,\rho) + \varphi_h(T_m-T_t) \qquad (7.10)$$

where

$$\varphi = \frac{\partial f}{\partial T}\Big|_{(T_t,\rho)} \quad .$$

Using $f_c^{\infty}= f_h^{\infty}$ at $T = T_t(\rho)$ and expanding the above equation to first order in $1/\ell$, the scaling form for T_m is found to be:

$$T_m(\rho,\ell) = T_t(\rho) + [B(T_t,\rho)/(\varphi_h-\varphi_c)]/\ell \qquad (7.11)$$

A least square fit of the data to the finite scaling form is used to extract T_t and the results are summarized in Fig. 7.3. Shown on the figure are both the finite size scaling estimate of the transition temperature T_t and the pseudo-transition temperature T_m for a set of systems of masses 32,

64, 128, 256 and 512. The phase diagram shares a number of common features with other calculations of the T-ρ nuclear phase diagram [BG86,FP81]. The T=0 coexistence region is over the same range of density (this isn't surprising). The critical temperature of 18.5 MeV and the critical density of $0.3\rho_o$ are close to other model estimates. What is new in this study is that the finite size effects are presented and shown to be nontrivial in the system sizes typical of systems used in nuclear reaction studies.

As an example of the finite size scaling form Eq. 7.11, we present the finite size data and the fits to it in Fig. 7.4a and 7.4b. Notice the close agreement between the fitted form and the data, leading one to conclude that the system sizes considered are in the scaling regime.

VII.4 Fluctuation Growth

We now wish to address the question of the connection between the instability region in the liquid-gas coexistence phase and the break-up of systems formed during nuclear reactions. A test for a connection between these two phenomena can be made by considering the time dependence of the density and its spatial fluctuations for two ideal systems. First we consider the growth of fluctuations in initially homogeneous nuclear matter systems and then compare these results with the fluctuation growth in excited ^{108}Ag nuclei.

To study the growth of fluctuations in homogeneous matter the constraint is removed from the constrained ground states generated in Sec 7.2 and the

evolution of the system is examined. As a measure of the spatial fluctuations the quantity $I=\langle\nabla^2\rho\rangle/\langle\nabla^2\rho_1\rangle$ is used. The quantity ρ_1 denotes the density distribution of a single isolated quasiparticle and the expectation $\langle\nabla^2 f\rangle \equiv \int(\nabla^2 f)f(\mathbf{r})d^3\mathbf{r} \,/\, \int f(\mathbf{r})d^3\mathbf{r}$. For small fluctuations I(t) should grow exponentially with time (i.e. $I(t) \sim \exp(t/\tau_f)$). To test this conjecture and to extract the time constant, τ_f, a scatter plot of dI/dt vs I is made for a number of different initial densities, and displayed in Fig. 7.5. From the plot it is clear that the data is clustered about a single straight line, indicating that the behaviour of I is exponential and independent of initial density. Furthermore, the inverse slope of the line gives a common τ_f=25 fm/c for all starting densities. This time constant indicates the rate at which clusters grow in the instability region.

Now we examine the time evolution and break-up of excited ^{108}Ag nuclei. The nuclei have been excited in one of two ways. The first way directs most of the excitation energy into radial motion and the second method produces a more thermal excitation. Both methods excite the system by modifying the momentum of the nuclear ground state. In the first method a random radial component is added to each QPD momentum, $\mathbf{P}$, to generate a new momentum, $\mathbf{P}' = \mathbf{P}+\Delta\hat{\mathbf{R}}$, where $\hat{\mathbf{R}}_i$ is unit along the direction from the centre of mass to the position of the i^{th} particle and the Δ's are uniformly distributed random variables in the interval (ω_1,ω_2). The choice of ω_1 and ω_2 will be discussed later. The second method randomizes the direction of the momentum vectors. In this case the new momentum is $P_i'^{\alpha} = S_i^{\alpha}P_i^{\alpha}$, where α=x, y, or z and the S's are random scale factors which are distributed uniformly in the interval $(-\omega,\omega)$.

Both of the above methods generate a distribution of energy states, which of course depends on the ω's chosen. To consider the dynamics of excited states in a given energy range we choose an ω that produces these states in relative abundance, typically about 1 in 10, and then generate a set of several thousand different excited states. This set is then sampled to select a collection of a hundred states within the desired energy range. Each of the states in this collection is then allowed to evolve for several hundred fm/c.

The evolution of these systems is investigated by examining the time dependence of the average central density $\langle\rho\rangle_c$ and central fluctuations $\langle\rho^2\rangle_c - \langle\rho\rangle_c^2$. The $\langle\ldots\rangle_c$ denotes both a spatial average over a sphere of radius R_c=4 fm centred on the centre of mass and an ensemble average over the 100 samples.

In Fig. 7.6 the time dependence of $\langle\rho\rangle_c$ is shown for a variety of initial excitations. In the upper plot the results for the radial excitation are shown for E^*/A = 4, 6 and 8 MeV. For low excitation energy the system exhibits a damped oscillation about an equilibrium value of the density. The period of this oscillation is about 75 fm/c and the relaxation time constant is τ_T=110 fm/c. The relaxation time represents the time constant associated with thermalization. The period of oscillation is nearly exactly the same as Ngô et al. find for ^{208}Pb within a liquid drop calculation [NNL88], although their calculation shows no damping. The main contribution to the relaxation process in the QPD model is due to the collision term in the equations of motion. In liquid drop models there is no process that can randomize the initial motion of the system, hence the

system will never thermalize. For E^*/A=8 MeV the system becomes unstable and breaks apart. During the break-up and expansion of the system, the central density $\langle\rho\rangle_c$ decays exponentially with a time constant of τ_e=20 fm/c.

In the lower part of Fig. 7.6 results are shown for the random excitation initialization. The first thing to notice is that the oscillations of the system are greatly suppressed, although the systems do relax. Secondly the systems are able to remain stable for much larger initial excitations.

It is of interest to see if the onset of fluctuation growth indicates the break-up of the system. To address this question we consider the trajectories of the radially excited ^{108}Ag in fluctuation-density space. In Fig. 7.7 a plot is made of $(\langle\rho_c^2\rangle/\langle\rho\rangle_c^2 - 1)$ vs $\langle\rho\rangle_c$ for a number of different initial excitations. Initially all the systems follow the same trajectory. The low energy trajectories split off from this common trajectory to follow separate "pig tail" paths to a thermalized state. However the large excitation energy system continues to expand and breaks apart. It appears that the initial fluctuation growth has little to do with the break-up of the system. Furthermore Fig. 7.5 time scales associated with fluctuation growth do not appear to depend on initial density. The break-up does appear to be sensitive to the initial excitation energy.

VII.5 Summary and Discussion

We began this chapter by considering the zero temperature properties of the QPD model. These properties are consistent with what one would predict with liquid drop fits to experimental data. This agreement gives a strong indication that the QPD model at least possesses the correct energetics for nuclear systems. At nonzero temperatures a Monte Carlo method is used to find the phase diagram for the QPD model. The resulting diagram is again consistent with the predictions of a number of other reasonable models. Given the above agreements we feel that we have developed a model that has included most of the physics of the thermodynamic state of nuclear matter.

The dynamics of fluctuation growth in a initially homogeneous and static system is explored next. It is found that the growth is exponential with a time constant of the order of τ_f=25fm/c, for all densities within the instability region. This is then compared with the expansion of a somewhat idealized excited ^{108}Ag system. The silver ion is excited in such a way to produce an expanding system. This excited state is much simpler and resembles more closely the state of expanding nuclear matter, than the excited state produced in a heavy ion collision. If the break-up of this idealized system is not describable in terms of spinodal decomposition, then certainly it will not be sensible to apply such a description to the break-up found in heavy ion collisions.

The spinodal decomposition description requires that the system change in a quasistatic way so that thermal equilibrium is maintained. This does not appear to be the case. The expansion time (τ_e=20 fm/c) is of the same

order as the fluctuation growth time (τ_f=25 fm/c) and short compared to the relaxation time (τ_T=110 fm/c), making a quasistatic assumption invalid. As further evidence against the spinodal decomposition description, notice that the instability sets in at a density of 0.042 fm^{-3}. This density is lower than the critical density of 0.05 fm^{-3} and therefore cannot be associated with any point on the spinodal curve. In particular, at low temperatures investigated here, the spinodal line lies closer to 0.1 fm^{-3}. The break-up density which we observed, ~0.25ρ_o, is similar to that found in classical argon-like droplets by Lenk and Pandharipande [LP85]. However, our conclusions as to the role of the spinodal decomposition are very different from theirs.

In conclusion we have used the QPD model to explore both the statics and dynamics of nuclear systems. In this exploration we have examined the influence that the thermodynamic state has on the break-up of heavy ions in a reaction study. Our simulation results show multifragmentation in the same bombarding energy range as is observed experimentally, and do not show spinodal decomposition as the source of multifragmentation.

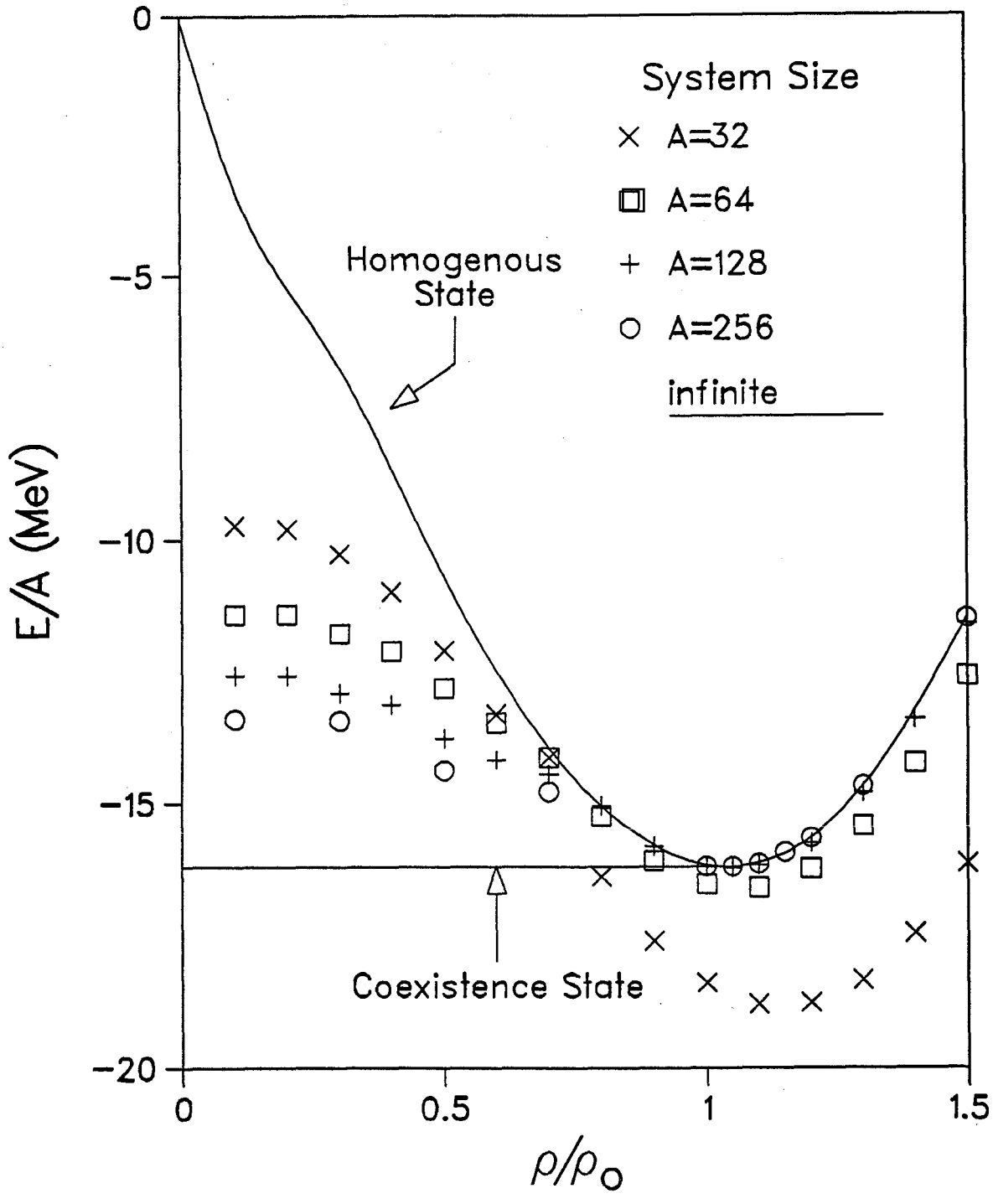

Fig. 7.1. The ground state energy per nucleon (E/A) as function of the reduced density (ρ/ρ_o) as predicted by the QPD model for both nuclear matter and finite systems. The data points represent the unconstrained minimum energy states of a number of isospin symmetric finite nuclear systems. The solid line marked "Coexistence State" indicates the minimum energy of unconstrained nuclear matter (infinite system) and the solid line marked "Homogeneous State" indicates the minimum energy of nuclear matter subject to the constraint that it is homogeneous.

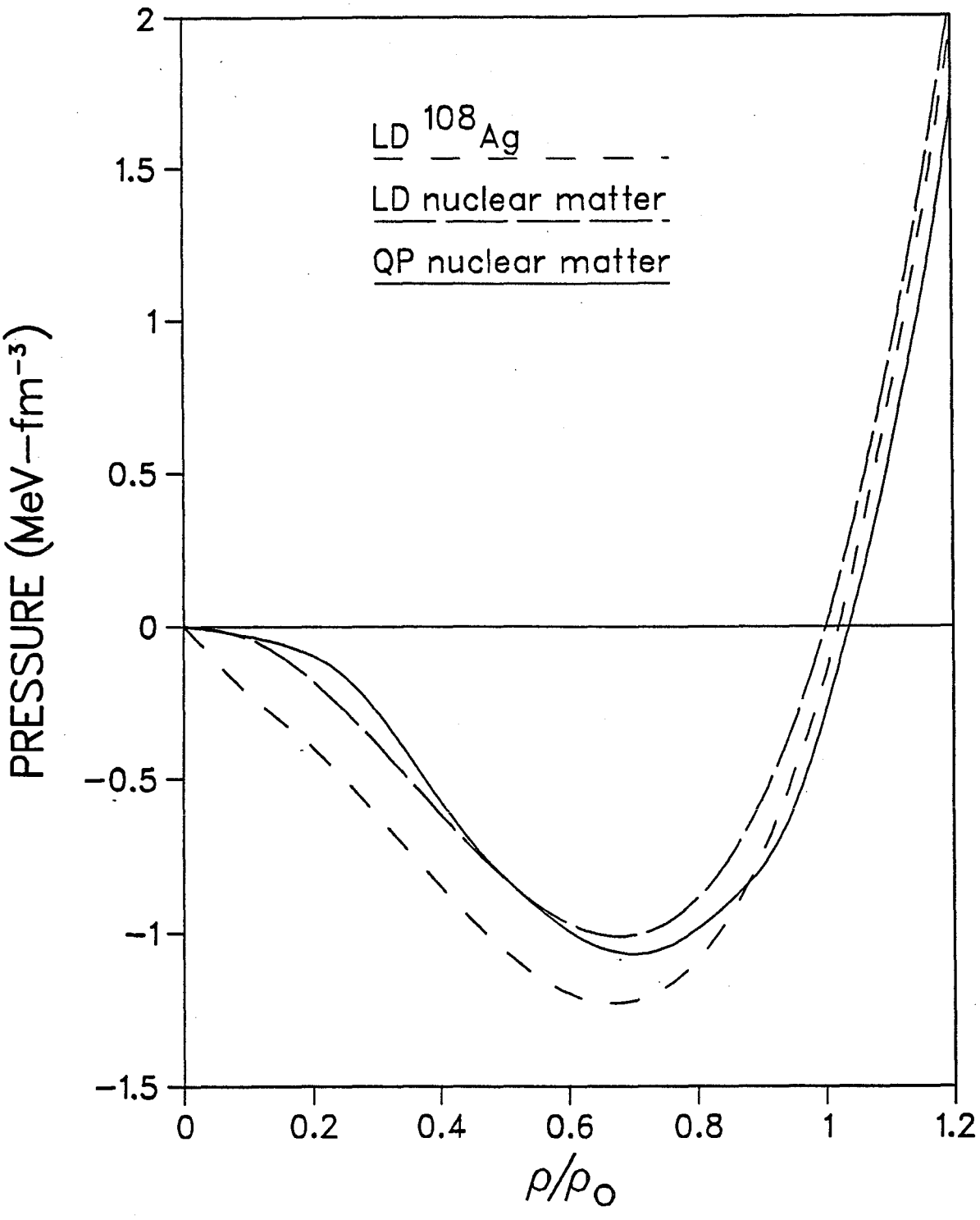

Fig. 7.2. Pressure vs. reduced density (ρ/ρ_o) at zero temperature for a number of different models. LD refers to the liquid drop calculations of Ngô et al. [NNL88,DBN87].

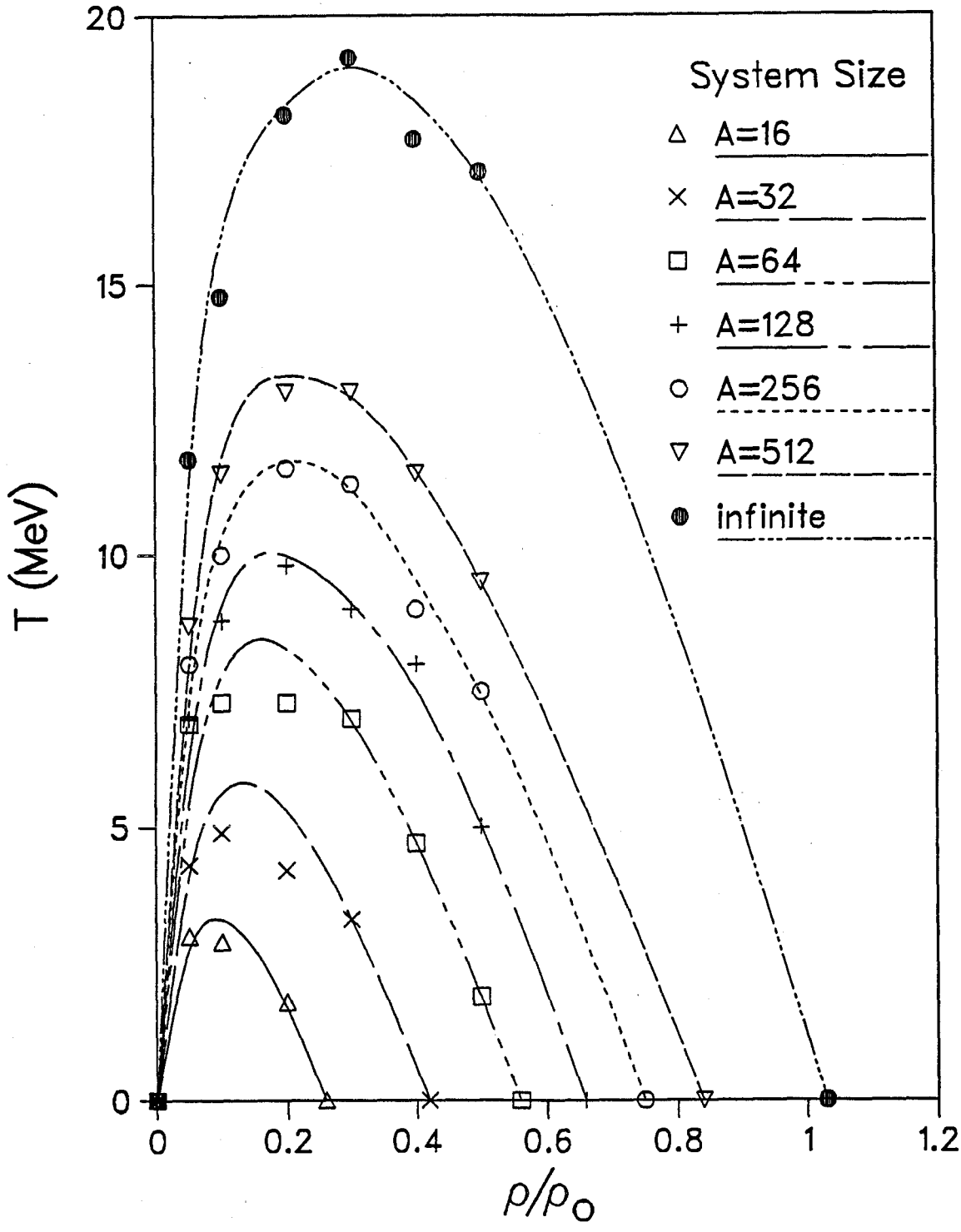

Fig. 7.3 The temperature (T) vs. reduced density (ρ/ρ_o) phase diagram of nuclear matter as calculated by extrapolating the temperature of the peak in the specific heat (C_v) at fixed density of the finite QPD system to infinite size. As well the locations of the peak in the specific heat for the finite systems are shown.

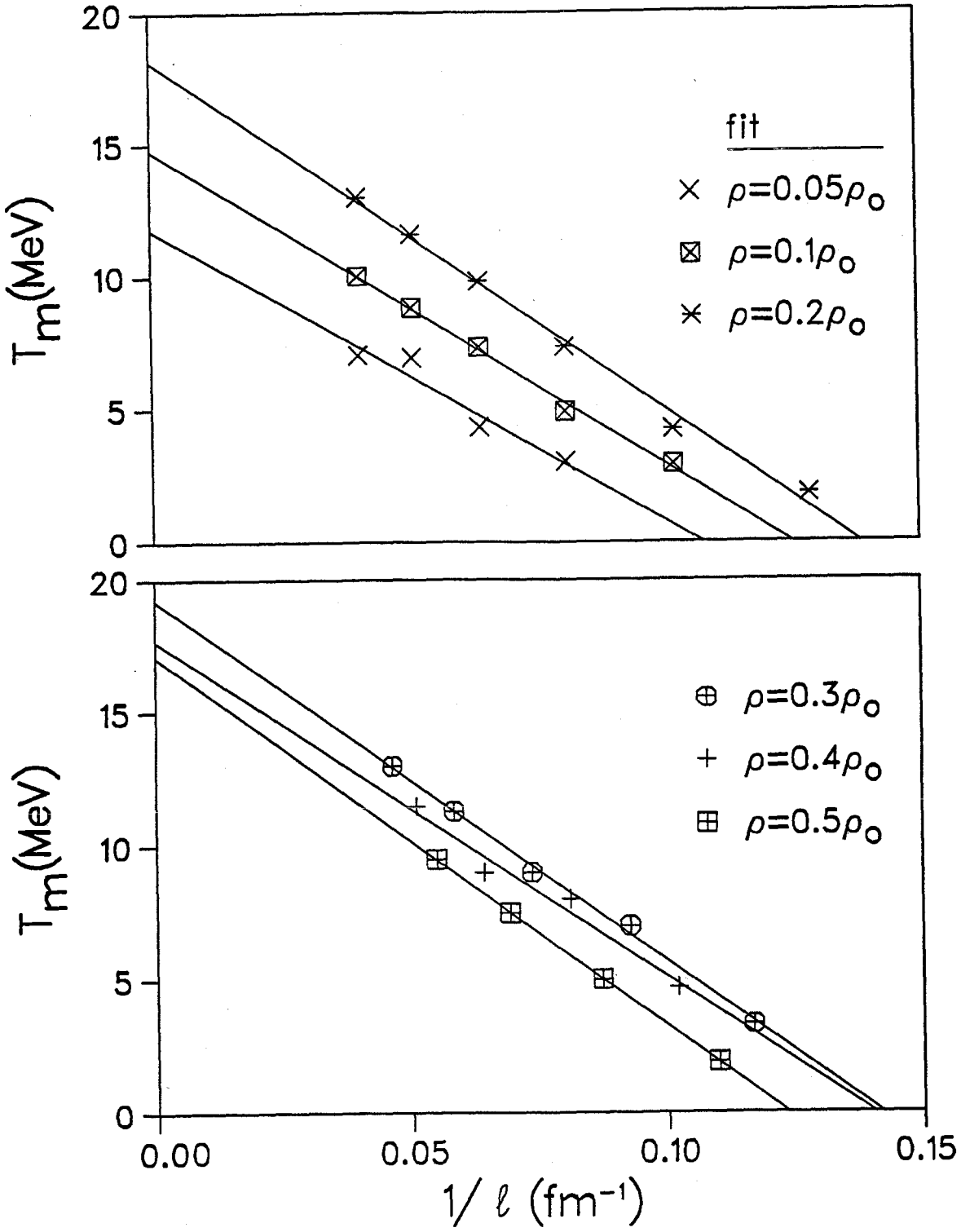

Fig. 7.4. An illustration of the goodness of fit of the T_m data to the scaling form, $T_m(\rho,\ell) = T_t(\rho) + A/\ell$, for a number of different densities. The y-intercept represents the infinite system transition temperature $T_t(\rho)$ as shown in Fig. 7.4.

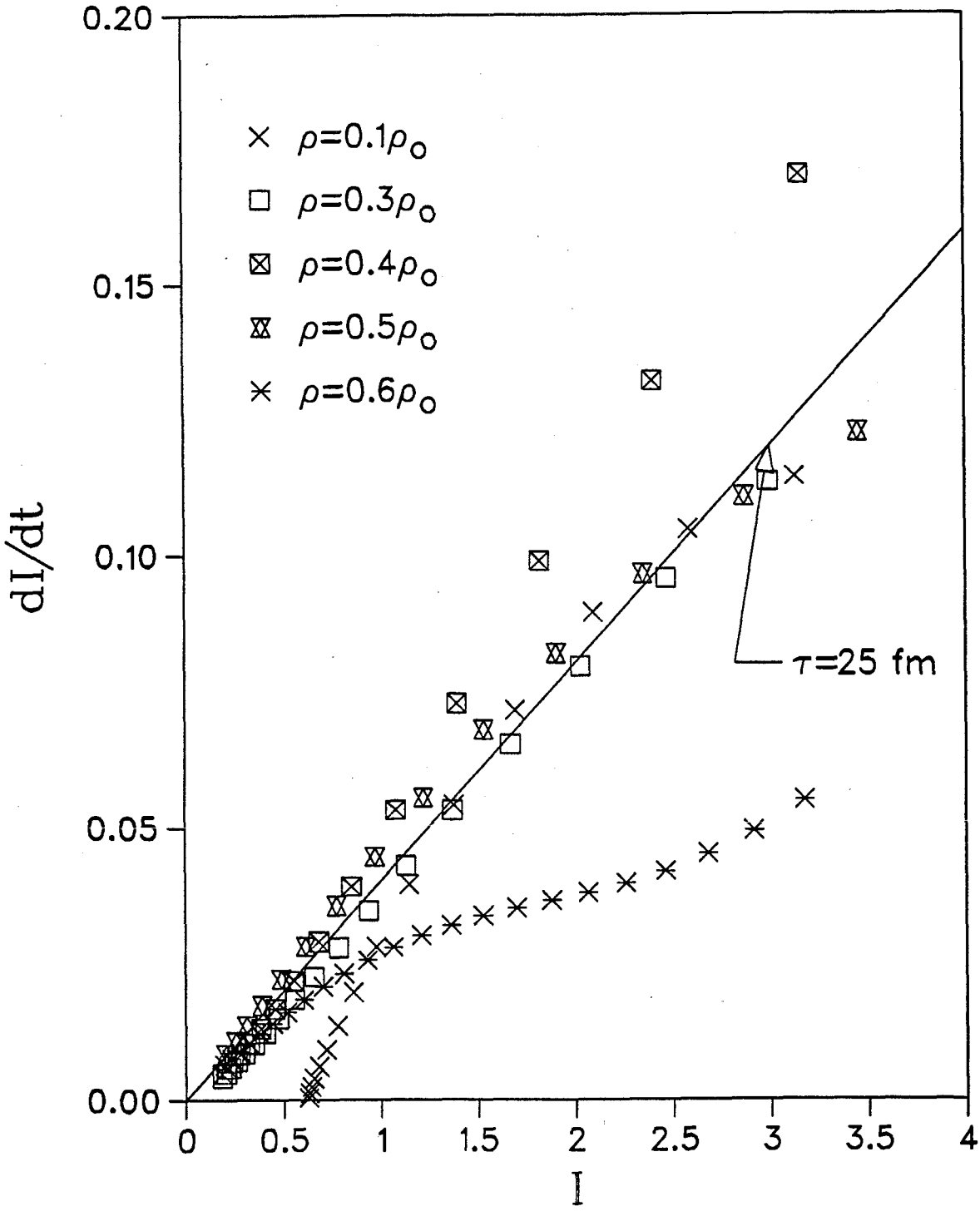

Fig. 7.5. Scatter plot of dI/dt vs I, where I is a measure of the fluctuations of the system (see text for definition of I). The fit to the straight line demonstrates the small time exponential growth of the fluctuations with time constant τ=25 fm/c.

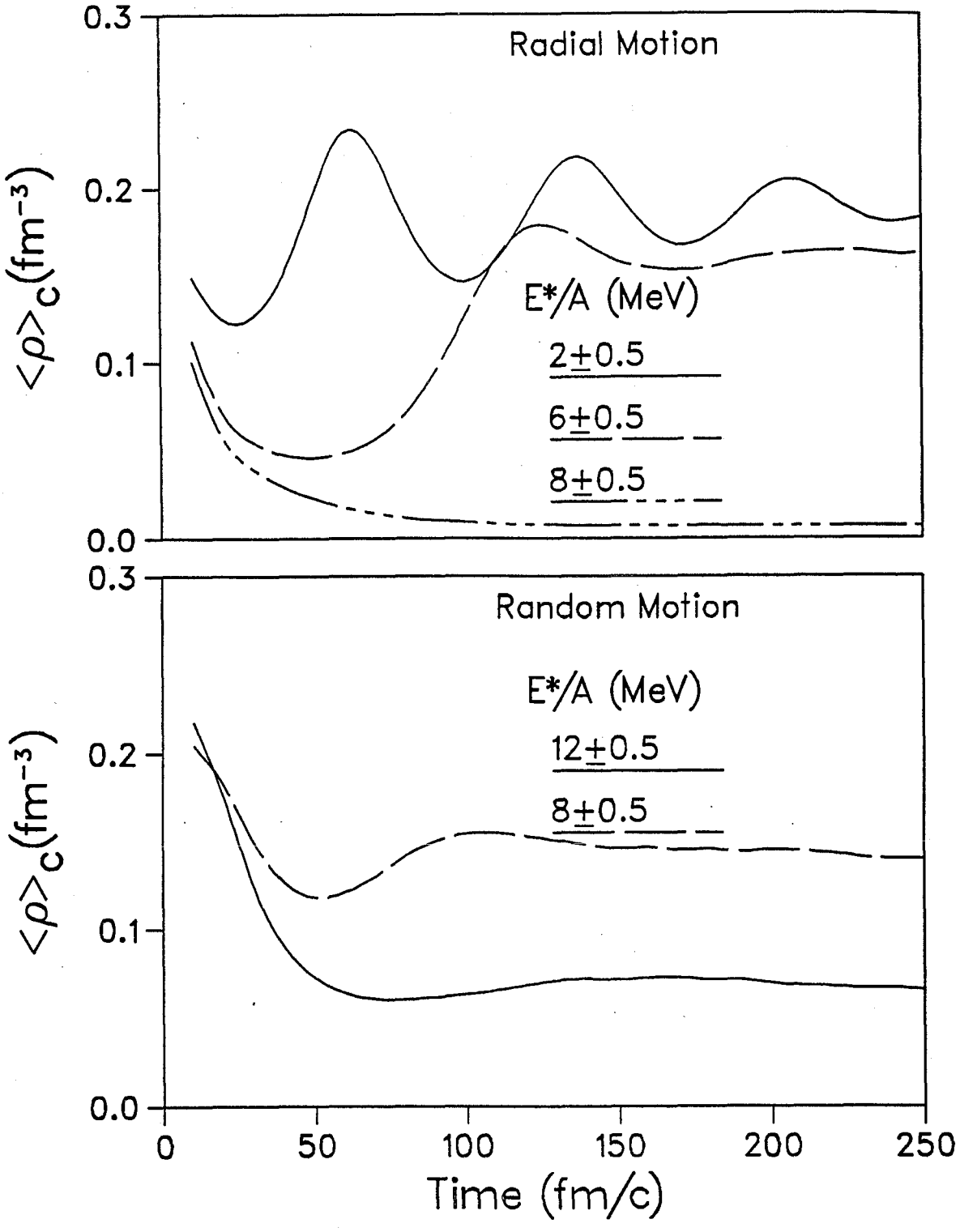

Fig. 7.6. The time dependence of the average central density ($<\rho_c>$) of excited ^{108}Ag nuclei. The upper diagram illustrates the behaviour for a radially outward directed excitation and the lower diagram illustrates the behaviour for a more random initial excitation.

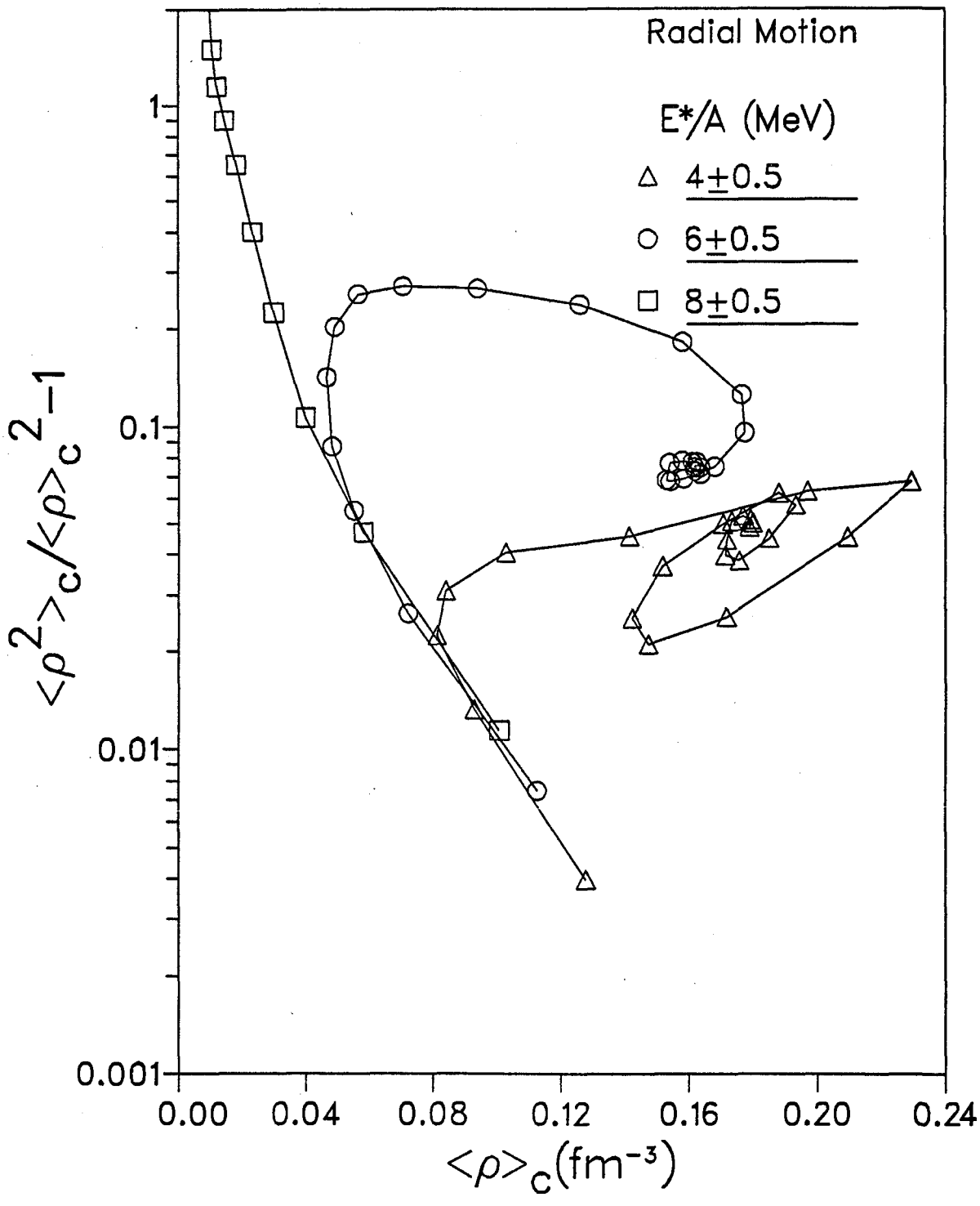

Fig. 7.7. The trajectories of the radially excited ^{108}Ag nuclei in density-fluctuation space.

VIII CONCLUSIONS

The motivation for developing the QPD model is to have at our disposal a computationally efficient nuclear model that is applicable to the study of intermediate energy heavy ion reactions. To be computationally tractable, models must have energy and force algorithms which can be evaluated within $O(A^2)$ operations. This condition limits the model to be classical or semiclassical in nature.

A completely classical picture of nuclear reactions is unable to describe much of the physics, so it is necessary to include at least some quantum mechanical aspects. To these ends, the development of our model begins with a wave function for the system, which ensures that the Heisenberg Uncertainty Principle has been incorporated. The wavefunction is then simplified by assuming that the state of the system can be expressed in terms of a product of single-particle fixed-width gaussian wavepackets. Each wavepacket's temporal evolution can be completely expressed by specifying its mean position $\mathbf{R}(t)$ and mean momentum $\mathbf{P}(t)$. It is therefore natural to associate with each gaussian wavepacket a classical particle with phase space coordinate $(\mathbf{R},\mathbf{P})$. To distinguish this particle from the underlying quantum mechanical particle we refer to it a quasiparticle. A natural generalization of the model would be to relax the restriction that wavepacket width α be fixed and allow it to be a dynamical variable. However in this work it has been fixed at a constant value of $\alpha=\sqrt{2}\ \mathrm{fm}^{-1}$.

To include the fermionic nature of the nucleon, the wave function must be antisymmetrized. The introduction of the quasiparticle notion into a

two-body fermionic system leads to a momentum-dependent interaction between quasiparticles, which we have called the Pauli potential, to represent the expectation of the energy of the fermion pair. For an A-particle system the expectation of the kinetic energy includes two-body through to A-body terms and is difficult to evaluate. To simplify the potential, the effects of the higher order terms are approximated by rescaling the magnitude two-body term. The ability of this potential to reproduce antisymmetrization effects is tested by considering a number of free fermion systems. The energy of a free gas of quasiparticles is calculated using the Pauli potential and compares well with the free Fermi gas for both zero and nonzero temperatures over the density range applicable to the study of intermediate energy reactions. As an example of fermions in a field, the Pauli potential is applied to fermions in a harmonic potential and predicts the energetics of this system with good accuracy compared to the exact quantum mechanical results.

In Chapter IV a Skyrme interaction is applied to the quasiparticle wave function to produce a density-dependent interaction. The gaussian forms allow the integrals associated with the density-dependent interaction to be evaluated and hence an explicit interaction term between quasiparticles can be determined. This interaction can be evaluated in $O(A^2)$ operations, in keeping with the goals for the model. Having found the form of the quasiparticle Hamiltonian (Pauli potential + Nuclear interaction), predictions are made for the ground states of real nuclei. By minimizing the QP Hamiltonian with respect to the QP phase space coordinates, ground state binding energies and RMS radii are predicted to be within 5-10% of the measured values over the entire periodic table, except for very light

systems.

The density-dependent term in the assumed nuclear interaction is of much the same form as the mean-field potential used in VUU calculations. For the same reason (transparency effect) that a collision term was introduced into the VUU calculations, a collision term is also introduced in to the QP model. The form of this collision term is not exactly the same as the VUU collision term but does share some similar features. The term is similar in that it involves stochastic instantaneous collisions that incorporate Pauli blocking. However, the QPD collision term ensures that not only are energy and linear momentum conserved but angular momentum is also conserved on an event-by-event basis. The Pauli blocking factor of the collision term is a further way in which the Pauli exclusion principle has been included in the model. This collision term reproduces reasonably well the nucleon-nucleon scattering data and removes the transparency characteristic of the Vlasov equation.

The first question that we use the QPD model to address is that of coarse time scales associated with intermediate nuclear reactions. The purposes of this investigation are two-fold; first, a computational determination of the model's ability to explore interesting physics and second, an investigation of the time scales associated with various stages of nuclear reactions. For a variety of intermediate energy reactions, it is found that the violent interaction associated with the initial impact of the colliding nuclei has disappeared by 100 fm/c after maximum overlap. It is clear that much of the fragmentation associated with intermediate energy heavy ion collisions occurs relativity early in the reaction (i.e. before

200 fm/c). To understand the modification of the fragmentation by long time decays, as well as to understand other long-time processes, it is not efficient (or even possible in some cases) to use the QPD model. Though the model can generate good data sets for reaction times of 100-500 fm/c, the many orders of magnitude increase in simulation times needed to see long-time processes is beyond present day computer hardware. However, the QPD model is successful in evolving the nuclear system through the initial far-from-equilibrium phase of the reaction to the quasiequilibrium state that has set in by 200 fm/c. A more efficient and desirable approach to understand the long-time processes is to use the output of the QPD model as input into a statistical decay model.

The QPD model has been used by a number of groups to investigate various nuclear reactions. R. Korteling of Simon Fraser Univ. has used the model to investigate proton-induced reactions on ^{108}Ag. For bombarding energies of 300 MeV the model reproduced the proton and neutron inclusive cross sections reasonably well [Kor89]. Boal and Wong [BW90] have used the model to explore gamma-ray polarization in ^{14}N + ^{154}Sm reactions at 35 A$\cdot$MeV. The inclusive cross sections for protons, deuterons and tritons they calculate have reasonable agreement with experiment. W. Bauer of Michigan State Univ. has investigated low energy C+C collisions with QPD and measured the single particle inclusive cross section [Ba89]. The low energy portion of the cross section is well reproduced by model, but the model under predicts the higher energy part of the distribution.

The ability of QPD to treat ground state and dynamical properties within a consistent framework makes it well suited to study excitation energy

distributions and temperature questions associated with nuclear reactions. A number of different measures of temperature have been proposed and applied to experimental systems. It is satisfying to see that the QPD model predicts both kinetic and chemical temperatures that are consistent with experiment. For intermediate energy reactions the chemical temperature is in the 2.5-3.5 MeV range, much lower than the kinetic temperature, and has only a small dependence on bombarding energy. The difference between the kinetic and chemical temperature is found to be established early in the reaction, thus demonstrating that long-time decays are not necessary to produce this effect.

Lastly, we consider the bulk properties of nuclear systems and how they effect fragmentation in nuclear reactions. We begin with zero temperature properties. The T=0 isotherm is found to have a minimum of -16.20 MeV at $\rho=1.03\rho_o$, and the compressibility is approximately K=400 MeV. The value of the compressibility is consistent with the form chosen for the nuclear interaction (i.e. stiff equation of state) but larger than the commonly accepted value of K=200 MeV. Next the T-ρ phase diagram is constructed by examining the temperature dependence of the specific heat. The phase diagram is consistent with a number of other analytical calculations. The agreement suggests that the QPD model is appropriate for investigating phase transition effects in nuclear reactions.

An interesting feature noticed in constructing the T-ρ diagram is the strong finite size effect. For example, the infinite-system transition temperature can be a factor of two greater than the pseudo-transition temperature (as defined by the peak in the specific heat at constant

volume) for system sizes typical of nuclear reactions. In light of this strong size effect the relationship between nuclear reaction phenomena, such as fragmentation, and bulk properties of phase transitions and spinodal decomposition is not transparent.

The role that thermodynamics has in describing phenomena of intermediate nuclear reactions is further investigated by considering the various time scales associated with decay times of excited nuclei. It is found that the expansion time and the fluctuation growth time are of the same order. Further, both of these time scales are short compared to the relaxation time, making the assumption of quasi-equilibrium invalid. In conclusion it appears that bulk thermodynamics has little to do with describing the physics of the highly excited systems that are produced in intermediate energy nuclear reactions.

One could proceed in a number of different directions to further this approach to nuclear dynamics. There are many simulations of interest to the experimentalist that can done and which would help define the reliability of the model. The calculation of particle-particle correlation functions and comparison with experiment are of particular interest. The questions of the existence and forms of Pauli potentials are areas which deserve more attention. Related concerns exist with the choice of the single-particle wave functions. What effect would it have on the model if the widths of the gaussian wavepackets were allowed to be dynamic variables. In all, we believe there are many interesting problems that the model can be used to explore and also there are many ways in which it can be improved.

APPENDIX A STABILITY OF THE ZERO MOMENTUM MODE OF THE QP MODEL ON A CUBIC LATTICE

Most classical systems possess a zero momentum ground state. However the introduction of a momentum-dependent interaction may cause the P=0 mode to become unstable. In this appendix it is shown that the P=0 mode of the QP model of noninteracting fermions can be unstable. For simplicity the quasiparticles are restricted to lie on a cubic lattice in real space with lattice spacing a.

The stability of the $\mathbf{P}_l=0$ will be determined by considering the curvature, with respect to $\mathbf{k}_l=\mathbf{P}_l/\hbar$, of the QP Hamiltonian $H(\mathbf{R},\mathbf{P})$ (see Eq. 3.8 for the definition of H). The curvature matrix M of H is defined as

$$M_{l\mu;m\nu} \equiv \left.\frac{\partial^2 H}{\partial k_l^{\mu}\partial k_m^{\nu}}\right|_{k=0} = \frac{\hbar^2}{m}\delta_{\mu\nu}\begin{cases} 1 + \sum_{j\neq l} f(\frac{1}{2}\alpha^2 R_{lj}^2) , & l=m \\ -f(\frac{1}{2}\alpha^2 R_{lm}^2) , & l\neq m \end{cases} \qquad (A.1)$$

where

$$f(X) = V_s\left(\frac{1}{e^X - 1} - \frac{X\, e^X}{(e^X - 1)^2}\right)$$

For a lattice model with periodic boundary conditions all lattice sites are equivalent, therefore the sum over particle label can be replaced by a sum over lattice sites:

$$\sum_{j\neq l} f(\tfrac{1}{2}\alpha^2 R_{lj}^2) = \sum_{\substack{R\neq 0 \\ R\in lattice}} f(\tfrac{1}{2}\alpha^2 R^2)$$

Defining

$$Q(X^2) = \begin{cases} 1 + \sum_{j\neq 1} f(\frac{1}{2}\alpha^2 R_{1j}^2) , & X=0 \\ -f(\frac{1}{2}X^2) , & \text{otherwise} \end{cases} \qquad (A.2)$$

Eq.A.1 can be rewritten as

$$M_{1\mu;m\nu} = \frac{\hbar^2}{m} \delta_{\mu\nu} Q(|R_1 - R_m|^2) \quad .$$

It will be demonstrated that

$$\left[V(q)\right]_{m\nu} = e^{-iR_m \cdot q} \ \omega_\nu$$

is an eigenvector of M for all $q=(q^x,q^y,q^z)$, $q^\mu \in (-\pi/a, \pi/a)$.

$$\begin{aligned} MV(q) &= \sum_{m\nu} M_{1\mu;m\nu} \, e^{-R_m \cdot q} \, \omega_\nu \\ &= \frac{\hbar^2}{m} \sum \delta_{\mu\nu} Q(|R_1 - R_m|^2) \times e^{-iR_m \cdot q} \, \omega_\nu \\ &= \frac{\hbar^2}{m} \sum \delta_{\mu\nu} Q(|R_1 - R_m|^2) \times e^{-i(R_m - R_1)\cdot q} \, e^{-iR_1 \cdot q} \, \omega_\nu \end{aligned}$$

Replacing the sum over particles with the sum over lattice sites,

$$\begin{aligned} MV(q) &= \frac{\hbar^2}{m} \omega_\mu \, e^{-iR_1 \cdot q} \sum_{R \in lattice} Q(|R|^2) e^{-iR \cdot q} \\ &= \lambda(q) V(q) \end{aligned}$$

where

$$\lambda(\mathbf{q}) = \frac{\hbar^2}{m} \sum_{\mathbf{R}\in lattice} Q(|\mathbf{R}|^2) e^{-i\mathbf{R}\cdot\mathbf{q}}$$

$$= \frac{\hbar^2}{m} \left[1 + \sum_{\mathbf{R}\in lattice} f(\tfrac{1}{2}\alpha^2 R^2) \; [1-\cos(\mathbf{R}\cdot\mathbf{q})] \right] \quad .$$

Hence $\mathbf{V}(\mathbf{q})$ is an eigenvector of M with eigenvalue $\lambda(\mathbf{q})$. The stability of the P=0 mode is determined by the sign of λ. If $\lambda(\mathbf{q})>0$ for all $\mathbf{q}$ then the zero momentum mode is stable. However if $\lambda(\mathbf{q}) < 0$ for some $\mathbf{q}$ then P=0 is a saddle point and unstable, hence the ground state will have a nonzero value of the momentum. In Fig. 3.1, $\lambda(\mathbf{q})$ is shown for V_s=1 and various α's along the line $q^x=q^y=q^z$. For $\alpha a<2.2$, the minimum value of λ is less than zero and the P=0 mode is unstable.

APPENDIX B MAXIMUM LIKELIHOOD ESTIMATORS ASSOCIATED WITH A BOLTZMANN DISTRIBUTION

The determination of the distribution that generated a given data set is a common statistical problem. Often a functional form of the distribution is known, but the determination of a number of unknown parameters is required to completely specify the distribution. The method of maximum likelihood provides a way to estimate these unknown parameters. The particular problem that this appendix addresses, will be how to make a maximum likelihood estimate (MLE) of the temperature, T, from a data set that is assumed to have a Boltzmann distribution.

The MLE of a set of unknown parameters is made by finding the value of these parameters that would maximize the probability of observing the given data set. More specifically, for a given data set $(x_1,\ldots,x_n)$ the MLE estimate is found by maximizing the value of the joint probability distribution $f(x_1,\ldots,x_n;\alpha_1,\ldots,\alpha_k)$ with respect to the unknown parameters $(\alpha_1,\ldots\alpha_k)$.

For the purposes of this appendix it is adequate to consider the case of one unknown parameter, α. Further, we assume that $(x_1,\ldots,x_n)$ are a set independent identically distributed random variables with distribution $g(x_i;\alpha)$. The independence of the observation allows the joint distribution to be factorized,

$$f(x_1,\ldots,x_n;\alpha) = \prod_{i=1}^{n} g(x_i;\alpha) \qquad (B.1)$$

To find the value of α, which will be denoted by $\hat{\alpha}$, it is common and

convenient to use the fact that $\hat{\alpha}$ will maximize both f and $\ell n(f)$. The value of $\hat{\alpha}$ can be found by solving the equation

$$\frac{\partial \ell n(f)}{\partial \alpha} = \sum_{i=1}^{n} \frac{\partial \ell n(g(\hat{x}_i;\alpha))}{\partial \alpha} = 0 \qquad (B.2)$$

The MLE $\hat{\alpha}$, of the parameter, α, has a number of desirable statistical properties. First it is a sufficient estimator of α and secondly it is asymptotically ($n \longrightarrow oo$) a minimum variance unbiased estimator of α as well (See page 267 of [Fre71]).

The Boltzmann distribution of a system is given by

$$g(E;T) = \frac{e^{(-E/T)}}{Z(T)} \qquad (B.3)$$

where Z(T) is the partition function. Given some set of observed energies $(E_1,\ldots,E_n)$ an equation for the MLE, $\hat{T}$, of the temperature, T, can be found by substituting Eq. B.3 into B.2,

$$\sum_{i=1}^{n} \left[(E_i/T^2) - \frac{\partial \ell n(Z)}{\partial T} \right] = 0 \quad . \qquad (B.4)$$

Using

$$\frac{\partial \ell n(Z)}{\partial T} = \langle E(T) \rangle / T^2$$

where < > represents the full ensemble average, Eq. B.4 is simplified to:

$$\bar{E} \equiv \frac{1}{n} \sum_{i=1}^{n} E_i = \langle E(\hat{T}) \rangle \qquad (B.5)$$

Typically <E(T)> is not known analytically, however a Monte Carlo procedure normally can be used to evaluate it.

To extract a temperature from a data set, a MLE based on the centre of mass kinetic energy also can be used. For many systems, including the QP model, the centre of mass kinetic energy, K, decouples from the rest of the Hamiltonian. This allows one to find an analytic form for the distribution function of K, and hence the expectation of the kinetic energy, $\langle K(T) \rangle = \frac{3}{2}T$. Using this relationship an additional MLE of the temperature is found.

$$\bar{K} \equiv \frac{1}{n}\sum_{i=1}^{n} K_i = \langle K(\hat{T}) \rangle = \frac{3}{2}\hat{T} \quad . \tag{B.6}$$

References

[Aic83] J. Aichelin, Nucl. Phys. A411, 474 (1983).

[AGH77] A.A. Amsden et al. Phys. Rev. 38, 1055 (1977).

[AHI84] J. Aichelin, J. Hüfner and R. Ibarra, Phys. Rev. C30, 107 (1984).

[AS85] J. Aichelin and J. Stocker, Phys. Rev. Lett. 165B, 59 (1985).

[AS86] J. Aichelin and J. Stocker, Phys. Lett. 176B, 14 (1986).

[Bau89] W. Bauer, (private commuication).

[BBW87] G.E. Beauvais, D.H. Boal and J.C.K. Wong, Phys. Rev. C35, 545 (1987).

[BBG87] G.E. Beauvais, D.H. Boal and J. Glosli, Nucl. Phys. A471, 427c (1987).

[BD88] G. Bertsch and S. Das Gupta, Phys. Rep. 160, 673 (1988).

[BFG76] J.P. Bondorf, H.T. Feldmeier, S.I.A. Garpman, and E.C. Halbert, Phys. Lett. 65B, 321 (1976).

[BG86] D.H. Boal and A. L. Goodman, Phys. Rev. C33, 1690 (1986).

[BG88] D.H. Boal and J. Glosli, Phys. Rev. C37, 91 (1988).

[BGG76] J.P. Blaizot, D. Gogny and B. Grammaticos, Nucl. Phys. A265, 315 (1976).

[BJ84] N.L. Balazs and B.K. Jennings, Phys. Rep. 104, 347 (1984).

[BKD84] G. Bertsch, H. Kruse and S. Das Gupta, Phys. Rev. C29, 673 (1984).

[BL55] S.Z. Bertini and L.D. Landau, Usp. Fiz. Nauk 56, 109 (1955).

[BL56] S.Z. Bertini and L.D. Landau, Nuovo Cimento Suppl. 3, 15 (1956).

[Bla80] J.P. Blaizot, Phys. Reports 64, 171 (1980).

[Blo86] C. Bloch et al., Phys. Rev. C34, 850 (1986).

[Blo87] C. Bloch et al., Phys. Rev. C36, 203 (1987).

[Blo88] C. Bloch et al., Phys. Rev. C37, 2469 (1988).

[Boa87] D.H. Boal, Annu. Rev. Nucl. Part. Sci. 37, 1 (1987).

[Boa84] D.H. Boal, Phys. Rev. C30, 749 (1984).

[Bon76] J.P. Bondorf, J. Phys. Suppl. 37, C5-195 (1976).

[Bon85] J.P. Bondorf et al., Nucl. Phys. A443, 321 (1985).

[BP77] A.R. Bodmer and C.N. Panos, Phys. Rev. C15, 1342 (1977).

[BPD86] W. Bauer, U. Post, D.R. Dean and U. Mosel, Nucl. Phys. A452, 699 (1986).

[BPM80] A.R. Bodmer, C.N. Panos and A.D. MacKellar, Phys. Rev. C22, 1025 (1980).

[BS83] G. Bertsch and P.J. Siemens, Phys. Lett. 126B, 9 (1983).

[BSG76] J.P. Bondorf, J.P. Siemens, S.I.A. Garpman, and E.C. Halbert, Z. Phys. A. 279, 385 (1976).

[BW90] D.H. Boal and J. Wong, Phys. Rev. C41 (in press).

[CB72] S.D. Conte and C. Boar, Elementary Numerical Analysis, McGraw Hill, New York (1972).

[Cer88] C. Cerruti et al., Nucl. Phys. A476, 74 (1988).

[Che87] Z. Chen et al., Phys. Rev. C36, 2297 (1987).

[CS86] R.B. Clare and D. Strottman, Phys. Rep. 141, 179 (1986).

[CWY79] D.J.E. Callaway, L. Wilets and Y. Yariv, Nucl. Phys. A327, 250 (1979).

[DBN87] J. Desbois, R. Boisgard, C. Ngô and J. Nemeth, Z. Phys. A328, 101 (1987).

[DDR87] C. Dorso, S. Duarte and J. Randrup, Phys. Lett. 188B, 287 (1987).

[DM81] S. Das Gupta and A.Z. Mekjian, Phys. Rep. 72, 423 (1981).

[DW69] T.W. Donnelly and G.E. Walker, Phys. Rev. Lett. 22, 1121 (1969).

[Eng66] H.A. Enge, Introduction to Nuclear Physics, Addision-Wesley, Massachusetts (1966).

[Fie87] D.J. Fields et al., Phys. Lett. 187B, 257 (1987).

[FP81] B. Friedman and V.R. Pandharipande, Nucl. Phys. A361, 502 (1981).

[Fre71] J.E. Freund, Mathematical Statistics, Prentice-Hall, New Jersey, (1971).

[FW71] A.L. Fetter and J.D. Walecka, Quantum Theory of Many-particle Systems, McGraw-Hill, New York (1971).

[GD85] C. Gale and S. Das Gupta, Phys. Lett. 162B, 35 (1985)

[GB87] C.K. Gelbke and D.H. Boal, Prog. Part. Nucl. Phys. 19 (1987).

[GKM84] A.L. Goodman, J.I. Kapusta and A. Mekjian, Phys. Rev. C30, 851 (1984).

[Gol48] M.L. Goldberger, Phys. Rev. 74, 1269 (1948).

[GT86] C. Grégoire and B. Tamain, Ann. Phys. Fr. 11, 323 (1986).

[Gre54] A.E.S. Green, Phys. Rev. 95, 1006 (1954).

[HAN76] F.H. Harlow, A.A. Amsden and J.R. Nix, J. Comp. Phys. 20, 119 (1976).

[Hof67] R. Hofstadter, in Nuclear Physics and Technology, Springer-Verlag, Berlin (1967).

[HOS84] M. Hillery, R.F. O'Connell, M.O. Scully and E.P. Wigner, Phys. Rep. 106, 121 (1984).

[HS87] D. Hahn and H. Stocker, Phys. Rev. C35, 1311 (1987).

[Kor89] R. Korteling, (private communication).

[LP86] R.J. Lenk and V.R. Pandharipande, Phys. Rev. C34, 177 (1986).

[LS84] J.A. Lopez and P.J. Siemens, Nucl. Phys. A431, 728 (1984).

[MS66] W.D. Myers and W.J. Swiatechki, Nucl. Phys. 81, 1 (1966).

[Mor75] P.A.P. Moran, Biometrika 62, 1 (1975).

[Mor84] D.J. Morrissey et al., Phys. Lett. 148B, 423 (1984).

[Mor85] D.J. Morrissey et al., Phys. Rev. C34, 761 (1985).

[Nix79] J.R. Nix, in Progress in Particle and Nuclear Physics (Vol 2), Pergamon Press, Oxford and New York (1979).

[NNL88] C. Ngô, H. Ngô, S. Leray and M.E. Spina, preprint (1988).

[Nor28] L.W. Nordheim, Proc. R. Soc. London, Ser. A 119, 689 (1928).

[PDG70] Particle Data Group, Lawrence Radiation Laboratory Report UCRL-200000NN, 1970.

[Po85a] J. Pochodzalla et al., Phys. Rev. Lett. 55, 177 (1985).

[Po85b] J. Pochodzalla et al., Phys. Lett. 161B, 275 (1985).

[Ser47] R. Serber, Phys. Rev. 72, 1114 (1947).

[SG86] H. Stocker and W. Greiner, Phys. Rep. 137, 277 (1986).

[SCM81] H. Stöcker, H. Cusson, J.A. Maruhn and W. Greiner, Prog. Part. Phys. Lett. 101, 379 (1981).

[SP87] T.J. Schlagel and V.R. Pandharipande, Phys. Rev. C36, 162 (1987).

[UU33] E.A. Uehling and G.E. Uhlenbech, Phys. Rev. 43, 552 (1933).

[VB72] D.Vautherin and D.M. Brink, Phys. Rev. C5, 626 (1972).

[VJP85] A. Vicentini, G. Jacucci, and V.R. Pandharipande, Phys. Rev. C31, 1783 (1985).

[WHK77] L. Wilets, E.M. Henley, M. Kraft and A.D. MacKellar, Nucl. Phys. A282, 341 (1977).

[WYC78] L. Wilets, Y. Yariv and R. Chestnut, Nucl. Phys. A301, 359 (1978).

[YF79] Y. Yariv and Z. Fraenkel, Phys. Rev. C20, 2227 (1979).

[YF81] Y. Yariv and Z. Fraenkel, Phys. Rev. C24, 488 (1981).